Final Technical Report
Development of Post-Installation Monitoring Capabilities

DE-EE0000301

March 2011 – December 2013

Principal Investigators

Mr. Craig Collar, P.E.

Public Utility District No. 1 of Snohomish County

(425) 783-1825, cwcollar@snopud.com

Dr. Brian L. Polagye, Ph.D.

Northwest National Marine Renewable Energy Center, University of Washington

(206) 543-7544, bpolagye@uw.edu

Recipient Organization

Public Utility District No. 1 of Snohomish County

2320 California Street

Everett, WA 98201

Team Member Organizations

Northwest National Marine Renewable Energy Center, University of Washington

Sea Mammal Research Unit, LLC

H.T. Harvey & Associates

Pacific Northwest National Laboratories (unfunded collaboration)

March 31, 2014

Acknowledgement and Disclaimer

Acknowledgment: This report is based upon work supported by the U. S. Department of Energy under Award No. DE-EE0000301.

Disclaimer: Any findings, opinions, and conclusions or recommendations expressed in this report are those of the author(s) and do not necessarily reflect the views of the Department of Energy.

Tables of Contents

List of Acronyms

AMP: Adaptable Monitoring Package

ADCP: acoustic Doppler current profiler

CPOD: cetacean click detector (Chelonia, Ltd.)

PNNL: Pacific Northwest National Laboratory

List of Figures

List of Tables

List of Appendices

Appendix 1 - Joslin, J. and B. Polagye (submitted), Biofouling mitigation methods for optical ports*, Submitted to IEEE J. Ocean. Eng.*

Appendix 2 - Joslin, J., S. Parker-Stetter, and B. Polagye (*revision submitted*) Development of a stereo-optical camera system for monitoring tidal turbines, *SPIE J. of Applied Remote Sensing*.

Executive Summary

The development of approaches to harness marine and hydrokinetic energy at large-scale is predicated on the compatibility of these generation technologies with the marine environment. At present, aspects of this compatibility are uncertain. Demonstration projects provide an opportunity to address these uncertainties in a way that moves the entire industry forward. However, the monitoring capabilities to realize these advances are often under-developed in comparison to the marine and hydrokinetic energy technologies being studied.

Public Utility District No. 1 of Snohomish County has proposed to deploy two 6-meter diameter tidal turbines manufactured by OpenHydro in northern Admiralty Inlet, Puget Sound, Washington. The goal of this deployment is to provide information about the environmental, technical, and economic performance of such turbines that can advance the development of larger-scale tidal energy projects, both in the United States and internationally. The objective of this particular project was to develop environmental monitoring plans in collaboration with resource agencies, while simultaneously advancing the capabilities of monitoring technologies to the point that they could be realistically implemented as part of these plans. In this, the District was joined by researchers at the Northwest National Marine Renewable Energy Center at the University of Washington, Sea Mammal Research Unit, LLC, H.T. Harvey & Associates, and Pacific Northwest National Laboratory.

Over a two year period, the project team successfully developed four environmental monitoring and mitigation plans that were adopted as a condition of the operating license for the demonstration project that issued by the Federal Energy Regulatory Commission in March 2014. These plans address near-turbine interactions with marine animals, the sound produced by the turbines, marine mammal behavioral changes associated with the turbines, and changes to benthic habitat associated with colonization of the subsea base support structure.

In support of these plans, the project team developed and field tested a strobe-illuminated stereo-optical camera system suitable for studying near-turbine interactions with marine animals. The camera system underwent short-term field testing at the proposed turbine deployment site and a multi-month endurance test in shallower water to evaluate the effectiveness of biofouling mitigation measures for the optical ports on camera and strobe pressure housings. These tests demonstrated that the camera system is likely to meet the objectives of the near-turbine monitoring plan and operate, without maintenance, for periods of at least three months. The project team also advanced monitoring capabilities related to passive acoustic monitoring of marine mammals and monitoring of tidal currents.

These capabilities will be integrated in a recoverable monitoring package that has a single interface point with the OpenHydro turbines, connects to shore power and data via a wet-mate connector, and can be recovered to the surface for maintenance and reconfiguration independent of the turbine. A logical next step would be to integrate these instruments within the package, such that one instrument can trigger the operation of another.

The partnership formed between the District and resource agencies in the development of these monitoring plans and monitoring technologies bodes well for a productive tidal energy demonstration project in Admiralty Inlet.

1 Introduction

Marine and hydrokinetic technologies have the potential to provide significant renewable electricity in the United States. However, there are equally significant environmental uncertainties associated with large-scale operation of these technologies. In 2010, an expert workshop identified interactions between stressors (i.e., turbine sound) and receptors (i.e., marine mammals) that might be environmentally significant, but presently have broad uncertainty (Polagye et al. 2011).The workshop brought together over seventy experts from academia, regulatory agencies, and industry drawn from the US, Canada, and Europe who identified critical knowledge gaps that hindered their assessment of environmental risks. One of the recommendations to come out of this workshop was to study these high-uncertainty environmental effects at the pilot scale as a mechanism to inform decisions about larger-scale deployments.

Figure 1 presents a modified stressor-reception interaction matrix developed by workshop participants for commercial-scale deployments (generalized over all sites and all turbine technologies). Each row corresponds to a category of environmental receptor and each column corresponds to an environmental stressor. The color of the intersecting cells denotes the severity of a potential interaction (i.e., red denotes a potentially significant interaction while green denotes a low significance interaction). Similarly, the number of triangles denotes the uncertainty around the significance of this interaction (e.g., three red triangles denote high uncertainty). Areas that are of potentially high significance but also have high uncertainty (yellow/red cells with three red triangles) should be focus areas for pilot project monitoring, in a general sense. However, the range of potential interactions meeting these criteria is too broad for any single pilot project to study all of them and prioritization is required.

The following considerations may be applied to prioritizing studies for pilot (or demonstration) projects[1]:

- Studies of cumulative effects of multiple stressors from a tidal energy project and ecosystem interactions are not likely to be possible because of the small scale of these projects relative to natural variability. A related, preceding step recommended by the workshop participants is to reduce the uncertainty associated with cumulative effects and ecosystem interactions by monitoring individual stressor-receptor interactions and then modeling the consequences of scale-up.
- Energy removal and far-field environmental effects (e.g., changes on the scale of an entire estuary) will be immeasurably small at the pilot scale and cannot be monitored for in most pilot projects (Polagye et al. 2009).
- Electromagnetic and chemical effects may be significant at the commercial scale, but at the pilot scale, the signal to noise ratio will likely be too low to effectively study.

Figure 1 shows the consequences of this prioritization by shading out those elements of the environmental uncertainty matrix that are not likely to be effectively studied at the scale of a demonstration project.

[1] These represent the opinions of the project team, not the general consensus of workshop participants.

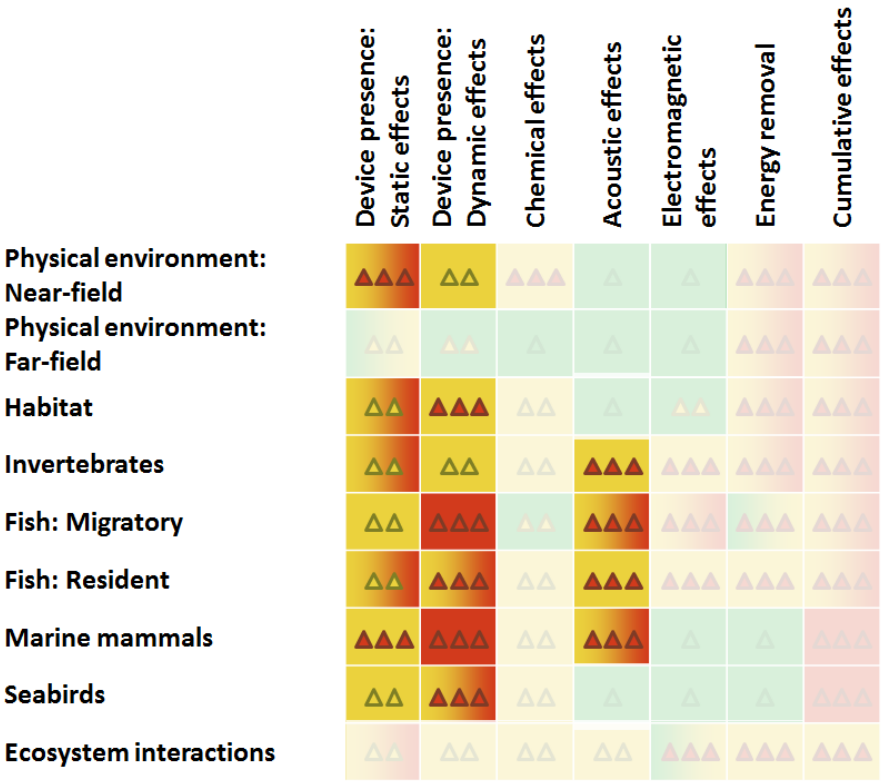

Figure 1 – Commercial-scale deployment generalized stressor/receptor significance (on a gradient green = low, red = high) and uncertainty (one green triangle = low uncertainty, two yellow triangles = moderate uncertainty, three red triangles = high uncertainty). From, Polagye et al. (2011), emphasizing focus study areas for pilot projects.

This prioritization results in the following high-value areas for demonstration project monitoring:

- Interactions between marine animals (invertebrates, fish, marine mammals, and seabirds) with a rotating turbine.
- Interactions between marine animals and the foundation of a turbine as an artificial reef is established over a multi-year period.
- The effects of turbine sound on marine animals.

Given these priorities, the questions then become:

1. How can monitoring plans be developed around specific hypotheses within these areas?
2. What technology options are available to implement such plans in the context of tidal energy sites (i.e., locations with extreme currents)?

Neither of these questions are easy to address and neither can be answered independently of the other. For example, monitoring plans that rely on non-existent monitoring technologies are no more likely to provide useful information than monitoring technologies that are deployed in a manner that does not address specific, high-priority hypotheses. The objective of this project was to provide an answer to these questions for a specific tidal energy demonstration in Admiralty Inlet, Puget Sound, Washington.

2 Background

2.1 Context

Public Utility District No. 1 of Snohomish County (the District) believes there is potential to generate renewable, emission free, environmentally benign and cost-effective energy from tidal flows at selected sites in Puget Sound, and that successful tidal energy demonstration in Puget Sound may enable significant commercial development that results in important benefits for both the northwest region and the country. The District is pursuing a tidal energy demonstration project to conduct in-water testing and evaluation of commercial/near-commercial tidal turbine technology representative of what would be expected to be used in a commercial-scale power plant. This will enable the District team to make an informed evaluation of whether, and to what extent, tidal energy should be included in the District's energy portfolio, while simultaneously facilitating the commercial development of this new industry.

The pilot tidal project will involve the deployment, operation, monitoring and evaluation of two 6-meter diameter hydrokinetic tidal turbines. The turbines are expected to generate 600 kW of electrical energy during periods of peak tidal currents with an average energy output of approximately 30 kW. While the project will be connected to the grid and produce a modest amount of energy, its primary purpose is to gather data to better inform the viability of commercial tidal energy generation from technical, economic, social and environmental standpoints. This data is critical to the responsible advancement of commercial scale tidal energy in the United States. Capabilities to collect project data (performance and environmental) are key to achieving this goal. In some cases, such as monitoring for blade strike in the immediate vicinity of the turbine rotor, these capabilities are less developed than the tidal turbines being monitored.

2.2 Objective

The objective of this project was to develop and verify monitoring capabilities necessary for post-installation data collection in areas of significant environmental uncertainty (Polagye et al. 2011). The primary focus was on the development of near-field monitoring capabilities to observe interactions in the immediate vicinity of turbine rotors that can address concerns about the risk of post-installation blade strike. This has been a persistent concern for tidal energy projects. Additionally, equipment suitable for post-installation passive acoustic monitoring was tested and a plan for integrated packaging of the instrumentation developed.

2.3 Approach

2.3.1 Near-turbine Monitoring

Because of the potential for injury caused by turbine blades striking a marine animal or marine animal colliding with turbine blades, resource agencies in the United States and Europe have focused on observations within the near-field. Field observations and laboratory experiments conducted to date for tidal and river turbines (Viehman and Zydlewski *in revision*, Normandeau 2009, Amaral et al. 2011) suggest that such interactions are likely to be rare. However, these results need to be confirmed for a broader set of locations and technology variants. Ideally, field observations should be able to discriminate between contact and a near-miss between marine animals and the turbine rotor, identify the marine animal involved to the species level, continuously observe the entire near-field, and cause

minimal behavioral changes. Simultaneously satisfying these constraints is not technically feasible, as evidenced by the variety of approaches employed to date, four of which are summarized here.

Verdant Power (East River, New York, United States)

Verdant Power operated an array of turbines near Roosevelt Island in the East River of New York from 2005 through 2008. The project used a combination of split-beam acoustic echosounders (BioSonics, DTX) deployed from shore and a vessel-deployed imaging sonar ("acoustical camera") (Sound Metrics, DIDSON) to monitor fish passage. The array of split-beam transducers (24 in total) was able to monitor targets passing through the project area, but could not be used to detect animal strikes with the device or to identify fish to the species level. The cost of the echosounder array exceeded that of the turbines, and the knowledge gained from this study was not considered proportional to its cost (Polagye et al. 2011). Vessel-based acoustical camera observations (3+ days) detected a single fish passing through the vicinity of one turbine during operation: the fish traveled along hydrodynamic streamlines and was not struck by the rotor. Verdant Power concluded that acoustical cameras could be an effective tool for animal strike monitoring if used for short-term deployments (2 to 3 weeks) coinciding with periods of peak fish abundance, but also concluded that data quantity, instrument reliability, and high cost combined to preclude acoustical camera use for longer-term observations.

Ocean Renewable Power Company (Eastport, Maine, United States)

Ocean Renewable Power Company tested a cross flow turbine from a barge near Eastport, Maine for two years (2010-2011). An acoustical camera (Sound Metrics, DIDSON) was deployed from the generator barge to monitor fish behavior around the operating rotor (Viehman and Zydlewski, in revision). These observations were the first documentation in the field of fish passage through a tidal turbine. While the positioning of the sonars did not allow individual fish to be tracked through the turbine, fish schools were observed entering the turbine and, having passed through, aggregating in the wake before continuing. Forty percent of individual fish detected by the imaging system were observed to interact with the turbine (i.e., passing through the turbine or resting in the wake). Reaction distance and type of interaction depended on the turbine operating state, fish length, and degree of aggregation, with schools interacting at a lower rate than individual fish. Avoidance of the rotor was observed less frequently at night than during the day, suggesting that visual cues played a role in behavior around the turbine.

OpenHydro (European Marine Energy Center, Orkney Islands, Scotland, United Kingdom)

OpenHydro used unlighted video to monitor fish interactions with its turbine at the European Marine Energy Center (Barr 2010). This approach was able to detect fish aggregations in the turbine wake during low current flows (e.g., < 1.5 m/s). No collisions with the device or blade strikes were observed and, unlike the field observations in Maine, fish were not reported to pass through the turbine once it began rotating. This turbine was deployed within the photic zone and monitoring was restricted to daylight hours. Observations were conducted with a single camera deployed from a spar on one side of the turbine.

OpenHydro (Fundy Ocean Research Centre for Energy, Minas Passage, Nova Scotia, Canada)

In the Bay of Fundy, an OpenHydro turbine was installed in November 2009 and removed in November 2010. The lack of a power and data cable precluded deployment of either optical or acoustical imaging

systems for monitoring. Consequently, researchers deployed an array of eight Vemco (VR2W) fish tag receivers around the turbine foundation and another array of eight receivers in a line across the channel to the east of the turbine. Over the course of the turbine deployment, approximately 100 fish were tagged and released in the upper Bay of Fundy. This study was able to identify periods of presence and absence, but could not be used to track individual targets because of the autonomous nature of the receivers.

Technologies for Near-Turbine Monitoring

Technologies potentially suitable for the study of near-turbine interactions include optical imaging, acoustical imaging, and animal-borne tags (i.e., tags actively transmitting an acoustic signal). Traditional fisheries trawls are unlikely to be feasible in close proximity to turbine rotors because of both the risk of net entanglement with the rotor and the difficulty of fishing effectively during periods of strong currents when interactions between turbines and fish are of greatest interest. In addition, as fish may experience injury or scale loss during capture in a trawl (Ryer 2004), it may not be feasible to determine if body trauma resulted from interaction with the turbine rotor or from trawl capture. The potential trade-offs between available technologies are summarized in Table 1, following workshop discussions summarized in Polagye et al. (2014). Of the available technologies, optical imaging may be best suited for discriminating between contacts and near-misses, as well as identifying targets to the species level, but subsampling in space and time are presently required due to data bandwidth. For example, a stereo imaging arrangement involving a pair of 2 megapixel black and white cameras with 16-bit resolution would produce more than 6 terabytes of uncompressed imagery per day when acquiring images at 10 frames per second. In contrast, a two-dimensional imaging sonar acquiring information at a similar rate produces only about 0.09 terabytes per day.

Table 1 – Capabilities of potential near-turbine monitoring technologies (adapted from workshop discussions documented in Polagye et al.).

	Optical Imaging	Acoustical Imaging	Animal-borne Tags
Discrimination between Contact and Near-Miss	Possible with stereo imaging	Not generally possible due to acoustic reflection from hard surfaces	Not possible
Identification to the Species Level	Possible at close range with stereo imaging	Possible for species with distinct shapes or swimming patterns. Requires additional information for similarly sized species about presence/absence	Inherent
Continuous Observations of Entire Near-field	Difficult due to positioning of cameras, data bandwidth, and functional range of cameras when artificial lighting is required	Difficult due to positioning of transducers and data bandwidth	Possible with an array of localizing receivers
Behavioral Changes	Artificial illumination will affect behavior	Minimal effect	Short-term effects after handling for tag insertion

2.3.2 Passive Acoustic Monitoring

Fish and marine mammals may be affected by the sound produced by tidal turbines (Polagye et al. 2011). However, given the disparity between the ranges at which turbine sound is likely to be received by these receptors (up to several hundred meters, Polagye et al. *in revision*) and the range of optical sensors and imaging sonars (less than 100 m), the detection of marine animal sound is an important tool for characterizing their presence and absence. Passive acoustic monitoring may be used to study fish and a broad set of marine mammals, but for this project is most relevant to studying mid-frequency cetaceans (e.g., Southern Resident killer whales) and high-frequency cetaceans (e.g., harbor porpoise) which are likely to vocalize and echolocate, respectively, within the range of passive acoustic detectors deployed on the turbines or surrounding inlet.

2.3.3 Current Velocity Monitoring

Understanding the structure of inflow currents and turbine wakes is essential to improving the understanding of structural loads on tidal turbines and inter-turbine spacing requirements. Current velocity monitoring is likely to make use of acoustic Doppler current profilers (Polagye and Thomson 2013, Richard et al. 2013) or acoustic Doppler velocimeters (Thomson et al. 2012). Depending on how these instruments are packaged, there is potential for these active acoustic instruments to interfere with the operation of high-frequency passive acoustic instruments, such as cetacean click detectors.

2.3.4 Component Packaging

Perhaps the most challenging aspect of post-installation monitoring is the high probability that access to components of the monitoring system will be required independent of the maintenance cycle for the

turbine. It is cost-prohibitive to recover the turbines to access the monitoring instrumentation and the project depth precludes the use of divers for any routine activities. Monitoring system servicing might be required to remove biofouling, upgrade components, replace malfunctioning electronics, or respond to requests for adaptive management by regulatory agencies. Given the power and data requirements for the monitoring system, a cabled connection is required. This is a challenge that multiple marine energy projects have encountered, but no commercially available solution yet exists to address it.

2.3.5 Monitoring Cost Estimation

A critical aspect of monitoring plan implementation is the cost. Monitoring plans that are scientifically sound and utilize realistic technologies, but present an uneconomic cost for project development are unlikely to advance the marine and hydrokinetic industry. This project sought to simultaneously develop monitoring plans and monitoring capabilities that could be implemented with an acceptable cost-benefit ratio. In doing so, five key principles were adopted that each monitoring plan needed to adhere to:

1. Establish why studying a particular interaction is important (i.e., establish that it is a high-priority environmental uncertainty).
2. Demonstrate that the study methodology is likely to detect environmental changes (since studies that show "no effect" for demonstration projects are unable to provide guidance on the effects of larger-scale projects).
3. Focus efforts on studies that can be published through the peer-review process since these are likely to be most readily transferable between projects and accepted by resource agencies (both domestic and internationally).
4. The cost of environmental studies should be proportional to the scale of the project and the value of the information obtained.
5. Studies should complement, not interfere with, turbine technology development.

These principles formed the basis of collaborative discussions between the project team and resource agencies that culminated in the adoption of four monitoring plans.

2.4 Team Qualifications

2.4.1 Public Utility District No. 1 of Snohomish County

Public Utility District No. 1 of Snohomish County is a leader in the development of marine and hydrokinetic energy in the United States. The District has been developing a demonstration project in Admiralty Inlet since 2006. Because this project is led by a utility, rather than a turbine technology developer, it offers an unprecedented opportunity for collection and dissemination of environmental, economic, and performance data.

2.4.2 University of Washington, Northwest National Marine Renewable Energy Center

The University of Washington leads tidal energy research within the Northwest National Marine Renewable Energy Center (a partnership with Oregon State University). NNMREC led the pre-installation environmental studies for the District's Admiralty Inlet demonstration project and has developed prioritized environmental frameworks for the environmental studies around demonstration projects (Polagye et al. 2011).

2.4.3 Sea Mammal Research Unit, LLC

Sea Mammal Research Unit, LLC led pre-installation monitoring of marine mammals and, consequently, was well positioned to develop plans for marine mammal monitoring and mitigation involving passive acoustic technologies. Sea Mammal Research Unit has also been involved in multiple marine and hydrokinetic energy demonstration projects globally. Though this, the organization has developed substantial intellectual capital around the feasibility of different marine mammal monitoring methodologies.

2.4.4 H.T. Harvey & Associates

H.T. Harvey & Associates has been involved in the development of near-turbine monitoring plans and preparation of regulatory documents for the demonstration project licensing proposal that was before the Federal Energy Regulatory Commission. The firm has also been involved in the development of several other marine and hydrokinetic energy projects and, consequently, has valuable experience in forming monitoring plan hypotheses that are scientifically grounded and meet the statutory needs of resource agencies.

2.4.5 Pacific Northwest National Laboratory

Pacific Northwest National Laboratory is a world-leader in the study of the environmental effects of marine and hydrokinetic energy and the development of risk assessment and mitigation tools. PNNL's concurrent development of a marine mammal detection system utilizing active and passive acoustics made a valuable contribution to the development of monitoring capabilities for the District's project. PNNL also played an instrumental role in the development of a risk assessment for the consequences of a collision between a Southern Resident killer whale and operating turbine (Carlson et al. 2012). This assessment was a turning point in the acceptance of the District's project by resource agencies.

3 Results and Discussion

3.1 Near-turbine Monitoring

Development of the near-turbine monitoring system proceeded through multiple phases. Prior to developing specifications for system operation, a monitoring plan was developed in consultation with a working group drawn from staff scientists and regulators at resource agencies, staff scientists from stakeholder organizations, university researchers, and the District. Once completed, this plan established the development tasks for the camera system. These tasks were centered around two questions:

1. What is the functional range (i.e., the ranges at which targets can be detected, discriminated, and classified) in northern Admiralty Inlet?
2. Can the system be expected to operate, in environments with likelihood of adverse biofouling, for periods of 3-6 months?

These questions were addressed through two types of field studies. The first question was the subject of field trials in Puget Sound in which the camera system and a frame equipped with static targets were deployed from a research vessel at two locations. The second question was the subject of a multi-month endurance test off a dock near Edmonds, Washington. The outcomes of the endurance test then motivated two primary redesigns to be incorporated into a second-generation camera system.

3.1.1 Near-turbine Monitoring and Mitigation Plan

The Near-turbine Monitoring and Mitigation Plan is the principle document describing the approach to monitoring for marine animal interactions with the turbine rotor and established several adaptive management triggers. In recognition of the high data bandwidths and potential for behavioral response by marine animals (fish, seabirds, marine mammals) to strobe illumination (which will be required at the turbine depth), monitoring will occur on a seasonal basis in the following sequence:

- Determine trends of presence/absence for fish species operating a stereo camera at low frame rate (1 s of imagery (10 frames/second) every 15 minutes).
- Evaluate the responsiveness of these species to strobe illumination, using an acoustical camera to identify when targets are in the field of view before activating the stereo camera and illumination strobes.
- Based on known presence/absence and responsiveness to strobe illumination, collect bursts of images when species are likely to be present to characterize interaction with the turbine rotor.

These studies will be conducted six times during the first year of project operations: seasonally and twice during periods of expected fish migration. After the first year, the optical and acoustical cameras are proposed to be used to study artificial reef effects. In future years, the system could also be used to study avoidance

3.1.2 System Overview

Mono- and stereo-optical imaging systems with artificial illumination have been deployed by several research groups to study the marine environment. Howland et al. (2006) developed a towed single camera system to capture high-resolution still imagery for scallop population density. Similarly, Rosenkranz et al. (2008) developed an imaging system to provide high-resolution images of benthic

habitats. Williams et al. (2010) employed stereo imaging to study rockfish abundance in untrawlable areas. These systems share a number of requirements with imaging of tidal turbines, such as operating depth and towing or current velocity, but were not developed for long term deployments or for use in areas with high levels of biological flocculent as would be the case for tidal turbine monitoring. Further, in reviewing the literature on stereographic imaging, there have been no standardized test cases for objective optimization of system performance.

Based on the requirements established by the project monitoring plan, the operational objectives for the imaging system are to classify targets (e.g., taxonomic classification to the species level, if possible) within the near-field environment (e.g., within 1-2 turbine diameters distance from the turbine and subsea base) of an operating hydrokinetic turbine, without significantly affecting animal behavior. During periods of strong currents, the relative velocity between the camera and these targets may be on the order of several m/s. Due to the difficulty and cost of maintaining the imaging system, which will require ROV operations for recovery to the surface (Joslin et al. 2013), the system will need to operate for multiple months at a time. For deployments of this duration, biofouling of the optical ports could rapidly degrade system effectiveness and will require mitigation. For the preliminary design, shore power up to 1 kW and fiber optic data connectivity with 1 Gb/s bandwidth were assumed to be available.

The imaging system developed in response to these objectives and constraints is a stereo-optical system, incorporating two machine vision optical cameras. Calibrated stereo cameras can provide information about the absolute position, size, and speed of targets. Target size is particularly relevant for classification.

The primary trade-offs in camera selection are resolution, bandwidth, and cost. High-resolution increases the potential for target classification, but at high frame rates (e.g., 10 Hz) data bandwidths can easily exceed the capacity of the communications system. To capture crisp images with relative motion on the order of 3 m/s, an exposure time between 2 and 50 µs is recommended (Gallager et al. 2005). This can be achieved by strobe illumination. Increased camera-light separation improves the effective range by reducing backscattered light from turbidity and flocculent (Jaffe 1988). However, the camera-light separation is constrained by the maximum practical package size for maintenance operations (discussed in Section 3.4).

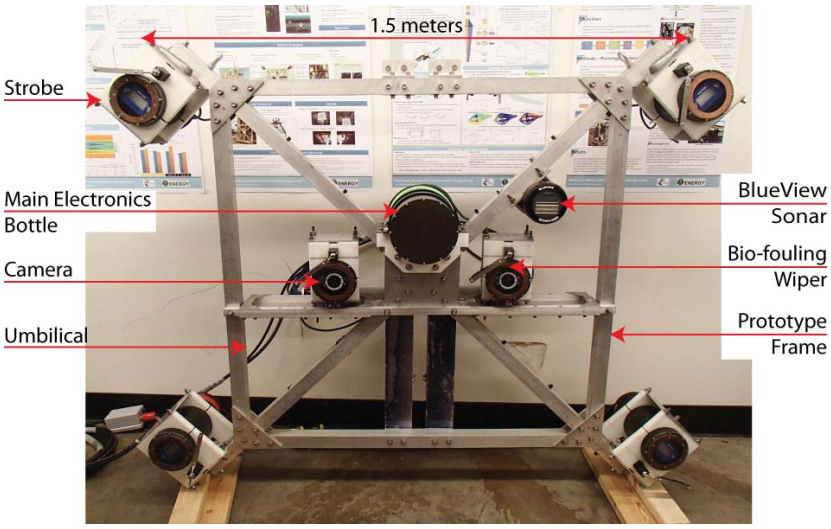

Figure 2 – Complete optical-acoustical camera system prior to salt-water endurance testing.

The principle components of the imaging system (Figure 2) were a pair of cameras (for stereo vision), four strobe illuminators for redundancy and even illumination of targets, and the power/communications architecture to integrate them and communicate with shore via the fiber optic link. In addition to the stereo-optical camera an acoustical camera was included in the package to meet the specifications established in the Near-turbine Monitoring and Mitigation Plan. The selected cameras were Allied Vision Technologies Manta G-201 B/Cs (2 Megapixel, www.alliedvisiontec.com). These were compact, industrial-grade machine vision cameras operating on Gigabit Ethernet (GigE) vision protocols. Each camera was equipped with a 5 mm focal length lens (Navitar NMV-5M23). A wider field of view could have been achieved with a shorter focal length lens, but at the cost of decreased image resolution. For strobe illumination, four Excelitas Technologies MVS-5002 units were selected on the basis of their performance in underwater camera systems with similar specifications (Howland 2006). The acoustical camera was a BlueView P900-2250 (www.blueview.com). The BlueView system was selected for three reasons:

- *Field of view*: the field of view is 45^{o} in the horizontal direction, which matches the optical camera field of view (i.e., the same target can be simultaneously imaged using optical and acoustic cameras).
- *Ease of integration*: the BlueView sonar is a self-contained unit, requiring only a connection to Ethernet communications and 12 V power. Both of these are readily supplied using the power and communications architecture developed for this project. No pressure cases, power, or communication modifications are required to accommodate the sonar.
- *Equipment Cost*: The BlueView sonar is less expensive than competitor sonars, such as the SoundMetrics DIDSON. Competing sonars offer higher resolution imaging, but this is not necessary for target detection if classification and identification are to be obtained from the optical cameras.

With the exception of the acoustical camera, the system components were not designed for underwater use and were enclosed within pressure housings. The pressure housings for the optical cameras and

strobes were anodized aluminum with acrylic optical view ports (planar)[2]. For testing, these modular components were mounted to an aluminum frame, as shown in Figure 2, which resulted in a camera-strobe separation distance of ~ 1 m. The frame allowed for the optical camera separation to be adjusted between 0.5 and 1.1 m with camera toe-in angles up to 10°.

To address biofouling concerns, a mechanical wiper (Zebra-Tech Hydro-wiper, www.zebra-tech.co.nz) was integrated into each housing and copper rings are placed around the perimeter of the optical ports. A commercially available antifouling coating that would complement the mechanical wiper could also be employed (Joslin and Polagye, *submitted*).

Off-the-shelf component specifications and costs are detailed in Table 2.

Table 2 – Component descriptions and costs for the stereo-optical camera system.

Component	Manufacturer	Description	Quantity Required	Unit Cost
Optical Cameras	Allied Vision Technologies, Manta G-201B/C	2 Megapixel, GigE Vision Camera with Sony ICX274 Sensor, 1624x1234 pixels, 4.4 μm pixel cell size, 1/1.8" sensor size, 14 fps.	2	$1600
Lenses	Navitar NMV-5M23	2/3" Megapixel format with manual focus from 0.05 m to infinity and 2.8 to 16 F-stop.	2	$500
Strobes	Excelitas Technologies MVS-5002	20 μs flash duration, 30 Hz maximum flash rate.	4	$1300
Acoustic Camera	BlueView P900-2250	Dual frequency sonar with 45° x 20° field of view, 60 m (900 kHz) and 8 m (2.25 MHz) maximum range.	1	$30,000
Mechanical Wipers	Zebra-Tech LTD	Brush style hydro fouling optical port wiper.	6	$1200

To minimize system cost and complexity, the primary communications bus operated on Ethernet protocol, with media conversion from copper to fiber to extend its range. A secondary communications bus operated on serial protocol (converted to Ethernet) and was used to monitor the health of various

[2] Early in the project, considerable thought went into the selection of optical ports for the camera and strobe pressure housings. Ultimately, a simple flat port was selected, but the logic process is instructive of the constraints on all selected components. To correct for refractive differences between air and water which reduce a lens' field of view relative to air-side operation, most underwater optical ports are domed, and act as a second lens. However, because of the biofouling mitigation measures employed, a domed port was not feasible. Specifically, a mechanical wiper was not compatible with a domed surface, meaning that the exterior of the optical port must be flat. The interior could, however, be domed (i.e., a plano-concave port). This possibility was investigated, but the benefit of a plano-concave port was determined to be marginal, particularly in comparison to the higher cost and complexity of this configuration. Consequently, a decision was made to use a simple flat port from abrasion-resistant cast acrylic (Spartech Polycast SAR).

components (current draw, temperature, and humidity) and control power distribution. The condition health monitoring system included automatic shut-off capabilities for individual pressure housings (including the main electronics housing) in the event that temperature, humidity, or current thresholds were exceeded. Low-cost media conversion limited the total bandwidth to 1 Gb/s (125 MB/s).

Power requirements for system components are described in Table 3. Custom power electronics stepped down the main supply power (375 VDC) to a 12 V component supply. These were built around Vicor (www.vicorpower.com) DC-DC converters. Medium voltage DC power supply was required to minimize resistive losses over the long cable run between the turbine and shore station. Temperature, humidity, and current monitoring in each pressure housing also utilized custom electronics.

Table 3 - Component power requirements at maximum data acquisition rates.

Component	**Mode**	**Power Requirement**
Optical cameras (2)	Acquiring at 10 fps	10 W
Strobes (4)	Strobing at 10 Hz	72 W
Mechanical wipers (6)	3 wiper motors locked (high failure rate)	18 W
Media conversion and auxiliary loads	Operating	30 W
DC Conversion Losses	80% efficiency	37 W
Total System Draw		**167 W**

System operation, monitoring, camera control, and optical image acquisition were performed with the National Instruments LabView serial communications (VISA) and image acquisition (IMAQ) modules (www.ni.com/labview). The image acquisition module was configured to allow a user to directly control a limited subset of camera settings accessible through GigE Vision protocol, such as frame rate, exposure time, digital gain, and strobe triggering. Simultaneous image acquisition from both cameras was achieved by a hardware trigger (i.e., electrical trigger connection between the master camera and slave camera) and the virtual shutter effect due to the short strobe duration (20 µs) in the absence of ambient light. Qualitative acoustical camera imagery was acquired using a proprietary software package (ProViewer, BlueView).

3.1.3 Puget Sound Field Testing

The objective of Puget Sound field testing was to establish the functional range of the camera system. Given the difficulty of accurately simulating flocculent and high relative velocities between targets and the camera in a laboratory setting, a field evaluation was undertaken with the imaging frame shown in Figure 3. The frame consisted of a mounting point for the imaging system located 4.5 m above the base of the frame. The frame had an in-air weight of approximately 1360 kg (3000 lbs). Relative water velocities of up to 2 m/s were achieved by towing the imaging frame from a high-tensile strength umbilical cable (Rochester A302351) with power conductors and optical fibers. Various targets were attached to platforms at camera-target separation distances of 1.5 m, 2.5 m, 3.5 m, and 4.5 m. These

targets included static objects, such as a single 10 cm square, standard eye charts, and line drawings of fish. The latter include large adult salmon (42 cm fork length), as well as small juvenile salmon and Pacific herring (5-11 cm fork length). Fish drawings were printed on a white or green background to provide either low or high contrast between the fish and background, respectively. As many fish expected at this site have a silver coloration, the white background provided a lower contrast around the edge of the printed image. In addition, tape streamers were attached to the frame and used to evaluate the ability of the camera system to capture rapid, complex motions without image blur. Other targets, including three-dimensional metallic objects and flash-frozen fish were considered and tested during methodology development. Preliminary testing demonstrated that these targets were more difficult to handle and did not provide more useful information than printed targets and streamers about system performance.

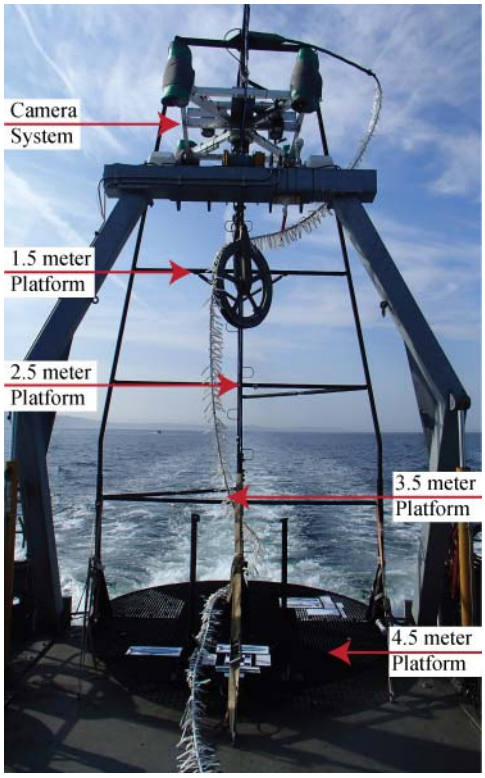

Figure 3 – Imaging frame for camera testing.

Field testing proceeded through three, sequentially more complicated and realistic, phases.

Phase 1: Frame Flight Test

In mid-October 2011, a "flight test" of the at-sea test frame was conducted. The original frame was designed to allow the camera system to positioned along the central support member at different heights to assess its capabilities to resolve imagery at different ranges in real-world conditions. To establish the feasibility of this method, the instrument frame holding all bottles (4 strobes, 2 cameras, and main electronics bottle) was positioned at the top of the test frame. All bottles were connected by cables, but no electronics (strobes, cameras) were placed in the bottles to prevent damage in the case that any bulkheads or seals were to leak during testing. The test frame was lowered to a depth of 40 m in Lake Washington and towed at speeds up to 2 m/s behind the *R/V Jack Robertson*, an Applied Physics

Laboratory research vessel. During the test, the umbilical wire angle was monitored to ensure that the load on the umbilical did not exceed the rating of the A-frame. Vibration was monitored by autonomous accelerometers mounted to the test frame. Stable “flight” and acceptable wire angles were achieved for tow velocities up to 2 m/s.

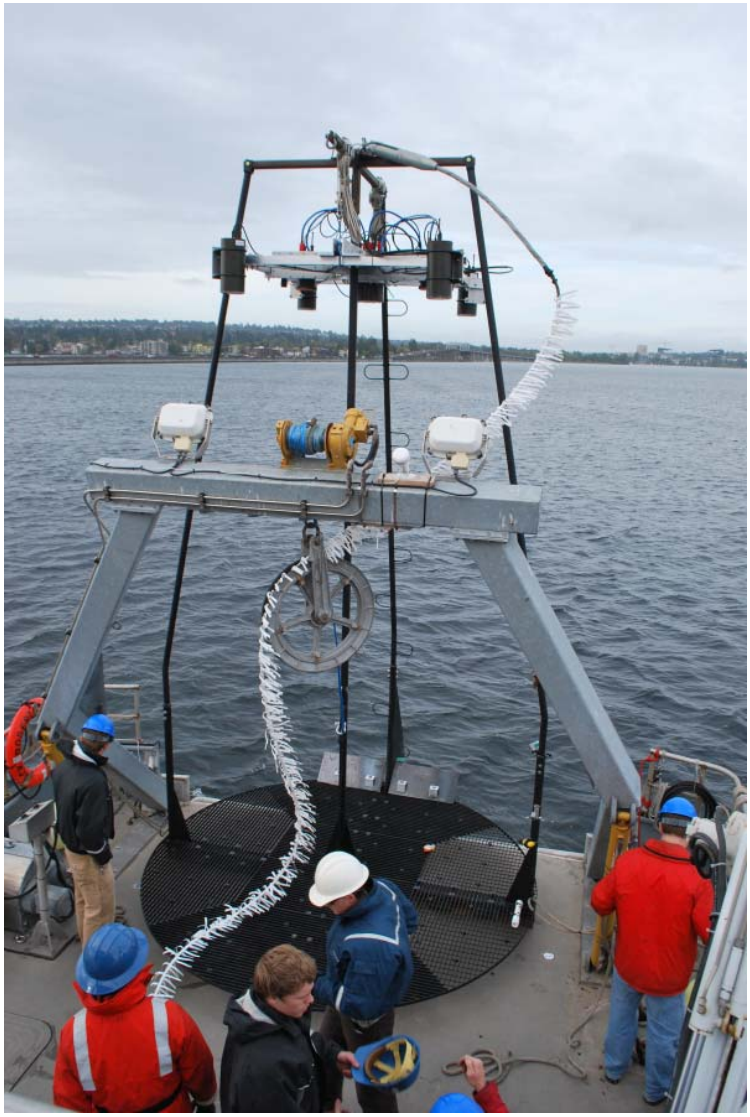

Figure 4 – Instrumentation frame mounted to at-sea test frame on Lake Washington in October 2011. White tags are an anti-strum faring on the camera umbilical (load bearing cable with power and fiber core).

Test operations revealed that it would be difficult to raise and lower the instrumentation frame holding the cameras and strobes during at-sea operations due to their significant weight and working height off the deck. Consequently, an alternative test plan was developed in which the cameras are to be positioned at the top of the test frame for all conditions and targets are to be positioned on a set of shelves at 1 m intervals down to the base of the frame (as shown in Figure 3).

Phase 2: Prototype System Test

The complete optical camera system (camera, strobes, and control system) was tested in early April 2012 in Puget Sound, just beyond the Ballard Locks. The water in this area of the Main Basin is deep and

surface conditions were calm. Metal grating platforms were welded to the test frame at distances of 1.5, 2.5, 3.5, and 4.5 m from the cameras. Full-size line drawings of individual fish of different species and size were printed out on waterproof paper and attached to a metal backing to evaluate the capabilities of the camera to detect, discriminate, and identify fish at various distances.

An image (single camera) obtained at 2 m/s tow speed is presented in Figure 5. Targets on "Platform A" (1.5 m distance) are clearly visible and species identification is possible for the larger targets, even without further image processing. Targets on "Platform B" (2.5 m distance) can be classified as fish, but species identification is more difficult. Targets are detectable on "Platform D" (4.5 m distance), but are difficult to classify or identify. However, Platform D is being shadowed by the upper platforms, which degrades the image quality. Consequently, for final field test, a decision was made to include only a single target platform for each test to minimize shadowing.

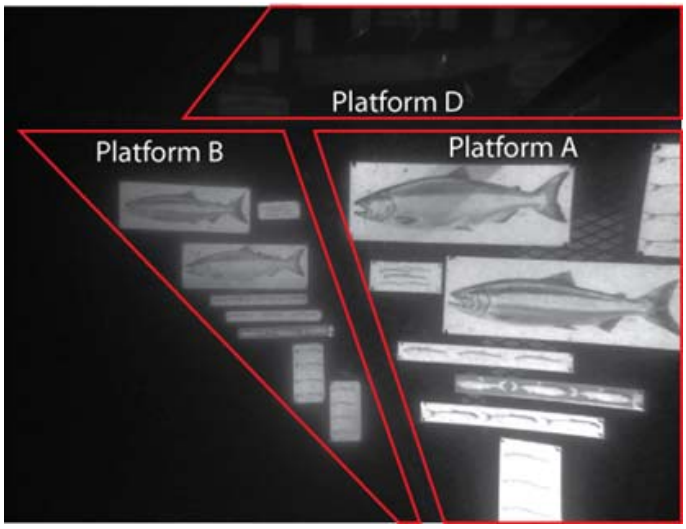

Figure 5 – Camera image (2 m/s tow speed).

Phase 3: Admiralty Inlet Field Test

Tow tests were undertaken August 13-16, 2012 in northern Admiralty Inlet, Puget Sound, Washington. All tows were conducted by the *R/V Jack Robertson*. Testing occurred during periods of falling tidal currents on greater ebb and flood to characterize performance during periods when biological flocculent would likely be suspended in the water column by intense tidal currents. There is also likely to be substantial seasonal variation in water clarity, with conditions in August likely to be on the lower end of seasonal clarity. Testing during this seasonal period was intended to demonstrate the system capabilities in a potentially "worst case" of water clarity. During each tow, static targets were positioned on the imaging frame at a camera-target separation distance of either 2.5 m, 3.5 m, or 4.5 m. Each test involved targets at a single camera-target separation distance and no tests were undertaken at separation distances ≤ 2.5 m (the April 2012 test having demonstrated that target classification was likely at a distance of 1.5 m). During each test, the imaging frame was lowered through the water column until the bottom of the frame (4.5 m distance from the cameras) was at a depth of 50 m. Images were acquired in blocks of fifty pairs at sampling rates of 5-10 frames per second under the following combinations of conditions:

- Camera-target separation: 2.5 m, 3.5 m, or 4.5 m
- Relative water velocity: near-zero (free-drift) or ~ 2 m/s (tow)
- Optical camera digital gain: 0*x*, 10*x*, or 20*x*

Each set of tests also included optical image capture with the strobes off and a camera gain of 20*x*, to confirm the expectation that observations at this depth and location required artificial illumination. Absolute measurement error was evaluated for the first thirty image pairs under each of the test

conditions using (10) to measure the length of one horizontal side of the 10 cm calibration square. This quantitative evaluation of the system performance was used to assess the variance of measurements of a target of known size conducted in each of the conditions described above. In other words, these tests represent the best case system performance in the given environmental conditions.

Table 4 details the conditions tested, in terms of the experimental variables and site conditions. Specifically, *z* is the depth of the camera frame, *H* is the total water depth, and *u* is the actual relative velocity between the imaging frame and the water. Two gain settings were not evaluated for quiescent conditions (i.e., 0 m/s nominal) with a 3.5 m camera-target separation because, even with the surface vessel drifting, the relative velocity between the test frame and currents exceeded 1 m/s. Quiescent conditions for other tests corresponded to a relative velocity of less than 0.5 m/s.

Table 4 – Camera evaluation cases from tow testing.

		Digital Gain		
Camera-Target Separation	**Nominal Relative Velocity**	*G* = 0x (no gain)	*G* = 10*x*	*G* = 20*x*
2.5 m	0 m/s	*z* = 46 m *H* = 61 m *u* = 0.2 m/s	*z* = 46 m *H* = 61 m *u* = 0.7 m/s	*z* = 46 m *H* = 60 m *u* = 0.2 m/s
	2 m/s	*z* = 30 m *H* = 70 m *u* = 1.9 m/s	*z* = 33 m *H* = 70 m *u* = 2.0 m/s	*z* = 31 m *H* = 69 m *u* = 1.8 m/s
3.5 m	0 m/s	*Not tested*	*Not tested*	*z* = 51 m *H* = 60 m *u* = 0.3 m/s
	2 m/s	*z* = 36 m *H* = 56 m *u* = 2.1 m/s	*z* = 37 m *H* = 56 m *u* = 1.7 m/s	*z* = 36 m *H* = 57 m *u* = 1.8 m/s
4.5 m	0 m/s[a]	*z* ~ 46 m *H* = 60 m *u* = 0.3 m/s	*z* ~ 46 m *H* = 60 m *u* = 0.2 m/s	*z* ~ 46 m *H* = 61 m *u* = 0.2 m/s
	2 m/s[b]	*z* ~ 30 m *H* = 66 m *u* = 2.1 m/s	*z* ~ 30 m *H* = 66 m *u* = 1.9 m/s	*z* ~ 30 m *H* = 66 m *u* = 1.9 m/s

[a] Pressure logger data unavailable. Camera depth estimated from umbilical length.

[b] Pressure logger data unavailable. Camera depth estimated from umbilical length and wire angle for other comparable platform tests and level of ambient light (zero reading on light meters).

Example images used for qualitative evaluation of the optical system are shown in Figure 6. As expected, image clarity degraded with distance (Figure 7) due to a combination of light attenuation, backscatter, and increasing pixel size. Strobe illumination was effective at freezing motion, with the streamers captured crisply in the frame (e.g., Figure 6*f*, 3.5 m, 20*x* gain). At most camera-target separations, some

degree of digital gain was required to detect the targets, though the high gain setting resulted in an over exposure of images at shorter separation distance (e.g., Figure 6*c*, 2.5 m, 20*x* gain). Flocculent was apparent in video sequences as black flecks, but the 1 m camera-strobe separation suppressed the majority of backscatter from strobe illumination. There were no distinguishing qualitative differences between images captured under tow, with a high flocculent flux through the field of view, and those captured free drifting, with a low flocculent flux.

As a point of comparison, the acoustical camera was capable of imaging the test frame and detecting streamer motion, but the two-dimensional images could, obviously, not be used to detect the static targets on the frame, as shown in Figure 8 for co-temporal video obtained by the two types of cameras.

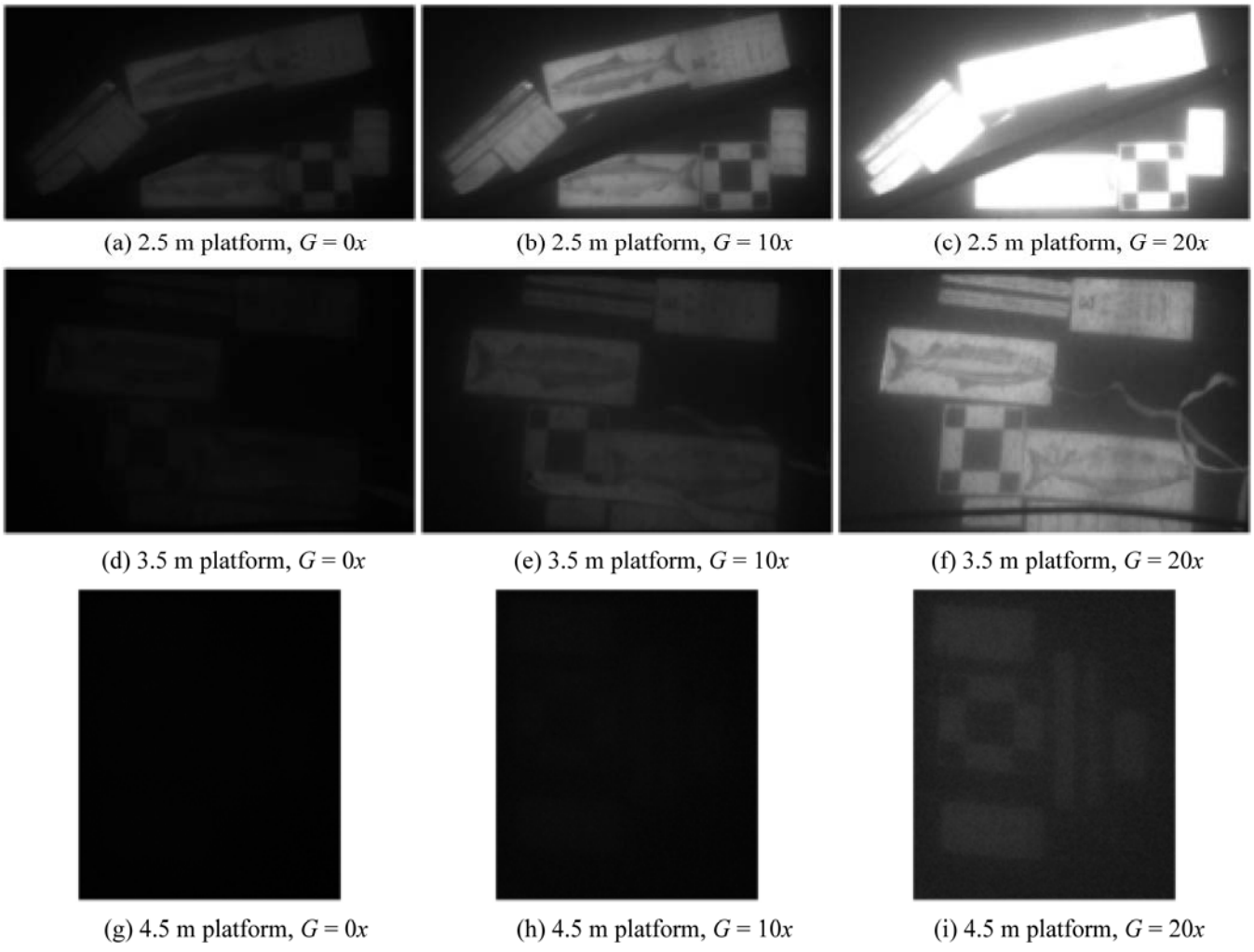

(a) 2.5 m platform, $G = 0x$ (b) 2.5 m platform, $G = 10x$ (c) 2.5 m platform, $G = 20x$

(d) 3.5 m platform, $G = 0x$ (e) 3.5 m platform, $G = 10x$ (f) 3.5 m platform, $G = 20x$

(g) 4.5 m platform, $G = 0x$ (h) 4.5 m platform, $G = 10x$ (i) 4.5 m platform, $G = 20x$

Figure 6 – Images acquired during testing under tow (*u* ~ 2 m/s) (image *h* detectable at full resolution on a large screen).

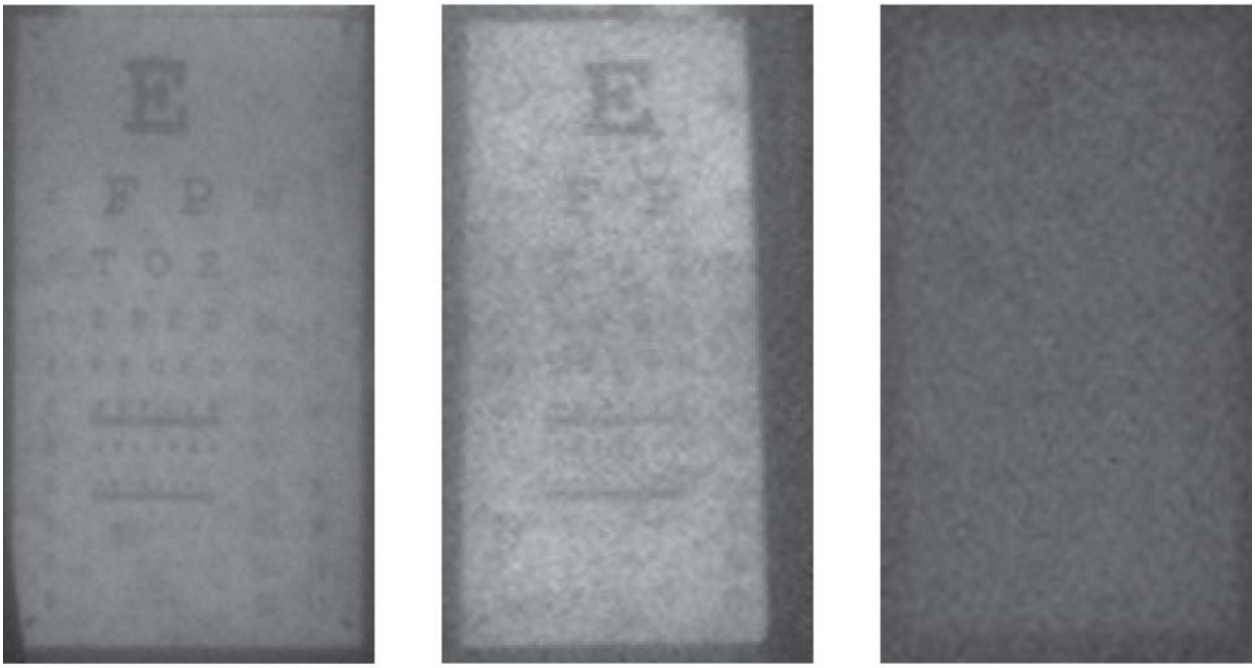

(a) 2.5 m platform, $G = 10x$ (b) 3.5 m platform, $G = 20x$ (c) 4.5 m platform, $G = 20x$

Figure 7 – Detail of eye charts (detail from same images as Figure 6).

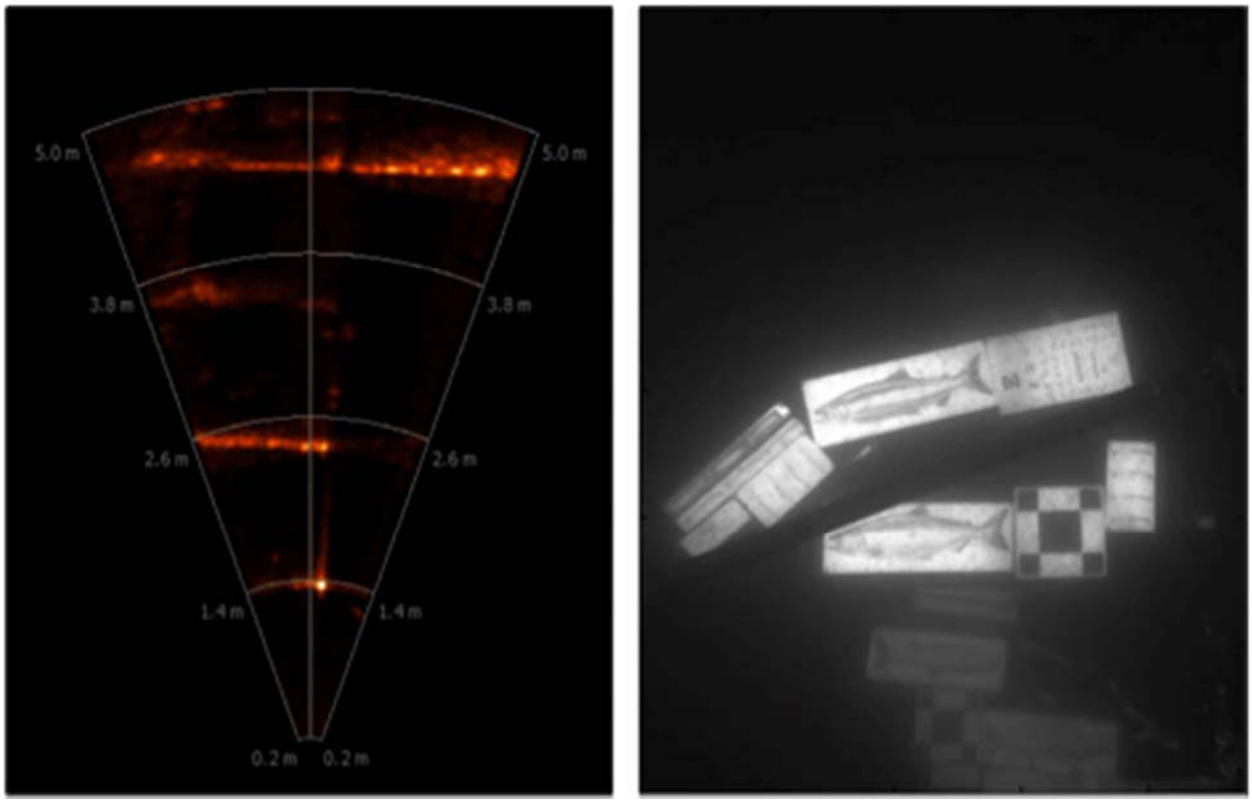

Figure 8 – Simultaneous acoustical (left) and optical (right) images. Acoustic returns at 1 m spacing correspond to the target-mounting platforms. Optical images with streamers and targets on 2.5 and 4.5 m platforms.

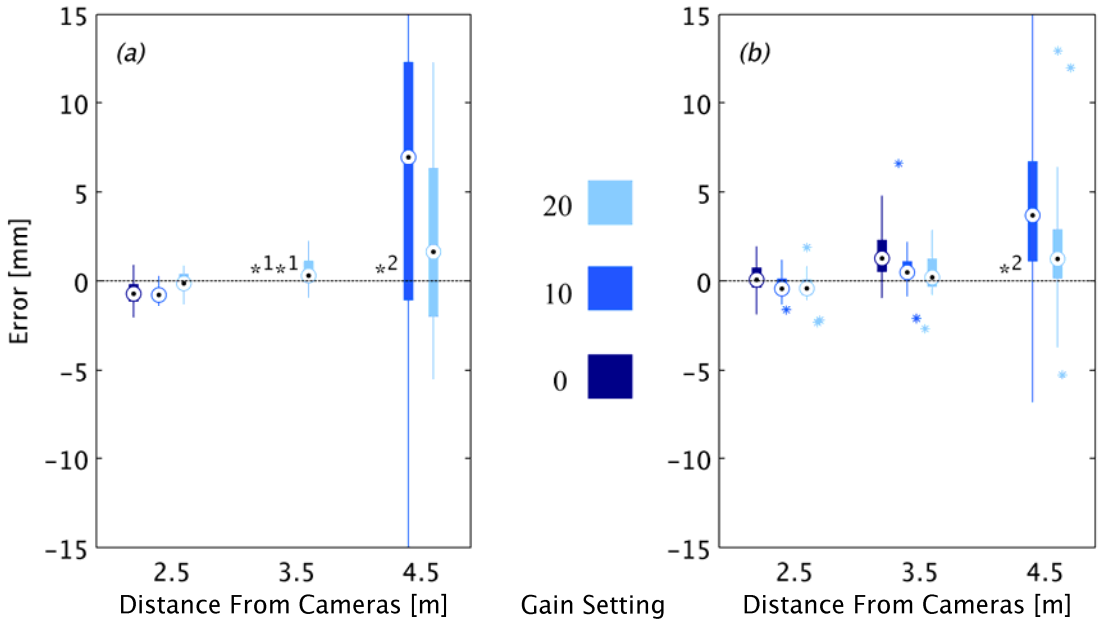

Figure 9 – Absolute measurement error for each gain setting and camera-target separation for *N* = 30 image measurements. (a) No relative water velocity. (b) Relative water velocity of ~ 2 m/s. Circles denote median values, lines denote the 25th to 75th percentile, thin bars denote the extent of measurements beyond the interquartile range, asterisks denote outliers that are beyond 1.5 times the interquartile range. 1: Case not tested. 2: Targets not visible at this gain setting.

Figure 9 shows absolute measurement errors in the length of one horizontal side of the 10 cm central calibration target square for 30 image pairs for each combination of gain setting and camera-target separation for the optical camera. At 2.5 m and 3.5 m camera-target separation there was a slight negative bias (length contraction) on the order of 2 mm and uncertainties were of similar magnitude. Bias may have been due to "trimming" of the black target area by over-exposure of the surrounding white space or errors in the estimates for camera system extrinsic parameters related to the calibration procedure. Although the individual camera pixel error was an order of magnitude smaller than the observed bias, compounding biases from both cameras and the identification of corresponding positions in the image pairs may have approached 2 mm. At a separation of 4.5 m, uncertainties were higher due to the degradation in image quality and length errors could exceed 1 cm (10% of target length). As shown in Figure 6, images at this distance had little contrast and the precision of corner detection was reduced. Difficulty associated with identifying the same target position in image pairs with low resolution and contrast contributed to greater uncertainty in the length measurement. Measurement errors under test conditions with high relative water velocity were not markedly different from the low water velocity for the 2.5 m and 3.5 m separations. Error decreased for the 4.5 m separation for the high relative water velocity case, likely due to decreased frame depth (30 m submersion due to high wire angle for fixed length umbilical) which increased ambient light levels to ~ 5 Lux. Consequently, ambient light was sufficient to illuminate the targets and provide additional contrast, which decreased the error beyond the anticipated conditions at turbine depth.

3.1.4 Camera System Optimization and Performance Quantification

In designing the optical camera configuration, there was uncertainty in the optimal separation between the cameras and the "toe-in" angle of each camera. Small camera separation with a modest toe-in angle maximizes the overlapping (and, therefore, stereographic) field of view, as shown in Figure 10. However, greater baseline separation between the cameras and a parallel configuration (no toe-in angle), improves system accuracy at greater range. This optimization trade-off requires information about the camera's functional range, which was unknown prior to field testing in August 2012.

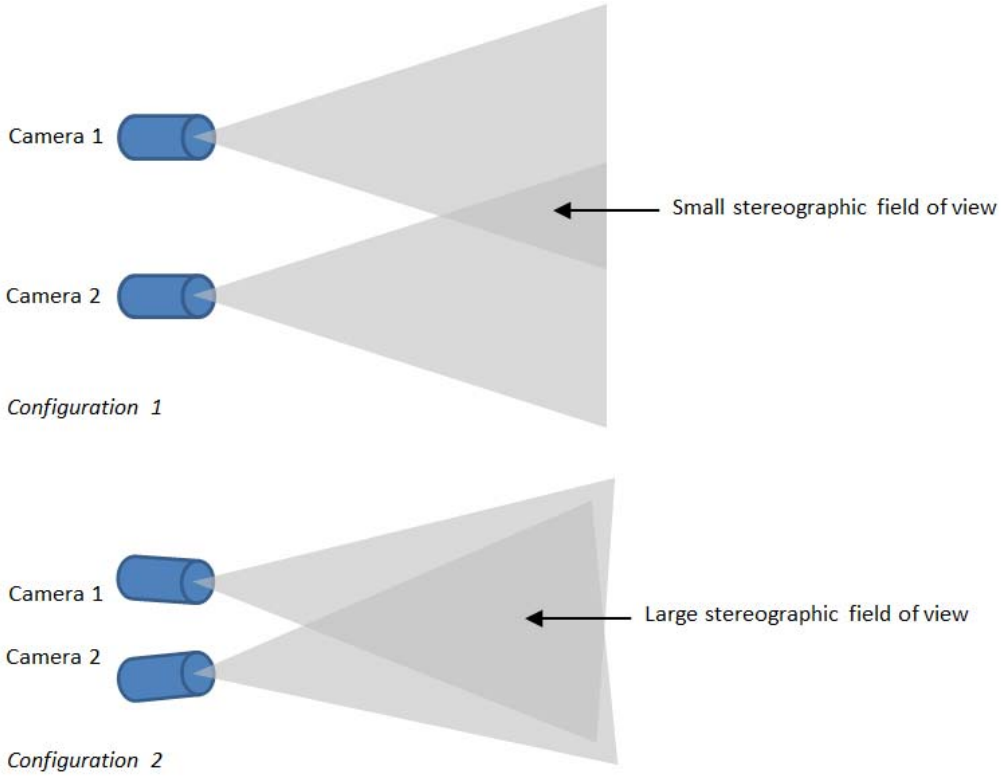

Figure 10 – Stereographic field of view optimization.

To evaluate the trade-off in accuracy versus stereographic field of view, the camera system was deployed in the test tank in the UW oceanography department, with the cameras in the minimum and maximum possible baseline separation on the imaging frame (50 cm and 100 cm, respectively). In both cases, calibrations using a standard checkerboard target were conducted and stereographic location errors (i.e., ambiguity in object location at a given distance from the camera) calculated in Matlab. For imaging distances up to 5 m (maximum functional range based on field test results), there was no statistical difference in location errors. Consequently, for deployment with the OpenHydro turbines, the optical cameras will be positioned with a baseline separation of 50 cm and a toe-in angle of 3.8^{o} (which maximizes the stereographic field of view). Camera system optimization is discussed further in Joslin et al. (*submitted*).

3.1.5 Endurance Test

Objective

The objective of the endurance test was to evaluate whether the optical-acoustical camera system intended to monitor near-field interactions with the OpenHydro turbines would be able to meet the planned 3-6 month maintenance cycle. The principle concern in meeting this cycle was biofouling of the optical ports on the camera and strobe pressure housings, which would degrade illumination and image quality. As originally scoped, the plan to test this had been to deploy a single optical camera housing (unpowered) on a Sea Spider in Admiralty Inlet. However, the availability of a dockside facility offered the opportunity to evaluate system functionality in a manner consistent with its intended operation.

Test Overview

For the endurance test, the camera system was attached to the top of the 4.5 m tall test frame and deployed in 20 m of water off a dock at the Sunset Bay Marina, north of Edmonds, WA. Static targets (test patterns, eye charts, and line drawings of fish) were attached to grating at the bottom of the frame as reference targets. The camera system was deployed on March 3, 2013 and recovered on July 2, 2013. During the test, the default configuration was for strobe illuminated imagery to be collected by a pair of cameras (one color, one black and white) for one second every fifteen minutes. This mirrors the proposed duty cycle for evaluating patterns of presence and absence of marine life around the OpenHydro turbines. Upon recovery, the system was deployed in a salt water tank at the University of Washington for a post-deployment calibration of the stereo optical cameras.

A common anecdotally reported problem with long-term optical system deployments is biofouling of the optical port, which degrades image quality. Bio-films begin to form shortly after a system is placed in the water and can degrade image quality in a matter of hours. While biofouling is most pronounced in the photic zone, experience with Sea Spider instrumentation tripods in Admiralty Inlet demonstrates that significant biofouling does still occur at greater depths, albeit with a seasonal variability.

To achieve the desired maintenance interval, the camera system incorporates mechanical wipers (Zebra-Tech, Inc.) and a copper ring around each optical port. In addition, optically transparent anti-fouling coatings have been reported to impede bio-fouling for multi-month oceanographic missions. However, the effectiveness of biofouling mitigation measures has not been quantified in the literature, meaning that limited, non-anecdotal guidance exists to design optical systems for extended deployments.

A test plan was, therefore, developed to quantify the effectiveness of different biofouling mitigation measures. One camera port was coated with ClearSignal (Severn Marine Technologies), while the other remained uncoated abrasion-resistant acrylic. Both cameras were fitted with a ring of LED lights (inside the housing) that can back-light the optical port. As the optical port fouls, more of the LED light would be reflected back to the camera lens. By capturing images at regular intervals with the strobes de-activated and LED lights activated, the degradation of image quality could be monitored and differential rates associated with the clear coat quantified. Additionally, one of the four strobe optical ports was also coated with ClearSignal. While the time-evolution of biofouling cannot be monitored for the strobe ports in the same way as the camera ports, a before-and-after comparison was possible.

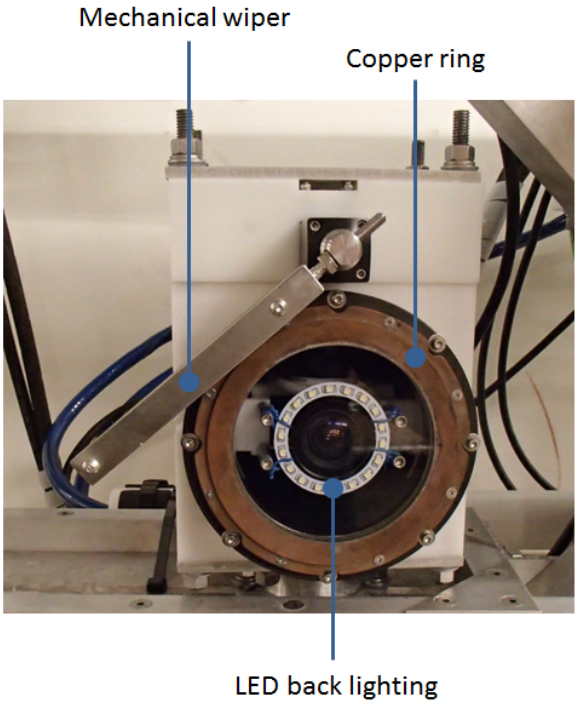

Figure 11 – Biofouling mitigation measures incorporated into optical camera system.

Results

The optical cameras (Allied Vision Manta G201) functioned well for the entire deployment, as did the strobes (Excelitas MVS 5002). The black and white camera displayed generally better contrast than the color camera and in future deployments both optical cameras would likely be black and white. No difference in the extrinsic properties of the camera pair were observed between pre-deployment calibration and post-deployment calibration.

The BlueView acoustical camera did not function well (interference patterns in acoustical imagery) and was recovered in early May during an inspection dive. The system was returned to BlueView where the technicians reported that the instrument housing had flooded, necessitating replacement of most of the electrical components. This repair was carried out under warranty by BlueView and appears to be an isolated malfunction that is unlikely to recur. This does, however, reinforce the need to be able to change out monitoring instrumentation, including off-the-shelf-instrumentation for the District's demonstration project.

The custom electronics developed for the camera system converts the supply voltage (375 V DC) to 12 V on four power busses (two rated at 120 W and two rated at 600 W). The logic board controls the power supplies and communicates with slave boards in each of the pressure housings (cameras and strobes) via an RS-232 serial communications bus. The power supplies functioned well for the entire deployment. However, the serial communications bus degraded over the course of the deployment (producing an increasing number of erroneous temperature and humidity readings from the slave boards), that made it difficult to control the optical cameras and strobes for extended periods of time after mid-May. The problem appears to be higher than expected electrical noise on the serial communications bus. While the precise root cause for the errors could not be established, it is believed that the grounding problems

discussed below also resulted in trace copper creep on the electronics bottle boards that introduced electrical noise into the serial communications bus.

There were three types of metals present in the camera system and target frame: aluminum (6061), stainless steel (316), and common steel. Superficial corrosion of the common and stainless steel was observed, similar to prior experience with Sea Spiders in Admiralty Inlet. The aluminum frame supporting the camera and strobe bottles was protected by zinc anodes and experienced moderate, but primarily superficial, corrosion, again similar to prior experience with aluminum hardware on Sea Spiders in Admiralty Inlet.

The pressure housings for the camera system (camera, strobe, and main electronics bottle) consisted of anodized aluminum bodies and end caps fastened together by stainless steel cap screws and sealed by double O-ring rubber gaskets. As shown in Figure 12, the pressure housings experienced severe corrosion, particularly at dissimilar metal interfaces between stainless fasteners and the anodized aluminum bodies. Corrosion occurred primarily on the end caps and was most severe on the strobe bottles. In one case, corrosion breached the first O-ring seal on a strobe, but the second O-ring seal kept water from intruding into the electronics compartment.

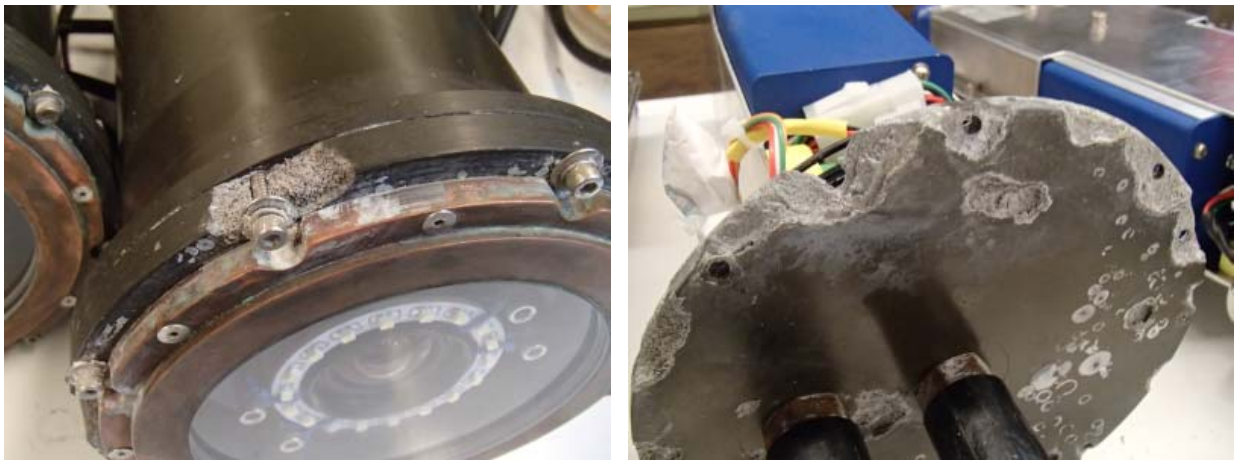

(a) Corrosion on a camera optical port end cap **(b) Corrosion on a strobe end cap**

Figure 12 – Corrosion on camera and strobe bottles

The observed bottle corrosion was exacerbated by the 0.6 V differential between the housings and seawater that occurred due to the conductive path between the housings and utility ground for the first 1.5 months of the deployment. This was corrected by breaking the utility ground connection in the shore station control box. However, the dissimilar metal corrosion between the stainless steel fasteners and aluminum body would likely have occurred to some extent even in the absence of this grounding problem. For example, on the strobe bottles, the stainless steel helicoil inserts used to jack open the end caps had, in several cases, completely “rotted out” of the aluminum end caps and were missing at system recovery.

Upon recovery, nearly every surface on the camera system and target frame had been colonized by barnacles, as shown in Figure 16. This biofouling was more severe than has been observed in Sea Spider deployments in Admiralty Inlet and, notably, the Sea Spider turned around on July 1, 2013 had only minimal barnacle growth despite being in the water for a similar period of time as the camera system.

Consequently, during the endurance test, the camera system was operating in a more extreme fouling environment than it would while monitoring the turbines. Given this, the measures taken to mitigate fouling of the optical ports (mechanical wipers, copper rings, and transparent coating) were successful. Even after four months immersion, the optical ports were in pristine condition upon recovery (Figure 16 c and d). The optical clear coat had, however, begun to delaminate. Given that the copper rings and mechanical wipers alone were sufficient to suppress biofouling, the use of an optical clear coat may not be necessary when there is sufficient power available to actuate the wipers. These results give high confidence that the system can be deployed for at least four months (and, perhaps, even as long as six months) in Admiralty Inlet without degradation of image quality. The effectiveness of the biofouling mitigation measures are discussed further in Joslin and Polagye (*submitted*).

During testing, the camera system was configured to acquire 1 s of strobe-illuminated imagery (at 10 frames per second) every 15 minutes. This long interval between short illumination periods is intended to avoid behavioral effects from the strobes (e.g., avoidance/attraction) and is proposed as the starting duty cycle for post-installation monitoring. A user interface was been developed in Matlab to facilitate image review and allow a user to enhance the image (increase brightness, saturation) to improve detectability of distant targets, note the degree to which targets can be detected, classified, or identified, and note the number and classification of targets.

Observations during the endurance test produced a number of exceptional images of fish schooling, as well as well as images of solitary invertebrates (e.g., crabs) which can remain in one place on the frame for several hours at a time. Water clarity at Sunset Bay was generally higher than during the field tests of the system in Admiralty Inlet in August, 2012 which may be either a consequence of seasonality or location. A few, representative, images from the black & white camera are shown in the figures below.

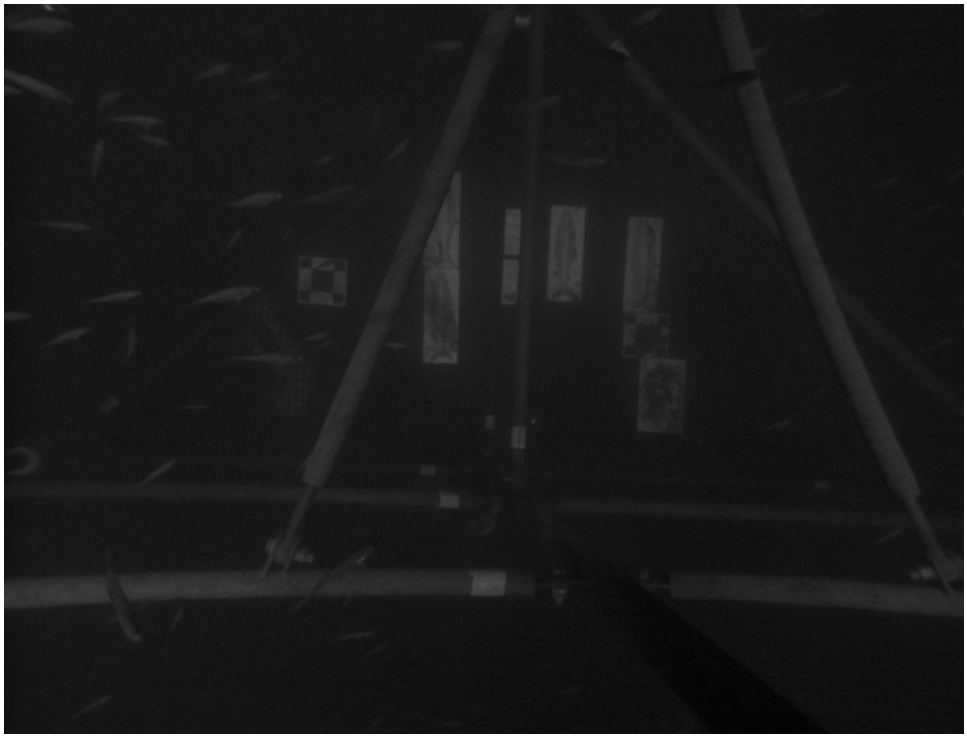

Figure 13 – Pacific herring school around camera frame (static line drawings are 4.5 m away from the camera).

Figure 14 – Crab on frame (top right) (static line drawings are 4.5 m away from the camera).

Review of daily imagery revealed expected diel trends in fish presence/absence, with large schools of targets most common at sunrise and sunset. This is not unexpected, but confirms that a staggered sampling scheme can patterns of presence/absence. This data collection scheme will be used by the District's tidal demonstration project to characterize patterns of use around the turbine and enable targeted studies of collision/strike without undue behavioral effect or extreme data volumes.

Due to the flooding of the acoustical camera housing, it was not possible to test the responsiveness of fish to artificial lighting in the same manner as is proposed for the District's demonstration project (i.e., using the acoustical camera to identify times with targets within the camera field of view, then engaging the strobes to study behavioral changes). However, sufficient ambient light penetrated to the depth of the cameras to identify fish with the cameras set to long exposure times and the strobes off. Preliminary tests of the effects of strobe lighting were conducted, noting that these effects are likely to vary with season, location, and depth. In some cases, strobe illumination caused fish to scatter in the near-field (i.e., within 1-2 m) but be unaffected in the far-field. In others, no behavioral change was observed. Frequent use of the strobe (i.e., several seconds each minute) does, however, appear to change use patterns (as observed by a departure from expected diel trends during a higher duty-cycle test). The results of this testing should not be taken to be representative of the effect that the cameras would have in Admiralty Inlet, but reinforce the need to characterize the behavioral effects of strobe illumination on marine life, prior to assessing interactions between marine life and tidal converters. The combined use of optical and acoustical imagery to investigate use/interaction does, however, continue to appear promising, given the clarity of images delivery by the camera system.

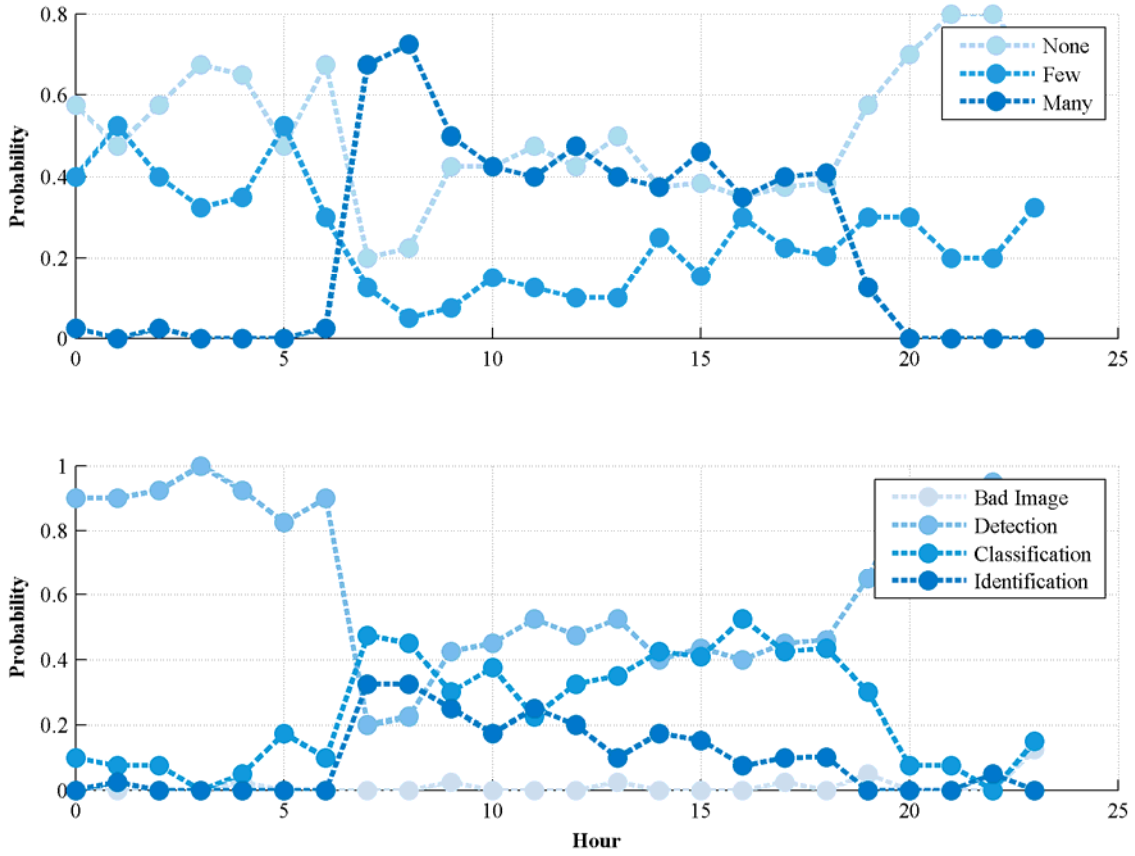

Figure 15 – Diel patterns in fish activity observed over one week of data collection. (top) Percentage of image sequences with many, few, and no targets. The morning spike in activity is apparent in the number of "many" sequences with fish around sunrise. (bottom) Percentage of image sequences allowing detection, classification, or identification. Identification is most likely during the diel migrations in the morning hours where many targets, at close proximity to the camera, are available for identification purposes.

Conclusions

The endurance test demonstrated the effectiveness of the biofouling mitigation measures for extended deployments of optical cameras in Puget Sound and indicated that the proposed duty cycle for camera system operation in the District's demonstration project would be sufficient to reveal patterns of use (thereby enabling targeted observations of collision/strike). The endurance of the biofouling mitigation measures provides confidence that the optical camera system will be able to operate with at least a 3 month maintenance cycle. This is a key, highly positive outcome of the test. The endurance test revealed two design flaws related to the serial communications bus and corrosion that were addressed prior to deployment as part of the District's demonstration project. Overall, the endurance test was well worth conducting and is recommended for further instrumentation development.

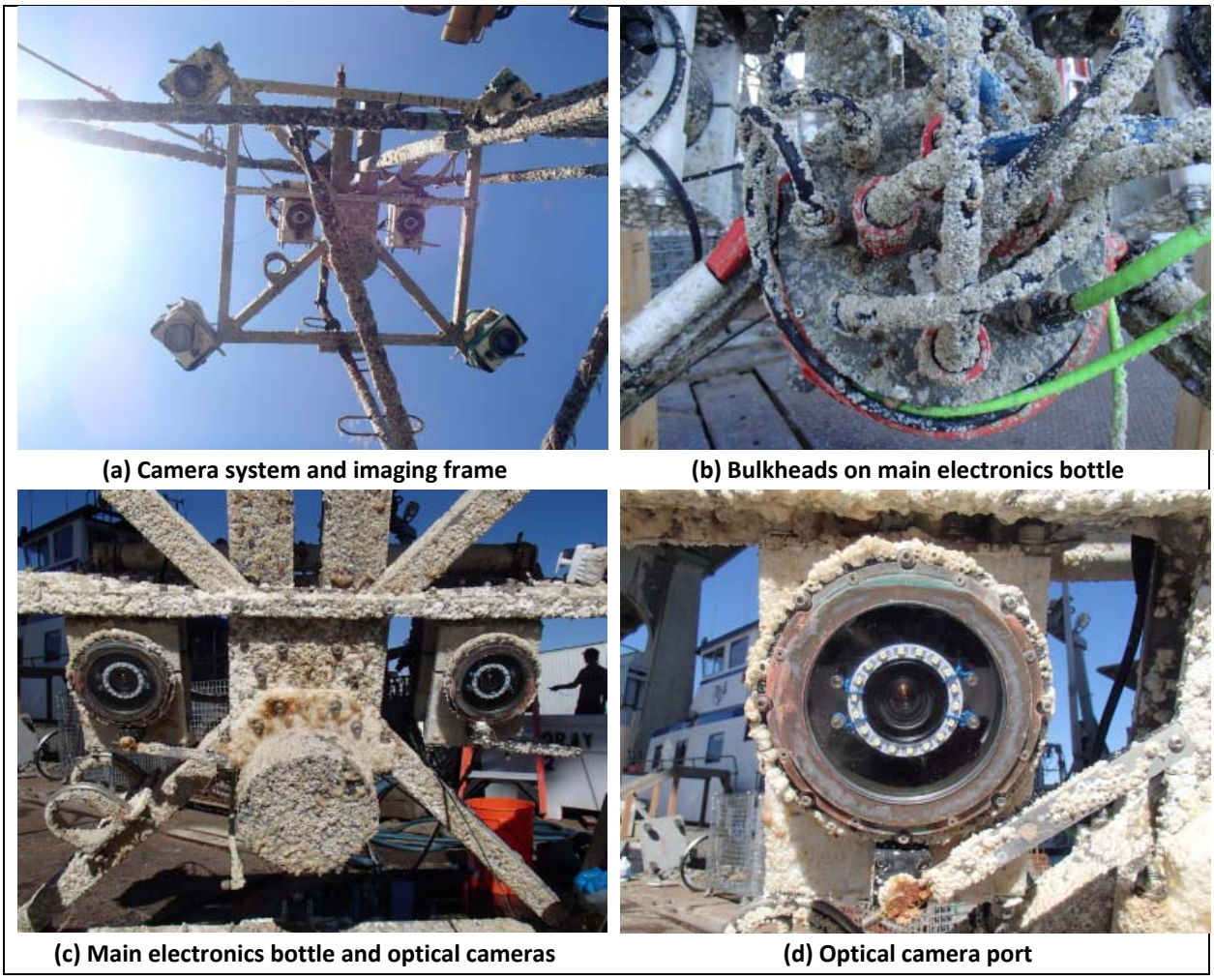

(a) Camera system and imaging frame

(b) Bulkheads on main electronics bottle

(c) Main electronics bottle and optical cameras

(d) Optical camera port

Figure 16 – Post-recovery biofouling.

3.1.6 Endurance Test Outcome: Pressure Housing Redesign

During the endurance test of the camera system, significant corrosion developed on the aluminum housings. While this was accelerated by the ground path between the bottle housing and utility ground on shore, it is likely representative of corrosion that would develop over a longer-term deployment. Corrosion occurred primarily at dissimilar metal interfaces, such as locations where stainless steel hardware was used to secure the end caps to the cylindrical bottle housings.

The electronics bottle (power supply, Ethernet distribution, etc.), camera bottles, and strobe bottles were redesigned to minimize corrosion in future, long-term deployments and reduce fabrication cost.

For the electronics bottle and strobe bottles, the following redesign measures were adopted:

- Replace customized aluminum bottle housing with standard schedule aluminum pipe (cost reduction measure).
- Replace aluminum end caps with PVC end caps (eliminate dissimilar metal contact between bronze bulkhead connectors and aluminum end caps).

- Replace end cap bolt fasteners with a filament retaining ring (eliminate dissimilar metal contact between stainless steel fasteners (bolts, washers, and helicoil inserts) and aluminum end caps and housing.
- Electrically isolate electronics from bottle wall.
- Incorporate a replaceable zinc anode into the anodized aluminum housing.

For the camera bottles, the following redesign measures were adopted:

- Replace customized aluminum bottle housing with standard schedule PVC pipe (cost reduction and corrosion elimination measures). This is possible for the camera bottles because heat transfer requirements (confirmed during testing) were lower than for the electronics bottle or the strobe bottles.
- Replace aluminum end caps with PVC end caps (eliminate dissimilar metal contact between bronze bulkhead connectors and aluminum end caps).
- Replace end cap bolt fasteners with a filament retaining ring (eliminate dissimilar metal contact between stainless steel fasteners (bolts, washers, and helicoil inserts) and aluminum end caps and housing.

These redesign measures are expected to inhibit corrosion of the anodized aluminum portions of the housing over a multi-year service life.

3.1.7 Endurance Test Outcome: Power and Communications Redesign

During the endurance test, the serial communications bus became increasingly unstable. While this may have been a symptom of the problems associated with the presence of a utility ground in contact with seawater ground, this suggested the benefit of a more reliable architecture. Two other factors also contributed to the need for a redesign. First, OpenHydro's final power supply specification was 48 V DC, rather than the 375 V DC the prototype camera system had been designed around. Second, with the decision to package all components in the Adaptable Monitoring Package (Section 3.4), it was desirable to design the system to be as compact as possible. This led to a decision to replace the multiple pressure housings (one housing for the camera system electronics, one for other oceanographic sensors, and several junction bottles) with a single bottle, power supply, and control system. Consequently, the power and communications system was redesigned to achieve these objectives, using I2C communications protocol for condition health monitoring (more robust than multi-drop RS-232) and power electronics adapted for a 48 V DC supply. The assembled second generation boards are shown in Figure 17 and will be tested over the course of the development of the Adaptable Monitoring Package (separate support). In addition, a more compact solution for media conversion (integrated media conversion with Ethernet switch, Moxa EDS-G308-2SFP) was adopted, reducing the footprint of the communications infrastructure in the electronics bottle.

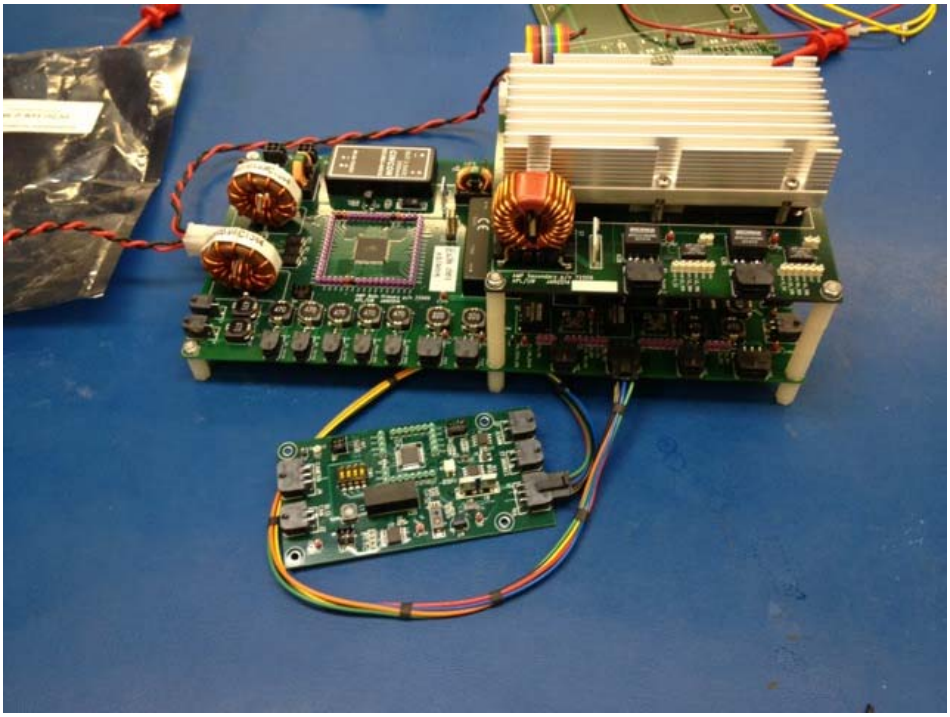

Figure 17 – Second generation electronics boards

3.2 Passive Acoustic Monitoring

Between project initiation and completion, the monitoring and mitigation plans that were anticipated to make use of passive acoustic monitoring underwent significant changes. At project initiation two plans: (1) the Marine Mammal Monitoring and Mitigation Plan and (2) Marine Mammal Operation and Protection Plan (targeted specifically at Southern Resident killer whales) had the least buy-in from all parties involved (i.e., the District, resource agencies, and stakeholders).

The Marine Mammal Operation and Protection Plan (MOPP) prescribed pre-emptive mitigation measures to protect Southern Resident killer whales. This plan would have required the turbines to shut down when Southern Residents were detected in Admiralty Inlet and remain shut down until it was confirmed that they had departed the inlet. Passive acoustic monitoring was expected to be the primary measure of detection to implement this plan. However, three problems were encountered in the plan development. First, given the masking noise associated with vessel traffic and sediment transport (e.g., movement of gravel, cobbles, and shell hash) hydrophones deployed in Admiralty Inlet would have intermittent availability to detect Southern Resident vocalizations. Second, not all Southern Resident transits were likely to involve vocalization. Active acoustic measures that could detect Southern Residents at comparable range to passive acoustics would likely harass harbor porpoises in the vicinity of the project and could not be readily adopted. Third, evolution of Open Hydro's technology improved the hydrodynamic performance of the turbine, rendering an electrical braking system impractical (engaging the electrical brake for extended periods, as originally envisioned, would no longer stop the turbine and would likely lead to catastrophic damage to the generator). These considerations led to a seemingly intractable impasse between the District and resource agencies by November 2011. Fortunately, this was resolved by analysis undertaken jointly by Pacific Northwest National Laboratory and Sandia National Laboratories (Carlson et al. 2012) that demonstrated that in the unlikely event that

a Southern Resident killer whale were to collide with an operating turbine, the forces imparted would be insufficient to cause significant biological trauma. Consequently, efforts turned away from mitigation efforts and towards approaches to monitor marine mammal activity in the vicinity of the turbines.

Collaborative discussions with the National Marine Fisheries Service led to the development of a marine mammal monitoring plan with two passive acoustic elements (1) a hydrophone array with the ability to localize marine mammal vocalizations and (2) cetacean echolocation monitoring.

3.2.1 Localizing Array

Marine mammal localization is achieved by hydrophone arrays that receive the same vocalization at slightly different times, due to the array elements being at slightly different distances relative to the source. Once these time delays are calculated for each hydrophone pair combination, a bearing to the source can be estimated based on the known hydrophone separation. In theory, three-dimensional localization can be achieved by three hydrophones. However, in practice, localization uncertainty is reduced by over-determined systems (e.g., arrays incorporating four or more hydrophones) and is preferred. Further, localization errors become large when the range to the target exceeds the separation between the hydrophone elements. For the purposes of passive acoustic localization in a tidal energy context, localization, with reasonable accuracy (i.e., no worse than 10s of meters), to a distance of several hundred meters is desirable.

Pacific Northwest National Laboratory (PNNL) had previously demonstrated the localization capability of a tetrahedral hydrophone array using playback of marine mammal vocalizations in Sequim Bay, WA. Because localization with a single array requires such a large baseline, PNNL's passive acoustic localization architecture involved two arrays of hydrophones separated by a significant distance (e.g., one array on each turbine). Each array produced an over-determined estimate for the three-dimensional bearing to the target, with the intersection of the two bearing estimates giving an estimate for the target positions (a three dimensional volume based on the intersection of the bearing estimates and their fields of uncertainty). However, the PNNL system used analog hydrophones and required a customized package to synchronize the hydrophones in the array and digitize the recorded signals for transmission to shore. An initial integration concept involved deploying this system on the subsea base of the turbines as fixed instrumentation for the duration of the demonstration project. However, given the critical nature of passive acoustic monitoring in the overall project scope, the ability to recover and service the package was desired. This precluded the use of an array with a larger instrumentation footprint.

Consequently, the localization system architecture designed in this project replaces the analog hydrophones with "smart" hydrophones (i.e., hydrophones incorporating an analog-to-digital converter on board). The cost of an individual smart hydrophones was higher than for conventional, analog hydrophones, but the overall cost was reduced and feasibility is improved in two ways. First, analog to digital signal conversion was distributed to the individual hydrophones, rather than being carried out by a central processing unit. This removed a single point of failure from the localization system architecture (i.e., if one analog to digital converter failed, the other three hydrophones in the array could continue to function and could provide a three-dimensional bearing). Second, hydrophone integration required a minimal degree of customization. Each hydrophone was tied back to a pressure housing containing only power distribution, a Gigabit Ethernet switch, and synchronization bus bar (used to align the clocks

between the four units in the array). This lended itself to a compact form factor and reduced the non-recurring engineering relative to the marinization of a four-channel analog to digital converter and synchronization system.

The Naxys Ethernet hydrophone was initially selected as the component “smart” hydrophone. However, discussions with SMRU, LLC indicated that the hydrophone was difficult to work with (e.g., IP address of the hydrophone set by firmware and not adjustable by end-users). An alternative hydrophone produced by OceanSonics was identified and demonstrated at the University of Washington by OceanSonics. The OceanSonics icListen HF architecture allows for multiple hydrophones to be synchronized to micro-second accuracy, making them suitable for localizing arrays. Four icListen HF hydrophones were received from OceanSonics in late April 2013. These were tested dockside at the Applied Physics Laboratory and in Port Townsend, near Admiralty Inlet. In both tests, the hydrophones performed well and were easily integrated with a data collection laptop. All four hydrophones were integrated with an Ethernet switch and assembled in a configuration for field tests. A preliminary design for a test frame was completed, as shown in Figure 18. The icListen HF hydrophones are the green cylinders. The aggregation bottle is the grey-walled cylinder with a blue end cap. For testing purposes, the system was designed to be suspended from a rigid overhead point in the Applied Physics Laboratory Acoustic Test Facility. In this configuration, the hydrophones formed a three-dimensional “L” with 1.5 m separation recoverable instrumentation package (Section 3.4). A review of the localization literature suggests that this arrangement could provide accurate estimates for three-dimensional bearing and would be as effective as more common tetrahedral configurations.

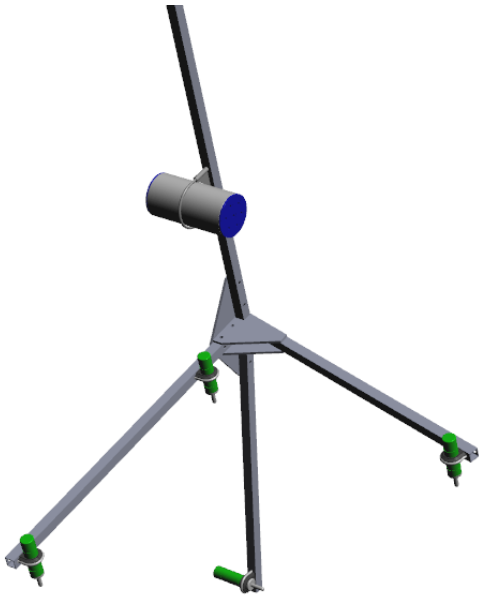

Figure 18 – Concept design for prototype testing.

3.2.2 Cetacean Echolocation Monitoring

Pre-installation studies in Admiralty Inlet used autonomous cetacean click detectors (Chelonia, Ltd. CPODs and TPODs) to monitor the presence/absence of echolocating cetaceans, such as harbor porpoises. Initially, there was interest in incorporating a cabled version of the CPOD that could enable real-time click detection. However, because marine mammal study plans for the demonstration project did not require real-time echolocation information and the cabled version of the CPOD (the "FPOD") remained in development, the autonomous instruments were determined to be sufficient and simpler to integrate with the recoverable instrumentation package. The use of CPODs would also allow direct comparison between pre- and post-installation measures of presence/absence.

When CPODs have been deployed in close proximity to active acoustic instruments on Sea Spider platforms in pre-installation studies, interference had been intermittently observed (i.e., the CPOD interpreted the active acoustic signal as cetacean clicks). This occurred only when the CPOD and active acoustic instrument were in close proximity and depended on relative orientation, as well as the configuration/frequency of active acoustic instrument[3]. The final version of the recoverable instrumentation package (Section 3.4) places the CPOD over 1 m away from any active acoustics, on the opposing end of the package's "hull" (Rush et al. 2014). This is likely to preclude the CPOD detecting signals from appropriately configured active acoustic instruments.

The use of CPODs in environmental monitoring has been complicated by instrument-to-instrument variability between individual CPODs. This was recently investigated by Dähne et al. (2013), who developed an approach for CPOD calibration in a laboratory tank. An equivalent test apparatus was developed for use during the District's demonstration project and could be used to verify CPOD performance over a multi-year period. An initial calibration of all CPODs that were likely to be used by the project was conducted and interpretation of the results is ongoing.

3.3 Current Velocity Monitoring

Monitoring current velocity is essential to interpret both the engineering performance and environmental interactions associated with a tidal energy demonstration project. Initially, acoustic Doppler current profilers were to be fixed to the turbine's subsea base in an upward looking configuration. These systems were intended to observe the vertical profile of inflow currents or the wake and would be complemented by a pair of Doppler profilers mounted to the turbine face, looking upstream and downstream. The latter, fixed instrumentation is standard equipment deployed by OpenHydro. However, similar wake/inflow information could be obtained along a horizontal profile parallel to the rotor face. The position of the recoverable instrumentation package (Section 3.4) allowed a Doppler profiler to be mounted in the desired configuration (i.e., with the ability to "look" across the wake). Incorporating the Doppler profiler into a monitoring package removed several components from

[3] For example, in one particular case, CPOD operation was degraded by a 600 kHz Nortek AWAC when the instrument sampling rate was slightly adjusted between deployments.

the subsea base (reducing cost) and allowed maintenance/upgrades to be performed on the profiler over the lifetime of the project.

The primary restriction on adding instrumentation to the recoverable package was an increase in form factor, which would both increase drag during package deployment and structural loads in operation. However, in early 2013, Nortek announced a version of its 1 MHz Aquadopp profiler (smaller sensor head than its Continental or AWAC models) that does not include a battery case. This reduced the length of the instrument by 50% and allowed it to be incorporated into the existing footprint for the recoverable package. This instrument would be suitable to studying mean wake/inflow velocity profiles and may be able to characterize turbulence (Richard et al. 2013).

3.4 Component Packaging

The development of a component packaging strategy was among the most significant outcomes from the project. It also involved the largest number of "moving parts", as it required specification of the components, which, in turn, required operational specifications from individual environmental monitoring plans.

3.4.1 Recovery Concept Development

Early on, a decision was made to pursue an integrated instrumentation package that would be positioned to one side of the turbine rotor, as shown in Figure 19. This package would be recoverable to the surface, independent of the turbine to facilitate instrumentation maintenance/reconfiguration and adaptive management requirements by resource agencies. Initial discussions centered on the size and capabilities of the recovery frame and supporting infrastructure on the subsea base. While it was considered desirable to be able to deploy instrumentation upstream and downstream of the turbine rotor, instrumentation on the side of the turbine with the apex of the subsea base would interfere with turbine recovery operations established by OpenHydro. Consequently, deploying instrumentation on both sides of the rotor would require a frame with characteristic length of 10 m to be recovered to the surface before the turbine could be recovered (or a pair of frames with a 5 m characteristic length). A frame of this size was deemed likely to drive design requirements for the subsea base and was, therefore, determined to be impractical. Subsequently, discussions converged on the concept of a compact recovery frame, as shown in Figure 19. Instrumentation would be deployed on only one side of the turbine rotor. To monitor upstream and downstream conditions on both ebb and flood, the two turbine foundations would be deployed in a mirrored configuration (i.e., one foundation will be rotated 180 degrees relative to the other), as shown in Figure 20.

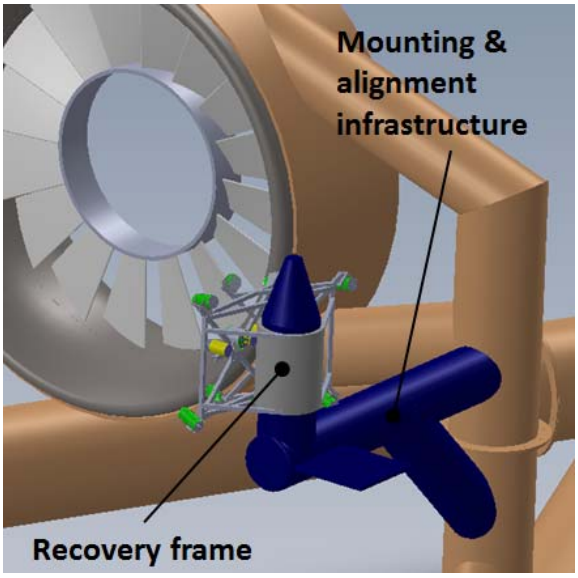

Figure 19 – Early concept for recoverable instrumentation package.

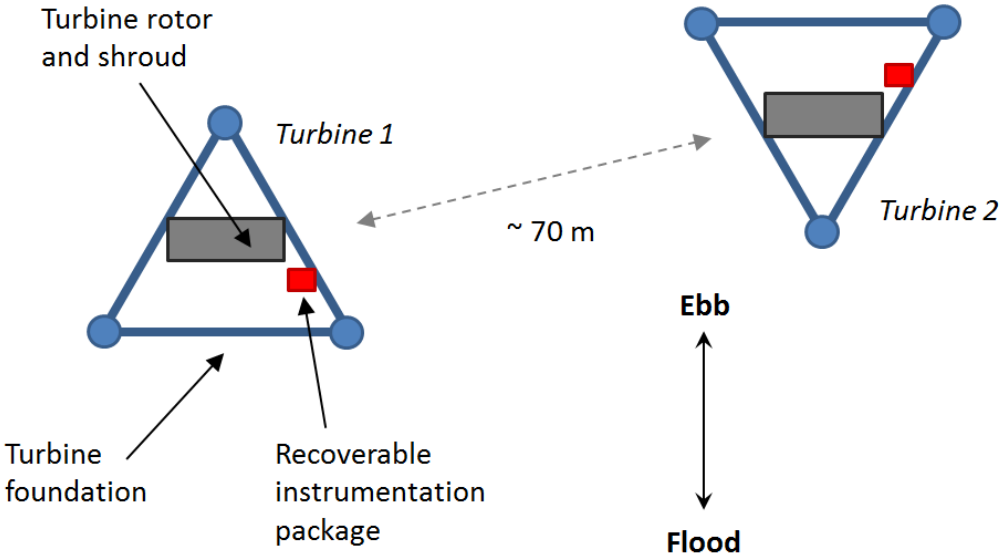

Figure 20 – Turbine and monitoring system arrangement.

In the initial concept, a cantilevered guide pin (Figure 19, blue cantilever and pin) was proposed to align the instrumentation frame (Figure 19, grey frame). The instrumentation frame would be recovered to the surface and redeployed by surface vessel, with an ROV used only to provide “eyes” and lighting for coarse-alignment of the frame from the guide pin. A wet-mate connector would be located at the base of the pin and electro-mechanical locks would engage to hold the frame in place, once mated.

While appearing attractive from the standpoint of limiting the recovery/redeployment infrastructure to a surface vessel and inspection class ROV, a concept that involved a surface vessel holding station at a tidal energy site while it lowered an instrumentation package onto a relative “bulls eyes” was ultimately deemed likely to involve a collision between theory and practice. To reduce operational risk during redeployment, several concepts were considered for a “guide line” to run from the top of the alignment

pin on the turbine frame up to the surface. If this line were to be remain under modest tension, passed through the cylindrical collar at the center of the instrumentation frame, and the turbine package were designed to be negatively buoyant, its rate of descent during deployment could be controlled by a deck winch on a surface vessel and rough alignment with "pin" on the turbine foundation might be more practical. Three options were considered for the provision of this guide line:

- *ROV assisted*: just prior to package redeployment, an ROV would bring the line down to the turbine and clip it in to the top of the alignment pin.
- *Spooling winch*: the guide line would be connected to the instrumentation frame and wound up as the package is lowered. The package would not be winching itself down, rather the package winch would be taking up slack as it was lowered from the surface.
- *Multiple release*: A configuration of releases and line canisters such that the instrumentation package pays out the guide line during recovery and the guide line is mechanically released by the re-engagement of the instrumentation package with the alignment pin during redeployment.

Of these options, the spooling winch was considered to be the least desirable as it required that the winch wind and unwind correctly during each deployment and recovery. If the winch were to bind, the instrumentation package could not be recovered or redeployed and could be "stranded" at mid-water, which would likely lead to catastrophic failure of the winch umbilical as the currents accelerated up from slack water. The multiple release option appeared feasible, but would have involved significant mechanical complexity. The ROV assist option would have involved the least mechanical complexity, but would have required a modest level of ROV intervention around the turbine to redeploy the system.

While improving the reality of effective coarse alignment, the precision of station keeping required by the surface vessel during redeployment remained problematic, as did the need for a winch with a heave compensation system to keep the package from "slamming" against the socket if the surface vessel was affected by wave action with the package close to the "docking station". Consequently, the proposed final design was for the development of a payload delivery system attached to the instrumentation frame and cabled back to the surface vessel by an umbilical. The payload delivery system would include thrusters (horizontal and vertical), cameras, and lights – essentially a purpose-built ROV. The compliant umbilical connection would decouple the instrumentation package deployment motion from the motion of a surface vessel, reducing the need for precise station keeping and heave compensation. Eliminating these requirements reduced the specialization of the surface vessel required to deploy the instrumentation package, transferring this specialization to a modular system that could be transferred between different vessels.

The payload frame would be attached to the instrumentation frame, with the combined package "flown" down to the socket on the subsea base. As with the previous iteration involving a guide line, an alignment structure (nominally, an inverted stab pin) would be used to align the instrumentation frame with the wet-mate power and data connection. The payload frame would then be decoupled from the instrumentation frame. If the payload frame was positively buoyant (several hundred pounds) and instrumentation frame was negatively buoyant (by the same amount), then the package could be

neutrally buoyant during deployment, able to engage the wet-mate connector with significant force, but not require thruster capacity beyond an inspection-class ROV for operations.

Package recovery would be by acoustic release, mirroring the approach used for the autonomous Sea Spider packages for pre-installation monitoring. While it would be possible to trigger the releases via a hard-wired connection, the use of autonomous releases meant that in the event that cabled power and communications were to be disrupted, the instrumentation package could still be recovered to the surface without need for ROV or diver intervention.

This concept formed the core of a funded proposal for the development of an Adaptable Monitoring Package (AMP) being undertaken by the Northwest National Marine Renewable Energy Center and the District (Rush et al. 2014, Joslin et al. 2014).

3.4.2 Wet Mate Connection to Shore

The leading candidate for the wet-mate connection between the recoverable package and turbine was determined to be the Teledyne ODI NRH connector. This was a hybrid, wet-mate connector that included two electrical circuits and four optical fibers. The cost was relatively high (> $100k for the connector) and the service life was on the order of 100 connect/disconnect cycles, but this would be sufficient for the lifetime of the District's demonstration project.

The export cable from each turbine included conductors to power instrumentation and fibers for control and data acquisition. These conductors and fibers would break out from the export cable in the Turbine Control Center (TCC, provisioned by OpenHydro) and connected to monitoring instrumentation via hard-wired dry mate connections.

3.4.3 Instrumentation Placement

Initially, instrumentation on the turbine was proposed to consist of recoverable instruments (such as the camera system) and fixed instruments (such as Doppler profilers) that would be connected directly to the turbine support structure and not recoverable independently from the turbine. The approach to integration would have involved several functional blocks – with each block corresponding to a pressure housing:

- *Junction bottles*: distribution of medium voltage power (400 V DC) and fiber optic communications
- *Control bottles*: transformation of medium voltage power to low voltage power (12 V DC) and conversion of fiber optic media to Gigabit Ethernet.
- *Serial bottles*: aggregation of serial communications from instruments and conversion to Gigabit Ethernet.

Monitoring instrumentation would have either connected directly to a control bottle or to a serial bottle. The approach would have mirrored that of the prototype camera system, with the control bottles patterned after the main electronics bottle.

However, as discussions with OpenHydro progressed, two obstacles to this approach became apparent. First, the power and communications infrastructure required to connect fixed instruments to the Turbine Control Center would likely have needed to be over-engineered to meet a five maintenance target. This would have substantially increase the cost of this instrumentation relative to including it in a

recoverable package. Second, instrument interface points, including mounting clamps and cable routing/securement would have required close coordination between OpenHydro and NNMREC engineers. To address these concerns, steps were taken to consolidate all instrumentation into the recoverable package without impairing the intended monitoring mission. This reduced the interface with OpenHydro to the mount point for the cantilever arm and routing for power and fiber connections from the Turbine Control Center to the wet-mate connection on the "docking station" for the recoverable package. The final adopted approach is shown in Figure 21.

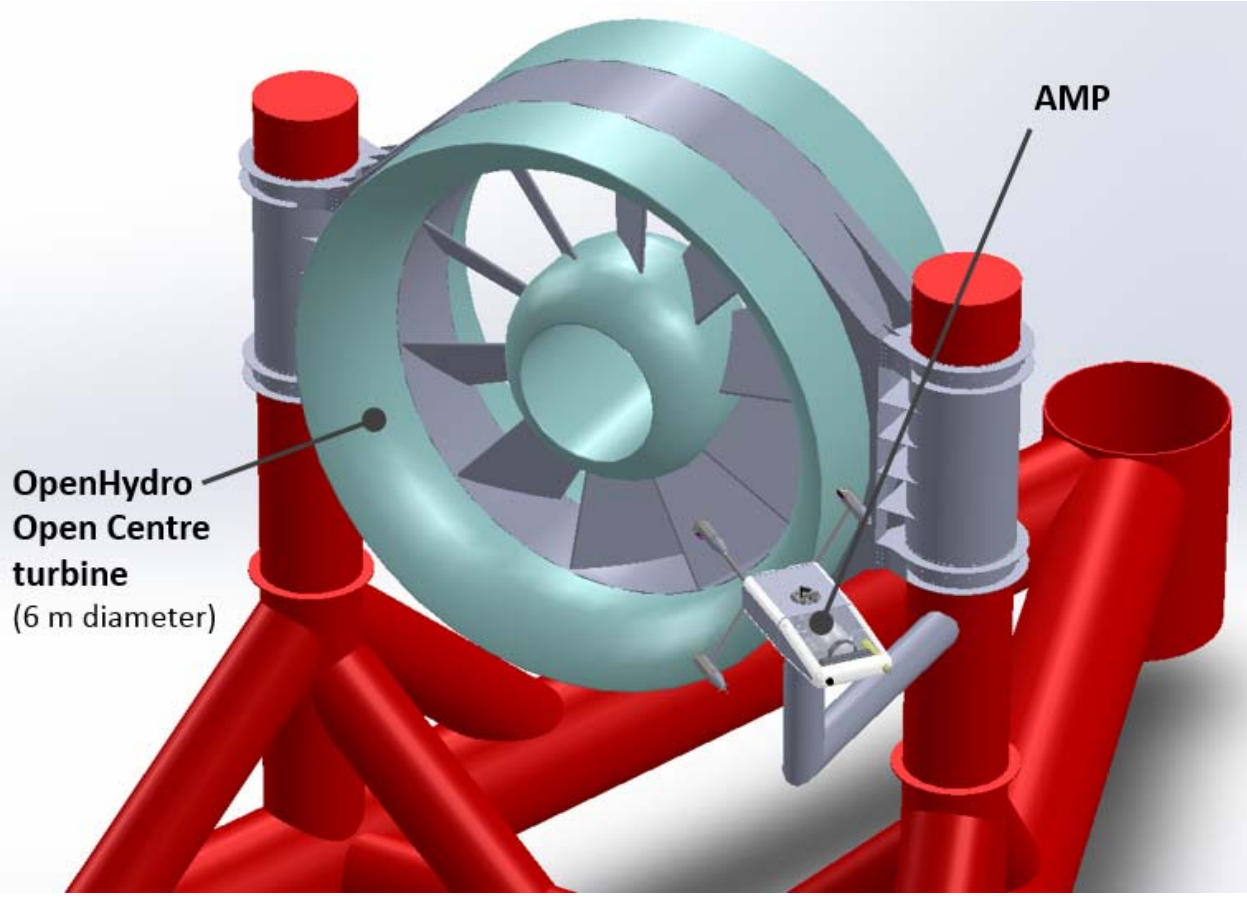

Figure 21 – Adopted approach for or recoverable instrumentation package (Adaptable Monitoring Package).

3.5 Monitoring Cost Estimation

Over the course of this project, final environmental monitoring and mitigation plans were developed, enabling an initial cost estimate to be made with respect to equipment and operations. Since this project began, most monitoring plans underwent significant revision and modification to address concerns of resource agencies and stakeholder groups, as follows:

- Near-turbine plan: Complete re-write, with modified hypotheses to determine, in sequence, (1) trends in presence/absence of marine animals (fish, marine mammals, and seabirds) in close proximity to the turbine rotor, (2) behavioral responses of these animals to artificial lighting to establish maximum operating thresholds for the camera and strobes, and (3) characterization of

direct interaction with the turbine rotor. These will be short-term studies conducted on a seasonal basis and/or at times that migratory species are expected to be present.

- Acoustic plan: Partial re-write, with modifications to plans to characterize turbine sound immediately following installation that do not rely on a turbine braking system.
- Marine mammal plan: Complete re-write, with hypothesis testing targeted at three groups of marine mammals: pinnipeds, harbor porpoise, and killer whales.
- Southern Resident Killer Whale MOPP: Eliminated following discussions with resource agencies and new risk assessment (Carlson et al. 2012).
- Benthic habitat plan: Complete re-write, with hypothesis testing emphasizing the potential for colonization of the turbine foundation by new benthic communities.
- Derelict gear plan: No changes.

These plans were adopted by the Federal Energy Regulatory Commission as a condition of the District's operating license.

Cost estimates to implement these plans are still subject to some uncertainty, given the adaptive management process and uncertainty over the length of project operations. The estimates shown in Table 5 and Table 6 assume that the project will operate for five years, with monitoring requirements changing minimally over that time. As environmental questions are addressed, these costs may change from year to year, decreasing as studies are phased out and increasing as new studies are required through adaptive management. Of these, the marine mammal and near-turbine monitoring plans are the most labor intensive and have the highest cost. Consequently, these are also the plans that would benefit most from automated post-processing or integrated instrumentation approaches that minimize the amount of information requiring manual review.

Table 5 – Equipment cost estimates for execution of monitoring plans.

Plan	Equipment Cost	Description
Benthic habitat	$0	ROV surveys only
Derelict gear	$0	ROV surveys and interventions only
Acoustic	$92,460	Drifting hydrophone packages for acoustic characterization
Marine mammal	$64,800	Shore observer instrumentation, upgrade to hydrophone at Port Townsend Marine Science Center
Near-turbine	$0	Included in Adaptable Monitoring package
Monitoring infrastructure	$991,033	Adaptable Monitoring packages for both turbines

Table 6 – Operational cost estimates for execution of monitoring plans.

Plan	Year 1	Year 2	Year 3	Year 4	Year 5
Benthic habitat	$38,625	$16,637	$17,136	$17,650	$18,179
Derelict gear	$243,750	$150,638	$155,157	$159,811	$164,606
Acoustic	$67,946	$ 59,992	$31,695	$32,810	$33,975
Marine mammal	$309,749	$50,578	$172,088	$178,844	$185,972
Near-turbine	$249,512	$241,205	$312,828	$310,765	$290,840
Instrumentation Maintenance	$285,219	$487,210	$406,520	$420,411	$434,888

4 Accomplishments

Under support from this award, substantial accomplishments were realized in all five task areas:

- Near-turbine monitoring
- Passive acoustic monitoring
- Current velocity monitoring
- Component packaging
- Monitoring cost estimation

The completion of these tasks advanced the general concepts for post-installation monitoring of the District's demonstration project to the point of realistic adoption.

4.1 Near-turbine Monitoring

The objective of this task was to develop and test an optical-acoustical camera system for near-turbine monitoring. Such a system would be necessary to evaluate interactions between marine animals and the turbine in the near-field (i.e., within 1-2 rotor diameters), which is an area of high environmental risk uncertainty (Polagye et al. 2014). Under support from this award:

- The specifications for a hybrid optical-acoustical camera system were established in consultation with a working group consisting of resource managers, scientists, and stakeholders.
- A final near-turbine monitoring plan making use of the specified system was developed in consultation with the National Oceanic and Atmospheric Administration and approved by the Federal Energy Regulatory Commission as a condition for demonstration project operation.
- A prototype system consisting of a strobe-illuminated stereo-optical camera and acoustical camera (i.e., imaging sonar) was developed and constructed.
- The prototype system was used to quantify and optimize performance through tank testing. In tank tests, the stereo-optical camera was able to determine the length of targets with errors on the order of 1% of total target length.
- The prototype system was towed through northern Admiralty Inlet at the hub height of the demonstration project turbines and found to be capable of detecting targets to a range of at least 4.5 m and classify targets at a range of approximately 3 m. This information informed the

placement of the camera system for the District's demonstration project – a key engineering constraint for the turbine supplier.

- The prototype system underwent a multi-month endurance test in a salt water environment. This test revealed a number of concerns related to the stability of the custom power and communications system, as well as the durability of the anodized aluminum pressure housings. These findings were used to redesign the pressure housings in a manner that will greatly suppress corrosion during extended deployments and to redesign the power and communications system. More importantly, the endurance test demonstrated that the biofouling mitigation measures developed for the optical ports were capable of minimizing biofouling even in environments conducive to rapid fouling.

4.2 Passive Acoustic Monitoring

The objective of this task was to specify passive acoustic systems capable of ambient noise and marine mammal monitoring, as well as detect Southern Resident killer whale vocalizations as part of a marine mammal mitigation plan. The passive acoustic system was specified, but the need to deploy the system to achieve mitigation obviated by the development of new information about the risk to marine mammals from tidal turbines. Under support from this award:

- A passive acoustic system capable of detecting and determining the bearing of marine mammal vocalizations was specified and components procured.
- Acoustic and marine mammal monitoring plans developed in consultation with the National Oceanic and Atmospheric Administration and approved by the Federal Energy Regulatory Commission as a condition for demonstration project operation.
- A calibration system for cetacean click detectors was developed to characterize the performance of these instruments over the lifetime of the demonstration project.

4.3 Current Velocity Monitoring

Under this award, an approach to current velocity monitoring was developed that eliminated the need to distribute instrumentation beyond the "footprint" of an integrated monitoring package. The potential for cross-talk between active acoustic instruments will be minimized through real-time control from the monitoring shore station.

4.4 Component Packaging

Under this award, a concept was developed for integrating all instrumentation necessary for the execution of the project monitoring plans into a single, cabled package. This packaging approach inherently minimizes the potential for cross-talk between active acoustic instruments by enabling adaptive duty cycles that are not feasible when instruments are deployed in a stand-alone manner. This concept forms the basis for the Adaptable Monitoring Package (Rush et al. 2014, Joslin et al. 2014) that is currently being developed under a separate award.

4.5 Monitoring Cost Estimation

Under this award, the costs to implement the four main monitoring plans for the District's demonstration project were evaluated. These estimates suggest that implementing the monitoring

plans would require expenditures of $1.3 M in equipment procurement and integration and $1 M/year of turbine operation.

4.6 Publications

This project has resulted in one conference proceeding, a trade journal publication, and two scientific journal publications that are under review.

- Joslin, J., B. Polagye, and S. Parker-Stetter (2012) Development of a stereo camera system for monitoring hydrokinetic turbines, *MTS/IEEE Oceans 2012*, Hampton Roads, VA, October 19-14.
- J. Joslin and B. Polagye (2013) Stereo-optical imaging for monitoring hydrokinetic turbines*, Sea Technology Magazine*, October:15-18.
- Joslin, J. S. Parker-Stetter, and B. Polagye (*revision submitted*) Development of a stereo-optical camera system for monitoring tidal turbines, *SPIE J. of Applied Remote Sensing*.
- Joslin, J. and B. Polagye (*submitted*) Field evaluation of optical port anti-fouling methods, *IEEE J. Ocean. Eng.*

5 Conclusions

This project developed several components necessary for effective environmental monitoring of early-stage marine and hydrokinetic energy demonstration projects. Monitoring of these projects is necessary to reduce environmental uncertainties that create barriers to market adoption (Polagye et al. 2011). Component technologies developed under this support included:

- A stereo-optical camera system with strobe illumination to monitor interactions between marine animals and the turbine within 1-2 turbine diameters of the rotor plane.
- An approach to localizing marine mammal vocalizations using a compact, recoverable array of "smart" hydrophones.
- Power and communications infrastructure to connect a range of instruments (e.g., camera system, imaging sonar, acoustic Doppler current profiler) to a shore station.

Significantly, this project also developed approaches in conjunction with resource agencies and the turbine supplier that would allow the instruments to be packaged in a way that meets the adaptive management needs of resource agencies without requiring that the turbine be recovered to for instrument reconfiguration.

One of the most challenging aspects of this project was interconnection between tasks. Specifically:

- Monitoring plans are required to specify the performance of instrumentation to meet specific study hypotheses, but in developing the plans, both resource agencies and the District wanted to ensure that the performance specifications were achievable.
- What is technically achievable depends on how instruments are packaged, but how they are packaged depends on the monitoring plans and practical aspects of integrating them with the turbine.

Consequently, close coordination was required between the District's team, OpenHydro, and resource agencies. This collaborative approach allowed the monitoring instrumentation and plans to evolve in parallel, breaking the "chicken and egg" problem associated with sequential development. These partnerships and the granting of a license for project operation based on the understanding developed through this process bode well for a productive tidal energy demonstration project in Admiralty Inlet.

6 Recommendations

Three general recommendations follow from the completion of this project.

First, while it may appear difficult to simultaneously develop monitoring capabilities and monitoring plans, this parallel development leads to valuable collaborations between researchers, technology developers, and resource agencies. This increases the likelihood that monitoring of demonstration projects will provide environmental information that reduces market barriers for the entire industry, rather than simply satisfying regulatory mandates for an individual project.

Second, endurance testing provides valuable insight into instrument durability, beyond that which can be obtained from bench testing or short-term field deployments. While time consuming, endurance tests can be carried out at low cost and provide valuable guidance for system refinement. Any necessary refinements can then occur ahead of critical deployments in conjunction with marine and hydrokinetic technology demonstrations when the systems must perform for extended periods of time.

Third, the conclusion of the monitoring capabilities development has resulted in a concept for combining multiple instruments into the same cable-connected, recoverable package. A logical next step would be to integrate these instruments within the package, such that one instrument can trigger the operation of another.

References

Amaral, S. et al., "Evaluation of fish injury and mortality associated with hydrokinetic turbines," Palo Alto, CA, Final Report 1024569 for EPRI (2011).

Barr, S. "Short term behavioural responses in fish species to the open –centre turbine," Open Hydro Unpublished memorandum, (2010).

Carlson, T., J. Elster, M. Jones, B. Watson, A. Copping, M. Watkins, R. Jepsen, and K. Metzinger (2012) Assessment of Strike of Adult Killer Whales by an OpenHydro Tidal Turbine Blade, Pacific Northwest National Laboratory technical report, PNNL-21177 (prepared for U.S. Department of Energy), February, 2012.

Dähne, M., VERFUß, U. K., Brandecker, A., Siebert, U., & Benke, H. (2013) Methodology and results of calibration of tonal click detectors for small odontocetes (C-PODs). *The Journal of the Acoustical Society of America*, *134*(3), 2514-2522.

Gallager, S.M., H. Singh, S. Tiwari, J. Howloand, P. Rago, and W. Overholtz (2004) High resolution underwater imaging and image processing for identifying essential fish habitat, In D.A. Somerton and C.T. Glendhill (eds.) Report of the National Marine Fisheries Service Workshop on Underwater Video Analysis, August 4-6, 2004, NOAA Technical Memorandum NMFS-F/SPO-68.

Howland, J. et al., "Development of a towed survey system for deployment by the fishing industry," *MTS/IEEE Oceans* (2006).

Jaffe, J. S., "Underwater optical imaging: the design of optimal systems," Oceanography, 40–41 (1988) [http://dx.doi.org/10.5670/oceanog.1988.09].

Joslin, J.B. et al., "Development of an adaptable monitoring package for marine renewable energy," *MTS/IEEE Oceans* (2013).

Joslin, J., B. Polagye, B. Rush, and A. Stewart (2014) Development of an Adaptable Monitoring Package for marine renewable energy projects, Part II: Hydrodynamic performance, *Proceedings of the 2nd Marine Energy Technology Symposium, Global Marine Renewable Energy Conference*, Seattle, WA, April 15-17.

Joslin, J. S. Parker-Stetter, and B. Polagye (*revision submitted*) Development of a stereo-optical camera system for monitoring tidal turbines, *SPIE J. of Applied Remote Sensing*.

Joslin, J. and B. Polagye (*submitted*), Biofouling mitigation methods for optical ports, *Submitted to IEEE J. Ocean. Eng.*

Normandeau Associates, "An estimation of survival and injury of fish passed through the hydro green energy hydrokinetic system, and a characterization of fish entrainment potential at the Mississippi Lock and Dam No. 2 hydroelectric project (FERC No. 4306)," Hastings, MN, Final Report Prepared for Hydro Green Energy, LLC (2009).

Polagye, B., M. Kawase, and P. Malte (2009) In-stream tidal energy potential of Puget Sound, Washington, *Proc. IMechE, Part A: J. Power and Energy*, 223(5).

Polagye, B., B. Van Cleve, A. Copping, and K. Kirkendall (eds.) (2011) Environmental effects of tidal energy development: Proceedings of a scientific workshop, March 22-25, 2010. *NOAA Technical Memorandum* NMFS F/SPO-116.

Polagye, B. and J. Thomson (2013) Tidal energy resource characterization: methodology and field study in Admiralty Inlet, Puget Sound, US, *Proc. Inst. MechE, Part A: J. Power and Energy*, doi: 10.1177/0957650912470081.

Polagye, B., A. Copping, R. Suryan, S. Kramer, J. Brown-Saracino, and C. Smith (2014) Instrumentation for monitoring around marine renewable energy converters: Workshop final report, PNNL-23110, Pacific Northwest National Laboratory, Seattle, Washington

Polagye, B., C. Bassett, M. Holt, J. Wood, and S. Barr (in revision) A framework for detection of tidal turbine sound: A pre-installation case study for Admiralty Inlet, Puget Sound, Washington (USA), *IEEE J. Ocean. Eng.*

Richard, J.B., J. Thomson, B. Polagye, and J. Bard (2013) Method for identification of Doppler noise levels in turbulent flow measurements dedicated to tidal energy, *International Journal of Marine Energy*, http://dx.doi.org/10.1016/j.ijome.2013.11.005

Rosenkranz, G. et al., "Development of a high-speed, megapixel benthic imaging system for coastal fisheries research in Alaska," *Fish. Res.*, **92**, 340–344 (2008)

Rush, B., J. Joslin, A. Stewart, and B. Polagye (2014) Development of an Adaptable Monitoring Package for marine renewable energy projects, Part I: Conceptual design and operation, *Proceedings of the 2nd Marine Energy Technology Symposium, Global Marine Renewable Energy Conference*, Seattle, WA, April 15-17.

Ryer, C. "Laboratory evidence for behavioral impairment of fish escaping trawls: a review," *ICES Journal of Marine Science,* **61**, 1157–1164 (2004).

Thomson, J., B. Polagye, V. Durgesh, and M. Richmond (2012) Measurements of turbulence at two tidal energy sites in Puget Sound, WA (USA), *IEEE J. Ocean. Eng.*, 37(3):363-374.

Viehman, H. and G. Zydlewski, "Fish interaction with a commercial-scale tidal energy device in a field setting," *Estuaries and Coasts*, *in revision*.

Williams, K., C. N. Rooper, and R. Towler, "Use of stereo camera systems for assessment of rockfish abundance in untrawlable areas and for recording pollock behavior during midwater trawls," *Fishery Bulletin*, **108**, 352–362 (2010).

Appendices

Biofouling Mitigation Methods for Optical Ports

James Joslin and Brian Polagye

Abstract

Biofouling mitigation measures for optical ports can extend the duration of oceanographic deployments, but there have been few quantitative studies of field performance. Results are presented from a four-month field test of a stereo-optical camera system intended for long term environmental monitoring of tidal turbines. A combination of passive (copper rings and ClearSignal antifouling coating) and active (mechanical wipers) biofouling mitigation measures are implemented on the optical ports of the two cameras and four strobe illuminators. Biofouling on the optical ports is monitored qualitatively by periodic diver inspections and quantitatively by metrics describing the quality of the images captured by cameras with different anti-fouling treatments. During deployment, barnacles colonized almost every surface of the camera system, excepting the optical ports with fouling mitigation measures. The effectiveness of the biofouling mitigation measures suggests that three to six month deployment durations are possible, even during conditions that would otherwise lead to severe fouling and occlusion of optical ports.

Index Terms

Biofouling, optical sensors, oceanic techniques, environmental and remote monitoring, field testing.

I. Introduction

Biofouling is often a limiting factor for long-term deployments of oceanographic optical instrumentation. While this study focuses on the fouling of camera optical ports, the methods and

Funding for this project is provided by the US Department of Energy and Public Utility District No. 1 of Snohomish County.

J. B. Joslin and B. Polagye are with the Northwest National Marine Renewable Energy Center, Department of Mechanical Engineering, University of Washington, Seattle, WA, 98195 USA (e-mail: jbjoslin@uw.edu and bpolagye@uw.edu).

outcomes are relevant to other instruments that rely on light transmission, such as absorption-attenuation meters (ac meters), photosynthetically active radiation (PAR) sensors, or fluorometers [1]. As biological growth colonizes a cameras optical port, image quality degrades and the monitoring mission may be compromised. With the proliferation of cabled ocean observatories [2]–[4], long-term deployments of optical instrumentation are becoming more common and biofouling mitigation methods are receiving more attention. Research in this field is generally focused on improving understanding of fundamental biofouling mechanisms (such as adhesion and growth) [5], [6] or development of biofouling mitigation measures. For example, Manov et al. [1] discusses the use of copper to prolong deployments of open, enclosed or semi-enclosed, and shuttered optical instrumentation and Debiemme-Chouvy et al. [7] describe applications of electrochemisty to produce a biocide on the optical port surface. Whelan and Regan [8] and Delauney et al. [9] provide reviews of existing biofouling mitigation techniques and their implementation on different sensors.

Marine renewable energy, including wave, tidal and ocean current, and off-shore wind energy, is a growing sector of the electricity generation industry that requires robust approaches to biofouling. Energy converters and their support structure are deployed in the marine environment for multi-year periods and cannot expect to receive significant maintenance if their cost of energy is to be competitive with conventional forms of electricity generation. While biofouling is possible on any of the converter surface, general-purpose biofouling mitigation methods may be different from the approach taken for more sensitive components, such as sensor transducers. Optical camera observations have been proposed to inform a number of critical environmental questions [10] and the shore cables for the energy converters provide sufficient power and data bandwidth to support high-resolution optical measurements over extended periods. This paper discusses the implementation of biofouling mitigation measures on the optical ports of a camera system developed for long term monitoring of marine energy converters [11]. This system will be recovered periodically for maintenance [12] and it is expected that optical port fouling will be the limiting factor for the length of maintenance intervals. Methods to quantitatively evaluate the effectiveness of these biofouling mitigation measures are developed and applied to a multi-month endurance test of the camera system.

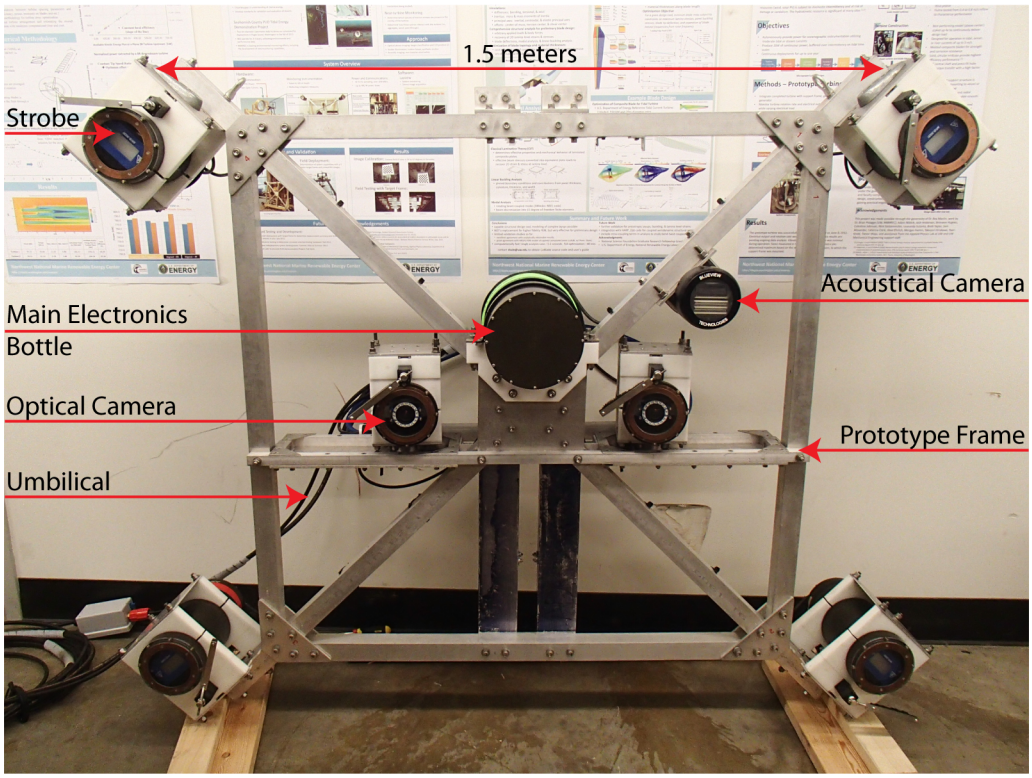

Fig. 1: Prototype imaging system showing principal components and scale.

II. Methodology

A. *Field Deployment Configuration*

Fig. 1 illustrates the hybrid stereo-optical and acoustical camera system developed for monitoring marine renewable energy converters [11]. The integrated system combines two Allied Vision Technologies Manta G-201 machine vision optical cameras, 4 Excelitas Technologies MVS-5000 strobes, a BlueView P-900/2250 acoustical camera and the supporting power and communications infrastructure to cable the system to a shore station. The system is controlled in real time by a computer on shore that can adjust camera settings (e.g. frame rate, exposure time, digital gain, and strobe triggering) and archive acquired stereo imagery. The optical cameras and strobes were marinized by enclosing them in aluminum pressure housings with planar acrylic optical ports.

A multi-month field trial was conducted during early 2013 to evaluate overall system endurance (hardware performance, software stability, corrosion, and biofouling). After an initial calibration

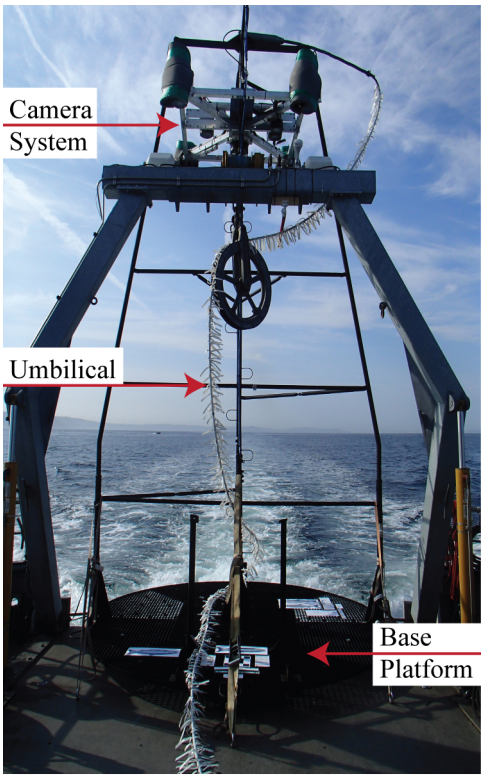

Fig. 2: Five meter tall field test frame on the deck of the deployment vessel RV Jack Robertson.

in a tank, the system was deployed from 24 January to 8 February in freshwater off of a dock on Lake Union, WA. Subsequently, the system was deployed in a saltwater environment from 3 March to 2 July off Edmonds, WA.

For the salt-water endurance trial, the camera system was mounted to the test frame shown in Fig. 2. The Applied Physics Laboratory vessel R/V Jack Robertson lowered the test frame to the seabed in approximately 20 meters of water at a point 100 meters from shore. Mounted to this frame, the camera system was suspended 5 meters above the seabed in a downward looking orientation. The power and fiber umbilical was terminated on shore and connected to a data logging computer. Divers from the Applied Physics Laboratory at the University of Washington visually inspected the system for biofouling and corrosion on 3 March, 11 April, 3 May, and 26 June.

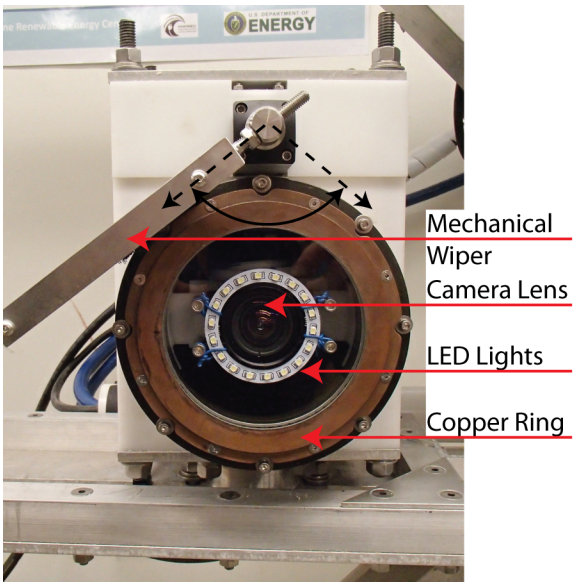

Fig. 3: Biofouling mitigation measures on the optical camera port (pre-endurance test).

B. Biofouling Mitigation Measures

A combination of active and passive biofouling mitigation measures was implemented on the optical ports of the two camera and four strobe housings. As shown in Fig. 3, each four-inch optical port had a ring of copper around its perimeter, which was intended to suppress biofouling at the edge of the optical port. Each housing was also equipped with a mechanical brush wiper manufactured by Zebra-Tech Ltd (http://www.zebra-tech.co.nz/Hydro-Wiper). In addition, one of each of the camera and strobe ports was coated with the ClearSignal fouling release coating produced by Severn Marine Technologies (http://www.severnmarinetech.com/).

The wiper, when triggered by the control computer in the shore station, swept a 90° arc across the copper ring and optical port before reversing direction and returning to its home position. This action was thought to potentially complement the copper ring by transferring trace amounts of copper across the optical port over the course of many wipe cycles. Throughout the endurance test, the wipers actuated once per hour during normal system operation. Electrical interference in the serial communications bus between the shore computer and camera system required the system to be shut down on six occasions, during which the wipers were not actuated. For the final month of the deployment, the system did not run continuously because of continued degradation of the communication bus. To continue collecting biofouling data during this period, the cameras

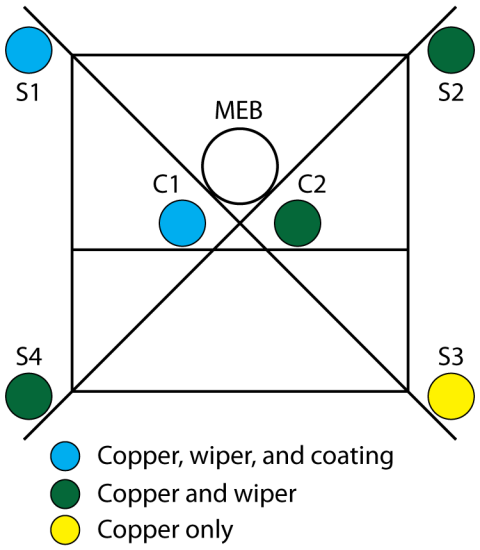

Fig. 4: Arrangement of anti-fouling measures on camera system optical ports (*S* denotes strobe, *C* denotes camera, and *MEB* denotes the main electronics bottle).

were brought on-line manually at night to capture images. Thus the mechanical wipers on the cameras were only active once per day and the wipers on the strobes were not active. During this same period, the mechanical wiper on Camera 2 malfunctioned and would periodically stop in front of the optical port after a wipe cycle, thereby blocking part of the image. This malfunction resulted from the gradual increase in friction between the wiper and the optical port and may be avoided by decreasing the interference between these two parts during installation.

Fig. 4 illustrates the arrangement of the biofouling mitigation measures on the six optical ports in the system. Strobe 3 was intended to serve as a control with minimal anti-fouling protection by disabling the wiper. However, an interruption to the bottle's power supply would cause the wiper to automatically actuate and since the system was power cycled on six occasions, the results for this optical port cannot be considered a true control. For the last month of the deployment, the mechanical wiper did not actuate on any strobe port.

C. Qualitative and Quantitative Evaluation of Biofouling Mitigation Measures

Performance of biofouling mitigation measures were monitored qualitatively during the endurance trial by diver inspections and quantitatively through the images captured by the cameras.

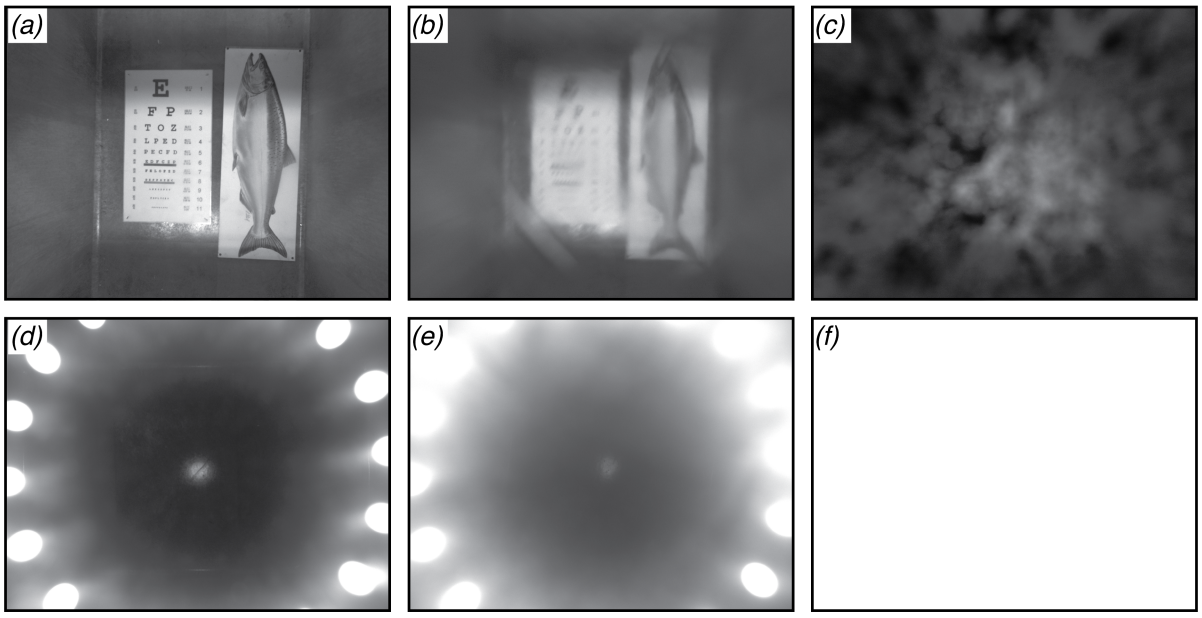

Fig. 5: Demonstration images for biofouling metric calculations with LED backlighting. *(a)* – *(c)* show representative image quality for a clear optical port with the LEDs inactive *(a)*, a partially obscured ($F = 0.37$) optical port *(b)*, and fully obscured ($F = 1.0$) optical port *(c)*. *(d)* – *(f)* show the corresponding image brightness with the LEDs active.

A final qualitative assessment of the biofouling on the system and all of the optical ports was conducted post-recovery on 2 July.

The optical cameras collected sequences of 10 images at 10 frames per second once every 15 minutes to monitor interactions between marine life and the frame (such as fish, crabs, and starfish) and provide some indication of test platform integrity between inspection dives. To monitor the biofouling levels on the camera optical ports, a ring of LED lights was installed within the camera housing, at the perimeter of the camera lens. On an hourly basis, sequences of 10 images were captured with these LEDs illuminated to backlight any growth on the optical ports. Biofouling that obscured the camera image by blocking the passage of light through the optical port would be illuminated by these LEDs and increase the image brightness relative to the initial condition. Similarly, images were captured spanning each wipe cycle to compare biofouling before and after individual wipes.

The brightness, B, of an image, i, collected with the LED illumination activated was calcu-

lated by summing the pixel grayscale values, *p(x,y)* as shown in Equation 1. For this camera configuration, the image resolution was n = 1624 and m = 1234 with a pixel grayscale range of 0 to 255.

$$B(i) = \sum_{x=1}^{n} \sum_{y=1}^{m} p(x, y) \tag{1}$$

A biofouling metric, *F(i)*, was calculated for each image as in Equation 2 by subtracting a baseline value, B_0, for each camera corresponding to the first night of the deployment and normalizing over the maximum possible image brightness, $B_{max} = 255n * m$. This biofouling metric ranged from the condition of the baseline images (*F = 0*) to a completely white image consistent with a fully obscured optical port (*F = 1*).

$$F(i) = \frac{B(i) - B_0}{B_{max} - B_0} \tag{2}$$

Fig. 5 demonstrates the effectiveness of this method for quantifying fouling on a cameras optical port by showing the image quality along with the biofouling for a clear (*F = 0*), blurry (*F = 0.37*), and fully obscured (*F = 1.0*) optical port. The artificial fouling in these images was simulated in the lab using a light coating of silicone grease as adhesive and fine sand to obscure the image.

The hourly biofouling images were collected in three sets of 10 images with camera exposure times of either 10 ms, 25 ms, or 50 ms. This range of exposure times was used to evaluate the method's sensitivity to camera configuration. For all three exposures, images were acquired at a rate of 1 frame per second, no digital gain was used, and the strobes were not triggered. By averaging the sets of 10 images collected each hour, the variations in backscattered light caused by moving flocculent in the water was reduced. Due to ambient lighting during the day, only images collected during night time hours were used to calculate a daily mean biofouling metric for each camera configuration. The images used to calculate the mean values were manually reviewed to ensure that camera settings and LED illumination corresponded to the expected configuration.

Fig. 6: Camera 1 images of biofouling on the field testing frame from *(a)* 19 March, *(b)* 15 May, and *(c)* 2 July prior to recovery.

III. Results

A. Field Deployment

Diving inspections confirmed increasing biofouling on the test frame throughout the deployment, as visible in the camera images, and divers generally noted that the optical ports appeared to remain clear. Fig. 6 shows the increasing level of biofouling on the test frame from camera images acquired over the course of the deployment.

B. Biofouling Mitigation Measures

Fig. 7 shows the calculated daily mean biofouling metric for each camera from the images collected with 50 ms exposure times throughout the endurance trial. The same trend was followed by the images acquired with the other two exposure settings, suggesting an insensitivity to exposure time. Highlighted periods represent interruptions in system operation due to software errors, electrical interference with serial communications, and wiper malfunctions. Images captured before and after individual wipe cycles had no quantitative difference in biofouling metric values.

The biofouling metric values shown in Fig. 7 are consistently below 0.04, indicating that both camera optical ports remained relatively clear throughout the deployment, which was confirmed upon recovery. Variation in the camera metrics is primarily attributed to changes in the water quality during the deployment because flocculent in the water close to the optical ports is illuminated and increases the value of F, without actually fouling the port. However, with the

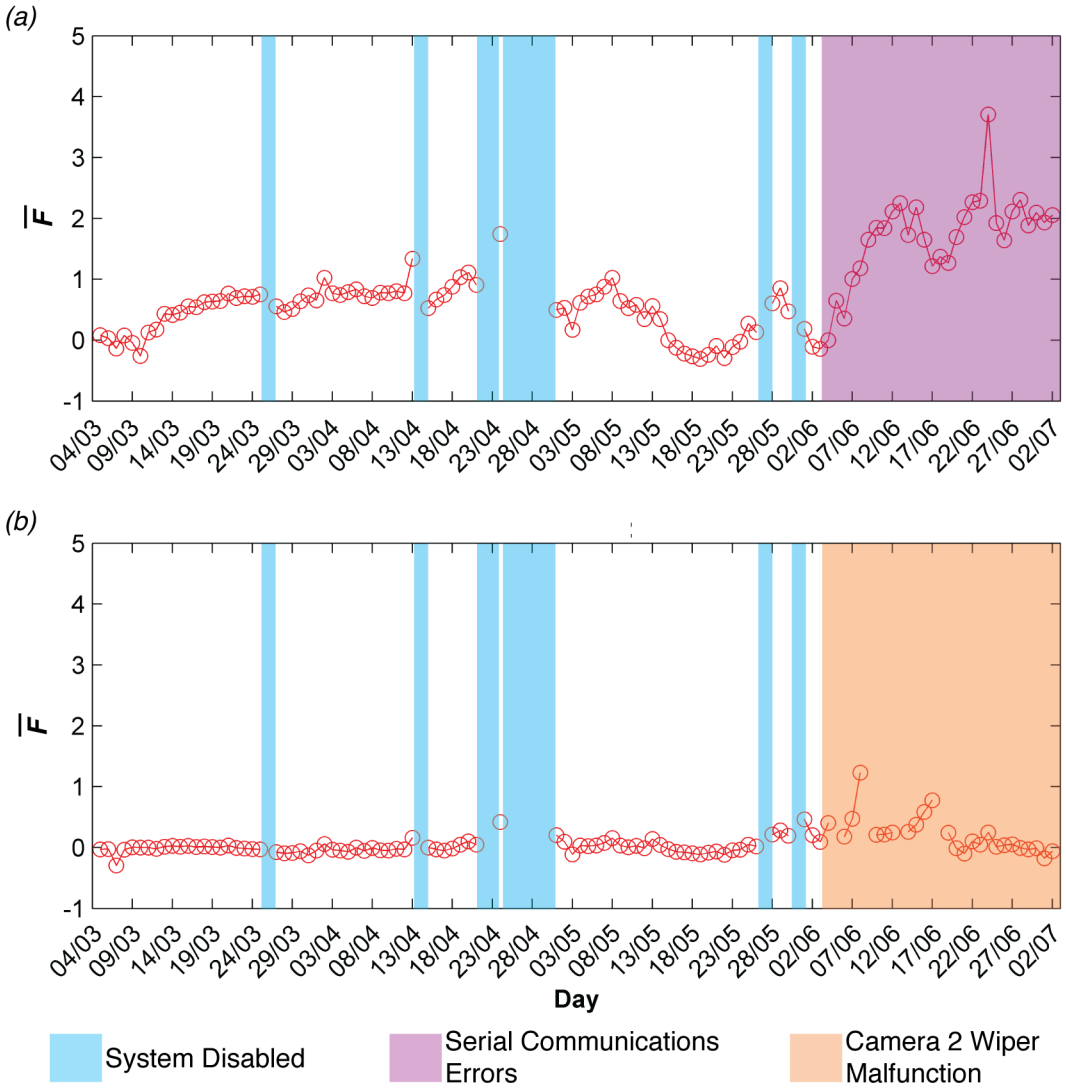

Fig. 7: Averaged nightly biofouling metric value on *(a)* Camera 1 and *(b)* Camera 2 optical ports throughout endurance test.

wipers activated only once per day at the end of the deployment, an increase is observed for Camera 1. Camera 1 images are consistently brighter than those from Camera 2 and have a larger range of variation, as a consequence of the ClearSignal coating on the Camera 1 optical port. While the image quality was not affected by the coating, the LED reflection was greater for the coated optical port.

Post-recovery inspection of the system revealed a high level of macro-fouling covering every

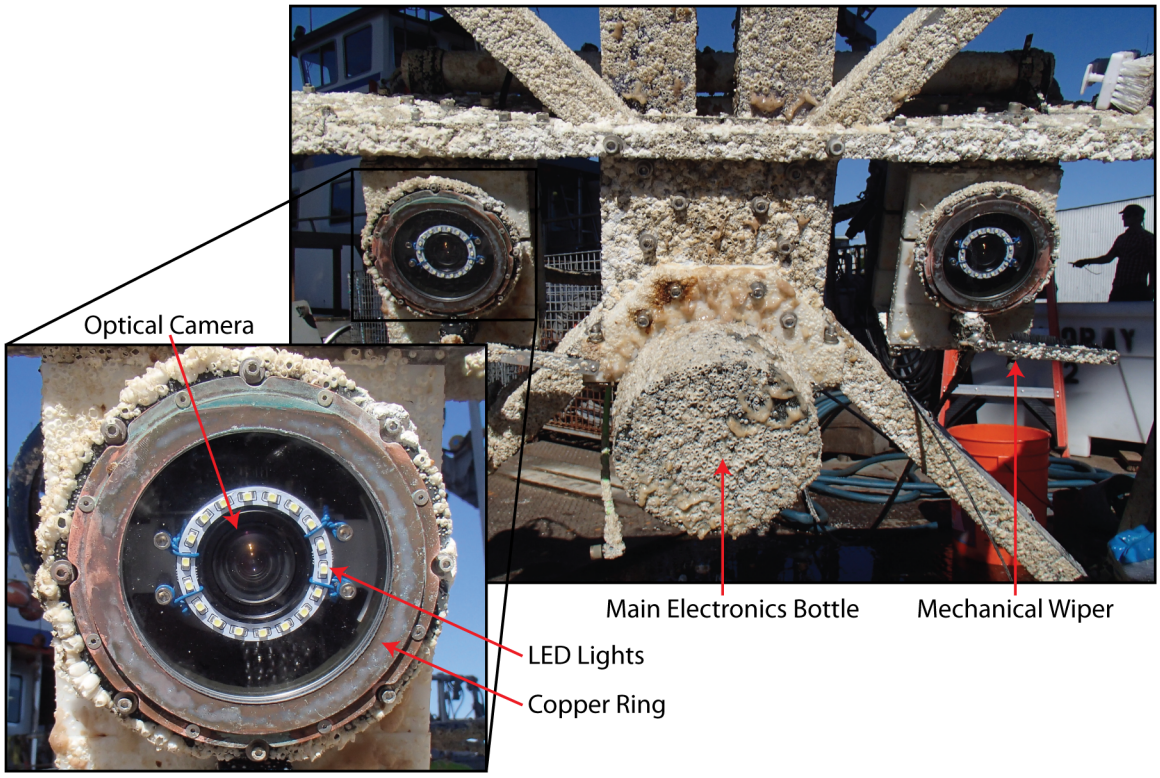

Fig. 8: Post recovery biofouling on aluminum frame and camera optical ports.

surface (including the back of the wiper blades) except for the optical ports. Fig. 8 shows the center of the camera frame with a close-up view of the Camera 1 optical port. Fouling on the system generally consisted of barnacles and algae.

The strobe optical ports, which were not monitored during the deployment, other than qualitatively by the diver inspections, are shown post recovery in Fig. 9. Due to the wipers being disabled over the last month of the deployment, all four optical ports exhibit some barnacle growth. Strobe 1 exhibits the most growth and, upon recovery, the wiper blade for this bottle is noted to have rotated out of the plane of the optical port, thus making it ineffective for a potentially longer portion of the test than the wipers on the other strobe ports. Comparison of the camera and strobe optical ports demonstrates the effectiveness of the mechanical wiper.

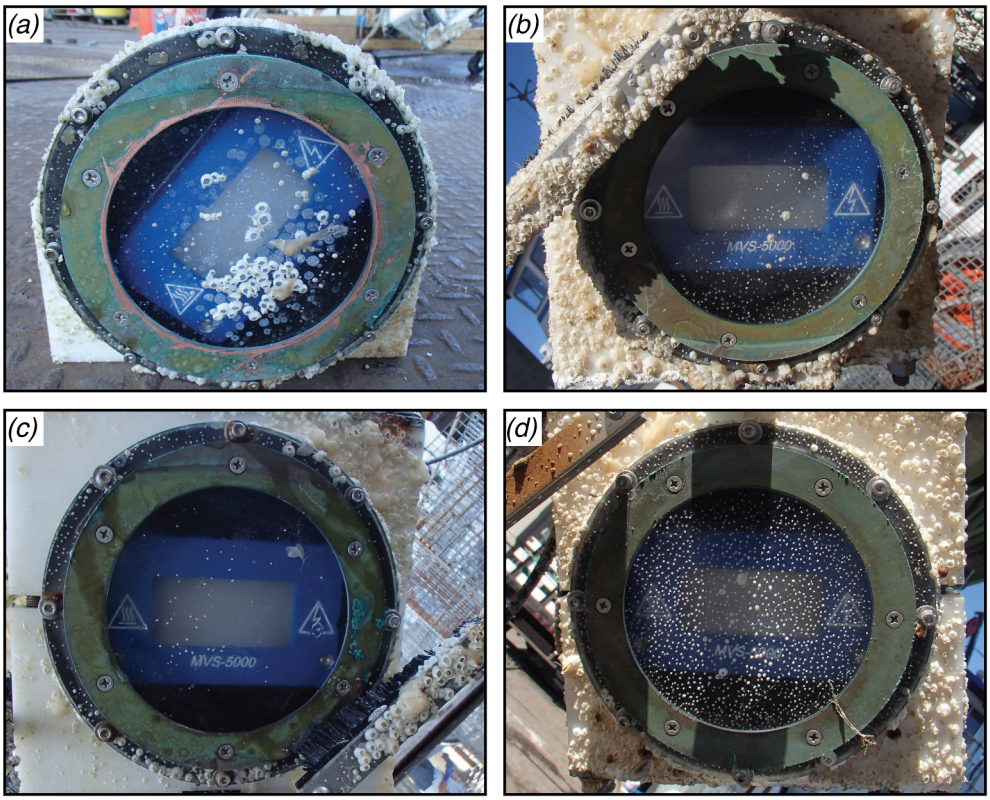

Fig. 9: Biofouling on strobe optical ports with *(a)* Strobe 1, *(b)* Strobe 2, *(c)* Strobe 4, and *(d)* Strobe 3. Ordering identical to treatment schematic in Fig. 4.

IV. Discussion and Conclusions

There are expected to be strong seasonal and spatial variations in biofouling within a region the size of Puget Sound [13]. The dates of this field deployment were chosen to span the spring and summer seasons, during which fouling is, historically, most severe. Since the endurance trial took place in calm waters with the camera system entirely within the photic zone, the biofouling observed during the trial is likely to be more severe than would occur at depth. Inspection of the images captured throughout the deployment, as represented in Fig. 6 and Fig. 8, revealed a high level of growth on the test frame.

Monitoring biofouling levels on camera optical ports in a quantitative manner is complicated by the variable nature of the imagery. This methodology of backlighting the optical ports with LEDs in the absence of other light provides a means of comparing images on a daily basis. While there was no visible degradation in image quality during the deployment, the biofouling

metric was able to detect more subtle changes than the human eye. An upward trend in this metric could, therefore, be used to predict the need for system maintenance before the optical port is visibly degraded, thus affording more time to plan system recovery (essential in marine renewable energy environments) and reducing system downtime.

The combination of biofouling mitigation methods effectively prevented macro-fouling growth that would have otherwise degraded system performance. The clarity of the camera optical ports in comparison to adjacent surfaces, as shown in Fig. 8, is a stark representation of this effectiveness. With no discernible difference between the clarity of the two camera optical ports, the benefit of the ClearSignal coating appears to be minimal. If a system deployment were to be power constrained, and the wipers could not be run as frequently (as would be the case for an autonomous deployment), then coatings may be helpful to maintain optical port clarity.

The clarity of images obtained during this endurance trial suggest optical sensor deployments of at least four months are possible in Puget Sound, even under adverse fouling conditions, provided that appropriate biofouling mitigation measures are employed. While this result is most applicable to optical monitoring in Puget Sound, projects elsewhere involving long-term deployments of optical sensors may benefit from similar biofouling mitigation measures. Future deployments of this camera system for environmental monitoring of tidal energy projects will provide additional information about seasonal effectiveness of the measures employed.

ACKNOWLEDGMENT

The authors would also like to thank Jeffery Thomas for use of his facilities at Sunset Bay Marina, Jim Thomson for coordination of the field deployment and inspection dives, Sandra Parker-Stetter and Sharon Kramer for recommendations on system testing, Capt. Andy Reay-Ellers for captaining the R/V Jack Robertson, Alex DeKlerk for designing and fabricating the imaging frame, Joe Talbert and Tim McGinnis for building the shore cable umbilical, Keith van Thiel for the design of the pressure housings and optical ports, Rick Towler and Kresimir Williams for insight into component selection and stereographic calibration, and last, but certainly not least, Randy Sindelar for his adaptable, custom electronics for power and communication.

REFERENCES

[1] D. V. Manov, G. C. Chang, and T. D. Dickey, “Methods for reducing biofouling on moored optical sensors,” *Journal of Atmospheric and Oceanic Technology*, vol. 21, pp. 958–968, 2004.

[2] B. Howe and T. McGinnis, "Sensor networks for cabled ocean observatories," in *International Symposium on Underwater Technology*, April 20-23 2004.

[3] A. M. Woodroffe, S. W. Pridie, and G. Druce, "The neptune canada junction box - interfacing science instruments to sub-sea cabled observatories," in *MTS/IEEE Kobe Techno-Ocean*, April 8-11 2008.

[4] A. D. Chave, M. Arrott, C. Farcas, and E. Farcas, "Cyberinfrastructure for the us ocean observatories initiative: Enabling interactive observation in the ocean," in *MTS/IEEE Oceans 2009 - Europe*, May 11-14 2009.

[5] I. Y. Phang, N. Aldred, A. S. Clare, and G. J. Vancso, "Effective marine antifouling coatings: studying barnacle cyprid adhesion with atomic force microscopy," *Nanos*, vol. 01, pp. 36–41, 2007.

[6] M. Salta, J. A. Wharton, Y. Blache, K. R. Stokes, and J.-F. Briand, "Marine biofilms on artificial surfaces: structure and dynamics," *Environmental Microbiology*, vol. 15, no. 11, pp. 2879–2893, 2013.

[7] C. Debiemme-Chouvy, U. Hua, F. Hui, J.-L. Duval, and H. Cachet, "Electrochemical treatments using tin oxide anode to prevent biofouling," *Electrochemica Acta*, vol. 56, no. 28, pp. 10 364–10 370, 2011.

[8] A. Whelan and F. Regan, "Antifouling strategies for marine and riverine sensors," *Journal of Environmental Monitoring*, vol. 8, no. 9, pp. 880–886, 2006.

[9] L. Delauney, C. Compere, and M. Lehaitre, "Biofouling protection for marine environmental sensors," *Ocean Science*, vol. 6, no. 2, pp. 503–511, 2010.

[10] B. Polagye, A. Copping, R. Suryan, J. Brown-Saracino, and C. Smith, "Instrumentation for monitoring around marine renewable energy converters: Workshop final report," Pacific Northwest National Laboratory, Seattle, WA, Tech. Rep. PNNL-SA-XXXX, 2014.

[11] J. Joslin, B. Polagye, and S. Parker-Stetter, "Development of a hybrid optical-acoustical camera system for monitoring tidal turbines," *SPIE Journal of Applied Remote Sensing*, In Review.

[12] J. Joslin, E. Celkis, C. Roper, A. Stewart, and B. Polagye, "Development of an adaptable monitoring package for marine renewable energy," in *Proceedings of the MTS/IEEE Oceans 2013 Conference*. San Diego, CA: MTS/IEEE, September 23-26 2013.

[13] T. D. Dickey and G. C. Chang, "Recent advances and future visions: Temporal variability of optical and bio-optical properties of the ocean," *Oceanography*, vol. 14, no. 3, pp. 15–29, 2001.

James Joslin James Joslin is a PhD student working with the Northwest National Marine Renewable Energy Center at the University of Washington in Seattle. His research focuses on the development of instrumentation to increase monitoring capabilities of tidal and wave energy converters. He completed his undergraduate and masters degrees at Dartmouth College and was introduced to marine engineering while working with Sea Education Association out of Woods Hole, MA.

Brian Polagye Dr. Brian Polagye is the co-Director of the Northwest National Marine Renewable Energy Center and an assistant professor in the Department of Mechanical Engineering at the University of Washington. His research focuses on marine renewable energy conversion. Dr. Polagye holds a bachelors degree from Princeton University and doctoral degree from the University of Washington.

Development of a hybrid optical-acoustical camera system for monitoring tidal turbines

James Joslin,[a] Brian Polagye,[a] Sandra Parker-Stetter[b]
[a]University of Washington, Northwest National Marine Renewable Energy Center, Department of Mechanical Engineering, Box 352600, Seattle, WA, USA, 98195-2600
[b]University of Washington, School of Aquatic and Fishery Sciences, Box 355020, Seattle, WA, USA, 98195-2600

Abstract - The development, implementation, and testing of a hybrid optical-acoustical imaging system suitable for environmental monitoring of a tidal turbine is described. This monitoring system is intended to provide real-time stereographic imagery in the near field (< 10 m) of tidal turbines proposed for deployment in Admiralty Inlet, Puget Sound, Washington. Post-deployment observations will provide necessary information about the frequency and type of interactions between marine animals and the turbine. A method for optimizing the stereo camera arrangement is given, along with a quantitative assessment of the system's ability to measure and track targets in three dimensional space. Optical camera effectiveness is evaluated under realistic field conditions to determine the range within which detection, discrimination, and classification of targets is likely. These field evaluations inform optimal system placement relative to the turbine rotor. Tests suggest that the stereographic cameras will likely be able to discriminate and classify targets at ranges up to 3.5 m and detect targets at ranges up to, and potentially beyond, 4.5 m. By pairing the optical cameras with an imaging sonar ("acoustical camera"), behavioral disturbances associated with artificial lighting can be minimized.

Keywords – Environmental Monitoring, Stereo Imaging, Hydrokinetic Energy, Tidal Energy.

Address all correspondence to: James Joslin, University of Washington, Northwest National Marine Renewable Energy Center, Department of Mechanical Engineering, Box 352600, Seattle, WA, USA, 98195-2600; Tel: +1 360-477-2901; Fax: +1 206-685-8047; E-mail: jbjoslin@uw.edu

1 Introduction

The energy in fast moving tidal currents is a potential source of renewable, predictable electricity. Tidal turbines harness tidal currents in a manner analogous to wind turbines. Benefiting from the lessons learned in the development of wind energy, single-turbine demonstration projects with rated electrical capacities exceeding 1 MW have been successfully deployed in tidal races.[1] However, before large-scale utilization of tidal current resources may occur, operation of turbines must be proven to be not just technically feasible, but economically viable, environmentally compatible, and socially acceptable.

Potential environmental impacts associated with tidal turbine operation have been evaluated by several groups.[1-3] However, the frequency with which the most significant potential impacts will actually occur is uncertain. Resource agencies have expressed particular interest in understanding the frequency and nature of close-range (defined as 1-2 diameters of the turbine rotor) interactions between marine animals (i.e., fish, large invertebrates, marine mammals, and diving seabirds) and tidal turbines. Possible interactions include collision/strike with the moving rotor, attraction due to the foundation as an artificial reef, and avoidance due to pressure fluctuations or sound. To date, there have been several attempts to collect this information with active acoustics (e.g., sonars or echosounders). These have provided valuable information about the behavior of fish in the vicinity of turbines,[4,5] but have reported difficulties achieving a fine level of taxonomic classification or characterizing the nature of interactions with the turbine rotor itself.

At present, there are several dozen tidal turbine designs in various stages of development. Khan et al.[6] provides an overview of proposed technologies and Polagye et al.[1] includes case studies of several demonstration projects. While turbine technology has yet to converge on a single archetype comparable to the three-bladed axial flow wind turbine, a trend has emerged in recent years for utility-scale tidal turbines. The rotors are dominantly axial flow designs (i.e., the axis of rotation is parallel to the direction of water motion) and utilize two to three rotor blades. However, it has been noted[7] that large-scale utilization of tidal current resources may require devices with fundamentally different rotor topologies (e.g., vertically-oriented cross flow rotors). To achieve rated electrical capacities greater than 1 MW, turbine rotors for axial flow commercial demonstration systems are on the order of 20 m in diameter. Hub heights (i.e., height of axis of rotation about rotor hub) relative to the seabed depend on the foundation and

mooring technology (monopiles, gravity foundations, or jacket structures). In general, current intensity increases away from the seabed, but foundation cost and complexity for bottom-anchored turbines also increases with hub height.[8] Consequently, depending on the turbine technology and deployment site, turbines can either operate entirely within the photic zone or at depths where there is negligible ambient light penetration.

1.1 Monitoring Near-Turbine Interactions

Because of the potential for injury caused by turbine blades striking a marine animal or marine animal colliding with turbine blades, resource agencies in the United States and Europe have focused on observations within the near-field. Concerns regarding blade strike primarily originate from the well-documented mortality of fish passing through conventional hydropower turbines[9] and tidal barrages,[10] as well as injuries to birds and bats caused by wind turbines.[11] Field observations and laboratory experiments conducted to date for tidal and river turbines4,[12,13] suggest that such interactions are likely to be rare. However, these results need to be confirmed for a broader set of locations and technology variants. Ideally, field observations should be able to discriminate between contact and a near-miss between marine animals and the turbine rotor, identify the marine animal involved to the species level, continuously observe the entire near-field, and cause minimal behavioral changes. Simultaneously satisfying these constraints is not technically feasible, as evidenced by the variety of approaches employed to date, four of which are summarized here.

1.1.1 Verdant Power (East River, New York, United States)

Verdant Power operated an array of turbines near Roosevelt Island in the East River of New York from 2005 through 2008. The project used a combination of split-beam acoustic

echosounders (BioSonics, DTX) deployed from shore and a vessel-deployed imaging sonar ("acoustical camera") (Sound Metrics, DIDSON) to monitor fish passage. The array of split-beam transducers (24 in total) was able to monitor targets passing through the project area, but could not be used to detect animal strikes with the device or to identify fish to the species level. The cost of the echosounder array exceeded that of the turbines, and the knowledge gained from this study was not considered proportional to its cost.[1] Vessel-based acoustical camera observations (3+ days) detected a single fish passing through the vicinity of one turbine during operation: the fish traveled along hydrodynamic streamlines and was not struck by the rotor. Verdant Power concluded that acoustical cameras could be an effective tool for animal strike monitoring if used for short-term deployments (2 to 3 weeks) coinciding with periods of peak fish abundance, but also concluded that data quantity, instrument reliability, and high cost combined to preclude acoustical camera use for longer-term observations.

1.1.2 Ocean Renewable Power Company (Eastport, Maine, United States)

Ocean Renewable Power Company tested a cross flow turbine from a barge near Eastport, Maine for two years (2010-2011). An acoustical camera (Sound Metrics, DIDSON) was deployed from the generator barge to monitor fish behavior around the operating rotor.[4] These observations were the first documentation in the field of fish passage through a tidal turbine. While the positioning of the sonars did not allow individual fish to be tracked through the turbine, fish schools were observed entering the turbine and, having passed through, aggregating in the wake before continuing. Forty percent of individual fish detected by the imaging system were observed to interact with the turbine (i.e., passing through the turbine or resting in the wake). Reaction distance and type of interaction depended on the turbine operating state, fish length, and degree of aggregation, with schools interacting at a lower rate than individual fish. Avoidance of the

rotor was observed less frequently at night than during the day, suggesting that visual cues played a role in behavior around the turbine.

1.1.3 OpenHydro (European Marine Energy Center, Orkney Islands, Scotland, United Kingdom)

OpenHydro used unlighted video to monitor fish interactions with its turbine at the European Marine Energy Center.[14] This approach was able to detect fish aggregations in the turbine wake during low current flows (e.g., < 1.5 m/s). No collisions with the device or blade strikes were observed and, unlike the field observations in Maine, fish were not reported to pass through the turbine once it began rotating. This turbine was deployed within the photic zone and monitoring was restricted to daylight hours. Observations were conducted with a single camera deployed from a spar on one side of the turbine.

1.1.4 OpenHydro (Fundy Ocean Research Centre for Energy, Minas Passage, Nova Scotia, Canada)

In the Bay of Fundy, an OpenHydro turbine was installed in November 2009 and removed in November 2010. The lack of a power and data cable precluded deployment of either optical or acoustical imaging systems for monitoring. Consequently, researchers deployed an array of eight Vemco (VR2W) fish tag receivers around the turbine foundation and another array of eight receivers in a line across the channel to the east of the turbine. Over the course of the turbine deployment, approximately 100 fish were tagged and released in the upper Bay of Fundy. This study was able to identify periods of presence and absence, but could not be used to track individual targets because of the autonomous nature of the receivers. Receiver arrays with clock synchronization capabilities have been shown to allow individual trajectory tracking,[15, 16] but this has not yet been attempted in a tidal energy context.

1.2 Technology Options for Near-Turbine Monitoring

As described in the case studies, technologies potentially suitable for the study of near-turbine interactions include optical imaging, acoustical imaging, and animal-borne tags (i.e., tags actively transmitting an acoustic signal). Traditional fisheries trawls are unlikely to be feasible in close proximity to turbine rotors because of both the risk of net entanglement with the rotor and the difficulty of fishing effectively during periods of strong currents when interactions between turbines and fish are of greatest interest. The trade-offs between available technologies is summarized in Table 1. Of the available technologies, optical imaging shows considerable promise for discriminating between contacts and near-misses and identifying targets to the species level, but subsampling in space and time are required. In particular, data bandwidths for optical imaging can be daunting in comparison to other approaches. For example, a stereo imaging arrangement involving a pair of 2 megapixel black and white cameras with 16-bit resolution would produce 80 megabytes of imagery per second when acquiring images at 10 frames per second. This translates to more than 6 terabytes of imagery per day. In contrast, a two-dimensional imaging sonar acquiring information at a similar rate produces only about 1 megabyte of data per second.

Table 1 – Capabilities of potential near-turbine monitoring technologies.

	Optical Imaging	**Acoustical Imaging**	**Animal-borne Tags**
Discrimination between Contact and Near-Miss	Possible with stereo imaging	Not possible due to acoustic reflection from hard surfaces	Not possible
Identification to the Species Level	Possible at close range with stereo imaging	Requires additional information about species presence/absence	Inherent
Continuous Observations of Entire Near-field	Difficult due to positioning of cameras, data bandwidth, and functional range of cameras when artificial lighting is required	Difficult due to positioning of transducers and data bandwidth	Possible with an array of localizing receivers
Behavioral Changes	Artificial illumination will affect behavior	Minimal effect	Short-term effects after handling for tag insertion[17]

1.3 Design Considerations for Stereo Imaging of Tidal Turbines

There are no "typical" tidal energy sites. Each has unique attributes that can either impair or facilitate the use of optical imaging techniques. The intended use of the system described in this paper is at a tidal energy site in northern Admiralty Inlet, Puget Sound, Washington. Public Utility District No. 1 of Snohomish County has proposed to deploy two turbines manufactured by OpenHydro (www.openhydro.com) at this location.[18] The turbines are axial flow devices 6 m in diameter and would operate for up to five years as a demonstration project to evaluate environmental interactions and turbine reliability. If the demonstration project is successful, Admiralty Inlet has significant potential for large-scale tidal energy utilization.[19] The water depth in the project area is approximately 55 m and the turbine hub height is 10 m above the seabed. During strong tidal exchanges, currents exceed 3 m/s.[20]

There is minimal ambient light at this depth, such that any optical imaging system deployed to monitor these turbines will require artificial illumination. Measurements indicate turbidity to be less than 1 NTU[20] but benthic habitat surveys utilizing remotely operated vehicles[21] have

encountered significant biological flocculent close to the seabed that limited the functional range of their camera systems. This flocculent can interfere with optical imaging by both obscuring the target and scattering artificial illumination back towards the cameras.

1.4 Study Description

Mono- and stereo-optical imaging systems with artificial illumination have been deployed by several research groups to study the marine environment. Howland et al.[22] developed a towed single camera system to capture high resolution still imagery for scallop population density. Similarly, Rosenkranz et al.[23] developed an imaging system to provide high resolution images of benthic habitats. Williams et al.[24] employed stereo-imaging to study rockfish abundance in untrawlable areas. These systems share a number of requirements with imaging of tidal turbines, but have not been deployed in the specific environments where tidal turbines would operate. Further, in reviewing the literature on stereographic imaging, there are no standardized test cases for objective optimization of system performance. Most lateral stereo arrangements are studied using parallel camera axes[25,26] or, more recently, to mimic human vision for 3d cinema.[27,28] Optimization methods for stereo vision generally focus on the correspondence problem (i.e., selection of points in stereo images that correspond to the same spatial location) and image matching (i.e., transforming data from stereo images into a single coordinate system) for computer vision.[29]

Section 2 presents a description of the hardware and software for the optical-acoustical camera system developed by the authors. Section 3 begins with a review of stereo imaging fundamentals relevant to optimization for near-turbine monitoring and presents the methodology used to determine the extrinsic and intrinsic properties of the optical camera system, evaluate triangulation errors, demonstrate target tracking, and establish the functional range in realistic

field conditions. Section 4 presents the results of the laboratory optimization and field testing. Section 5 discusses the implications of these results for near-turbine monitoring of the Admiralty Inlet tidal energy demonstration project.

2 Imaging System Description

The operational objectives for an imaging system for turbine monitoring are to classify targets (e.g., taxonomic classification to the species level, if possible) within the near-field environment (e.g., within 1-2 characteristic diameters) of an operating hydrokinetic turbine, without significantly affecting animal behavior. During periods of strong currents, the relative velocity between the camera and these targets can be on the order of several m/s. Shore power up to 1 kW and fiber optic data connectivity with 1 gigabit per second bandwidth need to be available. Due to the difficulty and cost of maintaining the imaging system,[30] the imaging system will need to operate for multi-month periods.

The imaging system developed in response to these objectives and constraints is a hybrid optical-acoustical system, incorporating stereographic optical cameras and a high-resolution acoustical camera. As described in Sec. 3.1, calibrated stereo cameras can provide information about the absolute position, size, and speed of targets. Target size is particularly relevant to classification.

To capture crisp images with relative motion on the order of 3 m/s, an exposure time between 2 and 50 μs is recommended.[31] This can be achieved by strobe illumination. Increased camera-light separation improves the effective range by reducing backscattered light from turbidity and flocculent.[32] However, the camera-light separation is constrained by the maximum practical package size for maintenance operations.

The use of full-spectrum, artificial light has the potential for behavioral effects on fish and invertebrate species (attraction or avoidance).[33-35] It is intended that the acoustical camera be used to characterize the effect of strobe illumination and determine a minimum "cool down" time between exposure to strobe illumination and resumption of pre-illumination behavior. For this reason, an acoustical camera with a field of view similar to the optical cameras is preferred.

The principle components of the imaging system are, therefore, a pair of cameras, four strobe illuminators, an acoustical camera, and the power/communications architecture to integrate them and communicate with shore via the fiber optic link. To minimize system cost and complexity, the primary communications bus operates on Ethernet protocol, with media conversion from copper to fiber to extend its range. A secondary communications bus operates on serial protocol (converted to Ethernet) and is used to monitor the health of various components (current draw, temperature, and humidity) and control power distribution. Low-cost media conversion limits the total bandwidth to 1 Gb/s (125 MB/s).

The primary trade-offs in camera selection are resolution, bandwidth, and cost. High resolution increases the potential for target classification, but at high frame rates (e.g., 10 Hz) data bandwidths can easily exceed the capacity of the communications system. The selected cameras are the Allied Vision Technologies Manta G-201 B/C (2 Megapixel, www.alliedvisiontec.com). These are compact, industrial-grade machine vision cameras operating on Gigabit Ethernet (GigE) vision protocols. Each camera is equipped with a 5 mm focal length lens (Navitar NMV-5M23). A wider field of view could be achieved with a shorter focal length lens, but at the cost of decreased image resolution. For strobe illumination, four Excelitas Technologies MVS-5002 units were selected on the basis of their performance in underwater camera systems with similar specifications.[22] A BlueView P900-2250

(www.blueview.com) was selected as an acoustical camera due to its similar field of view to the optical cameras, as well as ease of integration due its Ethernet-based communications bus.

With the exception of the BlueView acoustical camera, the system components are not designed for underwater use and must be enclosed within pressure housings. The pressure housings for the optical cameras and strobes are anodized aluminum with double seal O-rings on the end caps and acrylic optical view ports (planar). For testing these modular components are mounted to an aluminum frame, as shown in Fig. 1, resulting in a camera-strobe separation distance of ~1 m and nearly overlapping fields of view between the optical and acoustical cameras. The frame allows for the optical camera separation to be adjusted between 0.5 and 1.1 m with camera toe-in angles up to 10°. A method for determining optimized separation and toe-in angle is presented in Sec. 3.2.

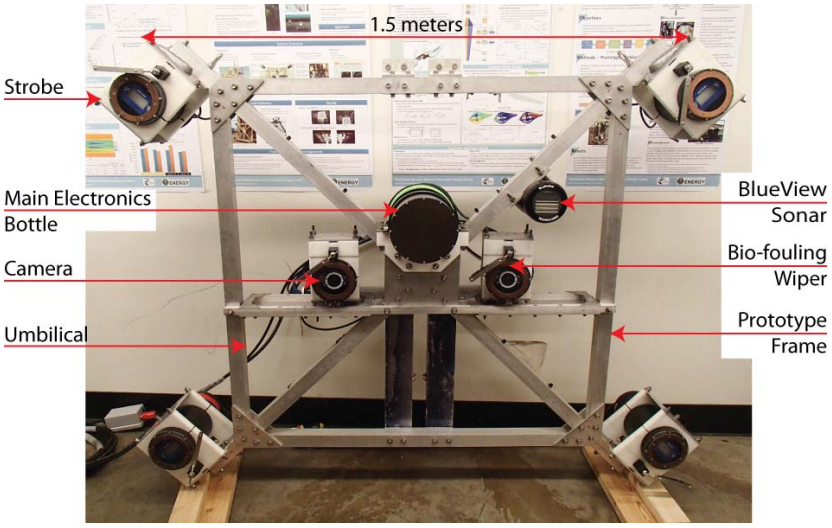

Fig. 1 – Prototype imaging system showing principal components and scale.

Without mitigation measures, biofouling of the optical ports will rapidly degrade system effectiveness.[36] To address this, a mechanical wiper (Zebra-Tech Hydro-wiper, www.zebra-tech.co.nz) is integrated into each housing and copper rings are placed around the perimeter of

the optical ports. A commercially available antifouling coating that would complement the mechanical wiper could also be employed.

Off-the-shelf component specifications and costs are detailed in Table 2.

Table 2 - Component, manufacturer, description, and equipment cost for the stereo-camera portion of the turbine monitoring instrumentation.

Component	Manufacturer	Description	Unit Cost
Optical Cameras	Allied Vision Technologies, Manta G-201B/C	2 Megapixel, GigE Vision Camera with Sony ICX274 Sensor, 1624x1234 pixels, 4.4 μm pixel cell size, 1/1.8" sensor size, 14 fps.	$1600
Lenses	Navitar NMV-5M23	2/3" Megapixel format with manual focus from 0.05 m to infinity and 2.8 to 16 F-stop.	$500
Strobes	Excelitas Technologies MVS-5002	20 μs flash duration, 30 Hz maximum flash rate.	$1300
Acoustic Camera	BlueView P900-2250	Dual frequency sonar with 45° x 20° field of view, 60 m (900 kHz) and 8 m (2.25 MHz) maximum range.	$30,000
Mechanical Wipers	Zebra-Tech LTD	Brush style hydro fouling optical port wiper.	$1200

Power requirements for system components are described in Table 3. Custom electronics step down the main supply power (375 VDC) to a 12 V component supply. These are built around Vicor (www.vicorpower.com) DC-DC converters. Medium voltage DC power supply is required to minimize resistive losses over the long cable run between the turbine and shore station. Temperature, humidity, and current monitoring in each pressure housing also utilizes custom electronics.

Table 3 - Component power requirements at maximum data acquisition rates.

Component	**Mode**	**Power Requirement**
Optical cameras (2)	Acquiring at 10 fps	10 W
Strobes (4)	Strobing at 10 Hz	72 W
Mechanical wipers (6)	3 wiper motors locked (high failure rate)	18 W
Acoustical camera	Acquiring at 15 fps	19 W
Media conversion and auxiliary loads	Operating	30 W
DC Conversion Losses	80% efficiency	37 W
Total System Draw		**186 W**

System operation, monitoring, camera control, and optical image acquisition are performed with the National Instruments LabView serial communications (VISA) and image acquisition (IMAQ) modules (www.ni.com/labview). The image acquisition module is configured to allow a user to directly control a limited subset of camera settings accessible through GigE Vision protocol, such as frame rate, exposure time, digital gain, and strobe triggering. Simultaneous image acquisition from both cameras is achieved by a hardware trigger (i.e., electrical trigger connection between the master camera and slave camera) and the virtual shutter effect due to the short strobe duration (20 μs) in the absence of ambient light. The acoustical camera imagery is acquired using a proprietary software package (ProViewer, BlueView).

Continuous monitoring of each pressure housing's temperature, humidity, and current draw provides metrics to evaluate system health. Each strobe housing and the main electronics housing is equipped with a circulation fan to increase the rate of heat transfer between electronics and the metal housing. Humidity monitoring is intended to detect leaks that could lead to catastrophic failure. A current spike beyond the normal operating limits of the electronics indicates a short circuit or ground fault between the main electronics housing and satellite pressure housings.

Each of these parameters can trigger an automatic power shutoff of the associated electronics if user-defined thresholds are exceeded.

3 Testing and Optimization Methodology

3.1 Stereo Imaging Fundamentals

Stereographic imagery uses multiple camera positions to map three-dimensional space from two-dimensional images. Many arrangements for stereographic systems have been proposed[26] each of which has various benefits and drawbacks to system performance. The system described here is a general two camera lateral arrangement (i.e., side-by-side cameras on a common lateral axis), as described in Alvertos et al.[26] The three parameters that describe this arrangement are (1) the rotation angle of the cameras, ω, (2) the baseline separation of the two cameras, b, and (3) the toe-in angle of the cameras, φ. Determination of appropriate values for each of these variables depends on the operating field of view of each camera, θ, and the expected target range. To fully describe the stereo system, the intrinsic parameters for each camera (such as the focal length, principal point, skew, and distortion coefficients) and the extrinsic parameter for the system must be measured experimentally. For simplicity in these calculations, the two cameras are assumed to be identical and modeled as ideal pinhole cameras. The pinhole camera model represents the camera as a single point in three-dimensional space through which light is projected onto an associated image plane, neglecting lens distortion effects.[37] Fig. **2** shows a generalized lateral arrangement with the right and left cameras located at C_1 and C_2 respectively and the associated image planes centered at O_1 and O_2. For the chosen machine vision cameras, the image plane is rectangular with the x and y axes containing 1624 and 1234 pixels respectively.

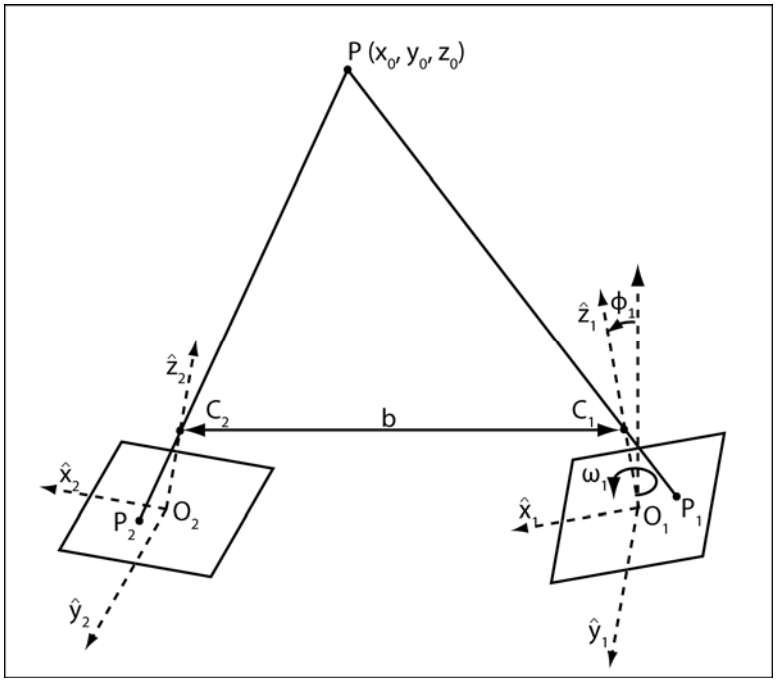

Fig. 2 - General 3 dimensional stereo camera arrangement.

Triangulation uses pixel coordinates in each image plane corresponding to the same point in three-dimensional space to determine that point's coordinates. Target size may be calculated from a pair of stereo images by computing the Euclidean norm between two triangulated points in the same image pair. Similarly, target velocity may be calculated from the distance a single point moves over sequential frames. As shown in Fig. 2, two coordinate systems are defined at the center of the right and left image planes as $(\hat{x}_1, \hat{y}_1, \hat{z}_1)$ and $(\hat{x}_2, \hat{y}_2, \hat{z}_2)$ respectively. These coordinate systems are related to each other by

$$\begin{pmatrix} \hat{x}_1 \\ \hat{y}_1 \\ \hat{z}_1 \end{pmatrix} = \begin{pmatrix} \hat{x}_2 \\ \hat{y}_2 \\ \hat{z}_2 \end{pmatrix} \mathbf{R} + \mathbf{T} \tag{1}$$

where ***R*** is a 3 x 3 orthonormal rotation matrix and ***T*** is a translation vector, which define the extrinsic parameters of the stereo system. For a fixed camera arrangement, these values are constant and are readily obtained by the calibration procedure discussed in Sec. 3.3.1. A target point (*P*) that is within the field of view of both cameras will have the coordinate (x_1, y_1, z_1) and

(x_2, y_2, z_2) in the right and left coordinate systems, respectively. Projections of this point on each two-dimensional image plane through the respective camera lens are identified as P_1, with coordinates (x_1^i, y_1^i, 0) and P_2, with coordinates (x_2^i, y_2^i, 0). These image coordinates are related to the three-dimensional target point coordinates in each system by

$$\frac{x_1}{x_1^i} = \frac{y_1}{y_1^i} = \frac{\lambda - z_1}{\lambda} \tag{2}$$

and

$$\frac{x_2}{x_2^i} = \frac{y_2}{y_2^i} = \frac{\lambda - z_2}{\lambda} \tag{3}$$

where $\lambda = C_1O_1 = C_2O_2$ (i.e., the camera focal lengths are equal). With a known set of extrinsic parameters, (1), (2), and (3) may be combined to determine the spatial coordinates of a target point, P, from the pixel coordinates of the target projection in each camera image. Choosing image coordinates that represent the same target point may be challenging due to the different perspectives of each camera and is referred to as the *correspondence problem* in machine vision.[26] Although the automation of target identification and tracking may necessitate further investigation of this problem in the intended application, more information about image quality and target frequency and size is first needed to constrain the problem.

3.2 Optimizing Camera Arrangement

Optimization of this camera arrangement for the purpose of measuring target location, size, and speed involves the maximization of the percentage of overlapping fields of view of the two cameras and the minimization of triangulation error due to depth perspective. The overlapping field of view of the two cameras is defined as the volume of space where a target appears in both camera images. Since the area captured in either image increases with distance from the camera, but target triangulation at any position in the near-field of a turbine is equally important,

volumetric overlap, as a percentage of an individual camera's volumetric field of view, is chosen as the optimization criteria. This percentage depends on all three of the arrangement variables (ω, b, and ϕ). The range over which the volumetric fields of view are calculated depends on the functional range of the system which is evaluated through field testing in Sec. 4.2.

The camera rotation angle that maximizes the overlapping field of view occurs when the image planes are aligned on the "horizontal" x-axis or side-by-side (where the x-axis is defined as the dimension of the image plane with the greatest number of pixels). In this arrangement, the "vertical" y-axis field of view is equal and the system orientation can be described entirely in the $\hat{x} - \hat{y}$ plane, as in **Fig. 3**.

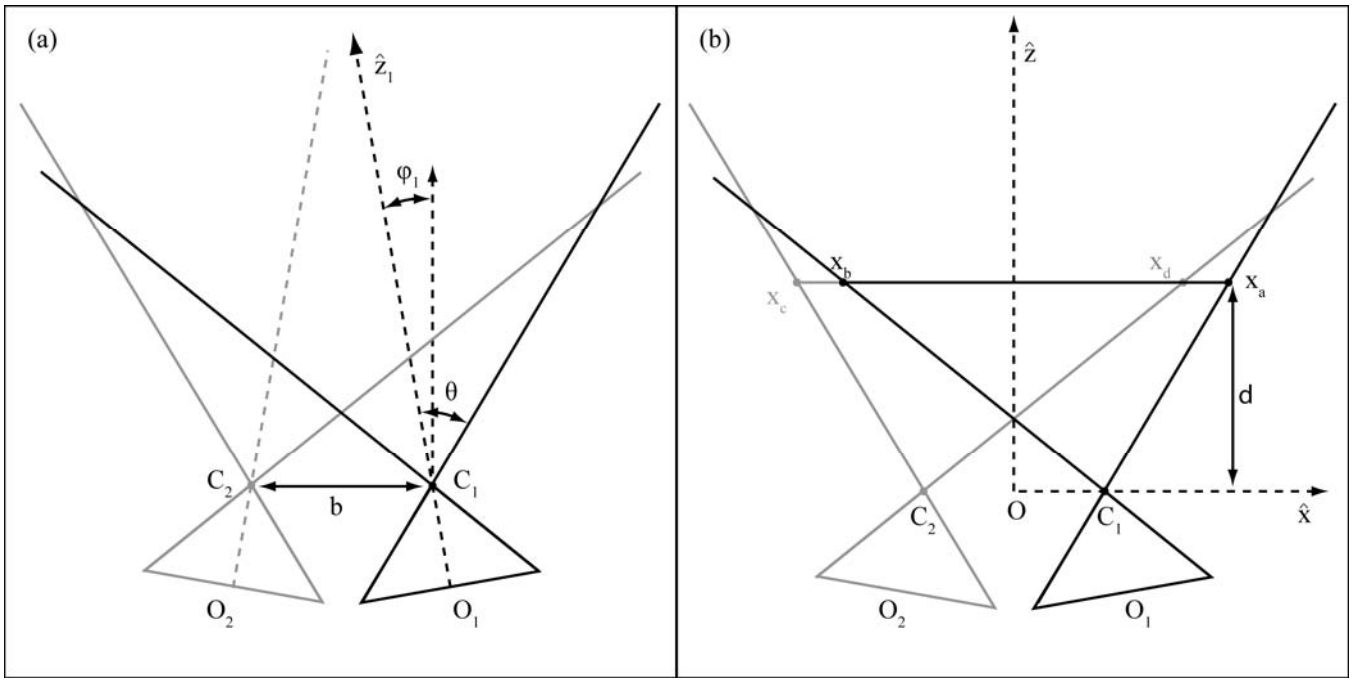

Fig. 3 – (a) Camera arrangement variables in the x-z plane and (b) variables describing the overlapping volumetric field of view at a given distance (d) from the camera.

Given a symmetric lateral stereo arrangement, the overlapping field of view may be calculated on the basis of a coordinate system centered between the two cameras at O. The percentage of the overlapping volumetric field of view of the two images on any plane parallel to

O may be written as a function of distance from O to a target, d, the horizontal field of view angle, θ, the toe-in angle, φ, and the baseline separation, b. First, let x_a, x_b, x_c, and x_d be the horizontal limits of the right and left camera images, respectively, at distance, d, as shown in **Fig. 3**b, which may be calculated as

$$x_a = b/2 + d\tan(\theta - \phi) \tag{4}$$

$$x_b = b/2 - d\tan(\theta + \phi) \tag{5}$$

$$x_c = -x_a \tag{6}$$

$$x_d = -x_b \tag{7}$$

Consequently, recalling that there is complete overlap in the y-direction, the percentage of the volumetric field of view that overlaps between the left and right cameras, FOV, is

$$FOV(d) = \begin{array}{c} 0 \\ 2x_b/(x_a - x_b) \\ -2x_a/(x_a - x_b) \end{array} \quad \begin{array}{c} \\ for \\ \\ \end{array} \quad \begin{array}{c} d \le (b/2)\tan(\theta + \phi) \\ (b/2)\tan(\theta + \phi) < d \le b/(\tan(\theta + \phi) - \tan(\theta - \phi)) \\ b/(\tan(\theta + \phi) - \tan(\theta - \phi)) < d \le d_{\max} \end{array} \tag{8}$$

Once the field of view and functional range have been established for a given application, (8) can be integrated over the functional range for various baseline separations and toe-in angles to evaluate the percentage overlap for a given configuration.

Intuitively, the greatest overlap occurs when the baseline separation is minimized. Target triangulation however, uses the disparity of the two images to measure the distance on the z-axis. This depth perspective increases with increasing baseline separation and, consequently, spatial triangulation errors may increase as the stereographic field of view is maximized. To understand the sensitivity of triangulation to the baseline separation, experiments were conducted with the cameras at the extreme limits of baseline separation (0.5 and 1.0 m) and with toe-in angles that maximize the percentage of overlap in a range of 1 to 5 m.

3.3 System Tank Testing

3.3.1 Intrinsic and Extrinsic Camera Parameters

The field of view of the individual cameras is measured empirically by acquiring images of a graduated rule at a known distance from the camera that spans the horizontal axis of the image. To account for lens barrel distortion and refraction at the air/water interface across the optical port on the pressure housing, images are acquired underwater.

The calibration procedure for the stereo camera pair closely follows the methods described in Williams et al.[24] Images of a one-meter square calibration target with a 7 x 8 checkerboard pattern of 10 cm squares are collected in an indoor, saltwater pool with a camera-target separation distance ranging from 3 to 6 m. With the camera system suspended approximately one meter below the surface of the water, the target is moved through the water while images are collected, yielding a set of images with the target at various three-dimensional orientations relative to the static camera position. For each combination of baseline camera separation and toe-in angle, fifty image pairs were collected.

The images are analyzed using the camera calibration toolbox for Matlab.[38] This software uses the Harris corner finding algorithm, which locates the square corners on the calibration target in each image based on color gradients.[39] From these coordinates, estimates of the intrinsic parameters of the individual cameras are produced, based on the known target size. These parameters account for all barrel distortion of the images and may be used to rectify images acquired by either camera. With the estimated intrinsic parameters for the individual cameras, a stereo calibration is used to estimate the extrinsic parameters of the camera system by analyzing the target position in the image pairs and iteratively computing the epipolar geometry.[40] Together

these intrinsic and extrinsic parameters represent a system model necessary for target triangulation.

3.3.2 Triangulation Accuracy

Along with the estimates for the intrinsic and extrinsic parameters of the camera system, the calibration procedure provides an estimate of "pixel errors." These errors are the differences between the pixel coordinates of the corners found using the Harris method during calibration and the expected corner location based on a reprojection of the target on each image. These errors are used to evaluate the calibration procedure and the accuracy of the corresponding system model for the camera pair. For example, the magnitude and distribution of these errors enables a comparison of accuracy trade-offs associated with different baseline separations and toe-in angles.

3.3.3 Target Tracking Capability

The system's ability to measure and track a target in three-dimensional space is demonstrated by moving a model killer whale (20 cm length) through the cameras' field of view. Images are collected at 2 frames per second for 30 seconds. For each image pair, the tip of the head and tail are manually identified. From this, an estimate is produced of the target length and spatial position.

3.4 System Field Testing

One of the key uncertainties regarding the integration of the optical imaging system with a tidal turbine is the functional range for detection, discrimination, and classification of marine animals by the stereographic cameras. The functional range establishes where the imaging system should

be deployed to observe interactions with the turbine rotor. A secondary question is the comparative effectiveness of the optical and acoustical camera systems to meet the objectives of near-turbine monitoring. The main variables that could affect imaging system effectiveness to classify a target are the target range and orientation, relative velocity between the target and camera, attenuation of artificial lighting by turbidity and flocculent, the optical camera digital gain setting, and behavioral effects of the strobe illumination. In this study, the first three of these are evaluated. Behavioral effects of strobe illumination will be evaluated once the system is developed with a tidal turbine, using the acoustical camera to observe the response of targets in the field of view to different strobe duty cycles.

Given the difficulty of accurately simulating flocculent and high relative velocities between targets and the camera in a laboratory setting, a field evaluation was undertaken with the imaging frame shown in Fig. 4. The frame consists of a mounting point for the imaging system located 4.5 m above the base of the frame. The frame has an in-air weight of approximately 1360 kg (3000 lbs). Relative water velocities of up to 2 m/s are achieved by towing the imaging frame from a high-tensile strength umbilical cable (Rochester A302351) with power conductors and optical fibers. Various targets are attached to platforms at camera-target separation distances of 1.5 m, 2.5 m, 3.5 m, and 4.5 m. These targets include static objects, such as a single square from the calibration image described in Sec. 3.3.1, standard eye charts, and line drawings of fish. The latter include large adult salmon (42 cm fork length), as well as small juvenile salmon and Pacific herring (5-11 cm fork length). Fish drawings are printed on a white or green background to provide either low or high contrast, respectively. In addition, tape streamers are attached to the frame and used to evaluate the ability of the camera system to capture rapid, complex motions without blur. Other targets, including three-dimensional metallic objects and flash-frozen fish

were considered during methodology development. It was concluded that these targets would be more difficult to handle and would not necessarily provide more useful information about system performance.

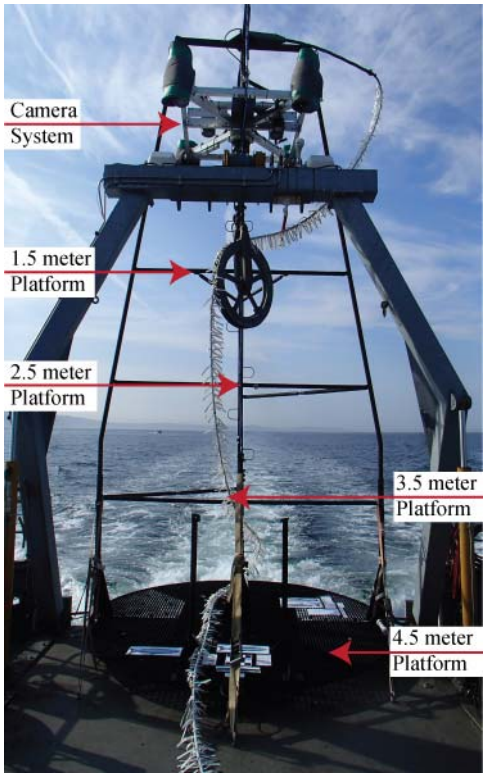

Fig. 4 – Imaging frame for camera testing.

In addition to image acquisition by the optical and acoustical cameras, several types of ancillary data are collected during field experiments. Cosine irradiance light meters (HOBO Pendant Temp-Light, www.onsetcomp.com) are attached to the camera frame and imaging frame platforms. These were intended to characterize the intensity of strobe illumination, but their response time is insufficient to achieve this, even at 10 Hz strobe rate and 1 Hz light meter sampling rate. However, information from the light meters is used to characterize the light attenuation coefficient tests and evaluate ambient light levels. Co-temporal profiles of depth and illumination obtained during deployment and recovery of the imaging frame are used to evaluate the attenuation coefficient by fitting them to a profile of the form

$$I(z) = I_0 e^{-cz} \quad (9)$$

where I is illumination (Lux), z is depth relative to the surface (m), and c is the empirical attenuation coefficient.[41] Pressure loggers (HOBO U20 Water Level, www.onsetcomp.com) are attached to the camera frame and the base of the imaging frame to monitor depth at a sampling rate of 1 Hz. During tows, the umbilical wire angle can be significant, up to 40^o at maximum tow velocities. Vibration is monitored by accelerometers on each platform and on the camera frame (HOBO Pendant G, www.onsetcomp.com) logging at 1 Hz. Relative water velocity between the tow frame and flocculent is monitored by a through-hull mounted Doppler profiler (RDI Workhorse 300 kHz, www.rdinstruments.com). Single-ping Doppler profiler data is recorded and ensemble averaged over the duration of image acquisition for a set of camera test parameters. Water depth is monitored by the tow vessel's echosounder and location is monitored by differential GPS, both logging at 1 Hz in Nobeltec software (www.nobeltec.com).

Qualitative assessments of imaging system performance include observations of flocculent and clarity of both the eye charts and fish line drawings. A quantitative assessment of performance is obtained by calculating the size of the black square on the calibration target from image pairs under different test conditions using the triangulation technique described in Sec. 3.1. Absolute measurement error for each image pair was defined as

$$e = L_{measured} - L_{actual} \quad (10)$$

where L_{measured} and L_{actual} are the stereographically measured and actual length of the calibration square, respectively. For simplicity of presentation, e is quantified in units of mm.

Tow tests were undertaken August 13-16, 2012 in northern Admiralty Inlet, Puget Sound, Washington. All tows were conducted by the University of Washington Applied Physics Laboratory's research vessel, the *R/V Jack Robertson*. Testing occurred during periods of falling tidal currents on greater ebb and flood to characterize performance during periods when

biological flocculent would likely be stirred up by intense tidal currents. There is also likely to be substantial seasonal variation in water clarity, with conditions in August likely to be on the lower end of seasonal clarity. During each tow, targets were positioned on the imaging frame at a camera-target separation distance of either 2.5 m, 3.5 m, or 4.5 m. Preliminary testing undertaken at an earlier date indicated shading of lower platforms by upper platforms could significantly degrade the quality of more distant images when multiple platforms were simultaneously employed. These earlier tests also indicated that targets were easily classified at 1.5 m range. Consequently, each test involved targets at a single camera-target separation distance and no tests were undertaken at separation distances less than 2.5 m. During each test, the imaging frame was lowered through the water column until the bottom of the frame (4.5 m distance from the cameras) was at a depth of 50 m. Images were acquired in blocks of fifty pairs at sampling rates of 5-10 frames per second under the following matrix of conditions:

- Camera-target separation: 2.5 m, 3.5 m, or 4.5 m
- Relative water velocity: near-zero (free-drift) or ~ 2 m/s (tow)
- Optical camera digital gain: 0x, 10*x*, or 20*x*

Each set of tests also included optical image capture with the strobes off and a camera gain of 20*x*, to confirm the expectation that observations at this depth and location require artificial illumination. Absolute measurement error is evaluated for the first thirty image pairs under each of the test conditions using (10).

4 Results

4.1 System Tank Testing

4.1.1 Intrinsic and Extrinsic Camera Parameters

The measured field of view of the individual cameras is approximately 54° in the horizontal direction (x-axis) and 42° in the vertical direction (y-axis). For reference, at a camera-target separation distance of 3.5 m, each pixel corresponds to a physical dimension of 2.10 mm by 2.17 mm and the field of view (including barrel distortion) is 3.4 m by 2.7 m.

As described in Sec. 3.3, uncertainty in the intrinsic parameters estimated through the calibration process is quantified by pixel error for each camera. Table 4 shows the standard deviation of the error values associated with the calibration procedure conducted prior to the field deployments and are representative of a typical calibration. This error varies throughout the stereographic field of view and causes a position bias for fixed points in space. At a distance of 3.5 m from the center of the camera pair, these values result in a spatial positioning error of approximately 0.2 mm.

Table 4 - Calibration reprojection error values for each camera.

	Camera 1	Camera 2
Horizontal and vertical pixel error (x,y)	(0.065, 0.059)	(0.14, 0.13)
Localization uncertainty at 3.5 m (x,y) [mm]	(0.081, 0.091)	(0.17, 0.20)

Raw and rectified images from each camera are shown in **Fig. 5** with the barrel distortion effects clearly visible in the curvature of the windows along the edges of the original images.

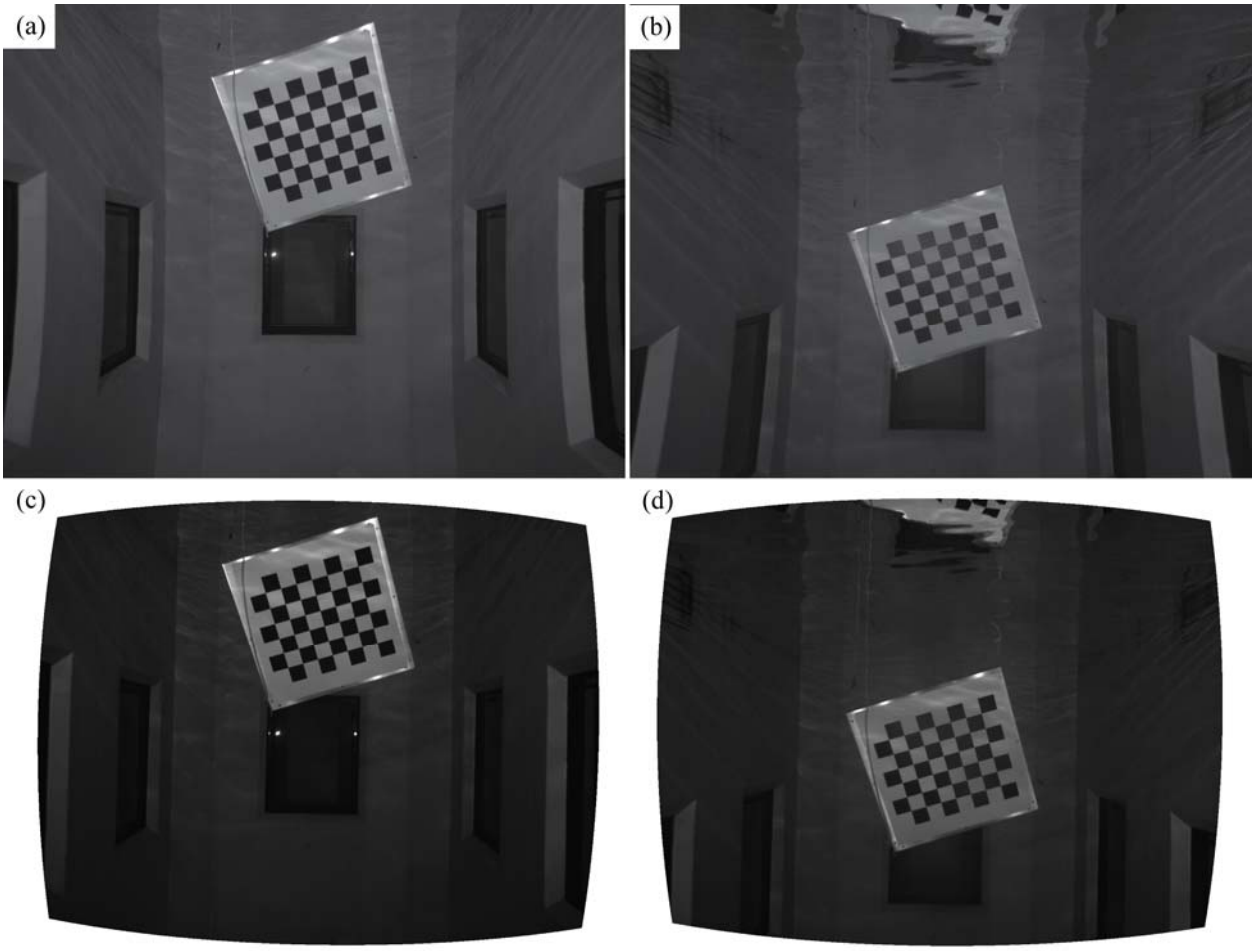

Fig. 5 - Camera 1 (left) and Camera 2 (right) calibration images before (a and b) and after (c and d) rectification. Effects of barrel distortion are visible in the curvature of the tank windows and target frame in the unrectified image.

4.1.2 Optimized Camera Arrangement

The objective of camera arrangement optimization is to maximize the stereographic field of view without significantly reducing triangulation accuracy. Fig. **6** shows the percentage of the overlapping field of view with baseline separations (*b*) of 0.5, 0.75, and 1.0 m over a range of toe-in angles and a field of view defined by a camera-target separation distance (measured from the center of the camera pair) of 1 to 5 m.

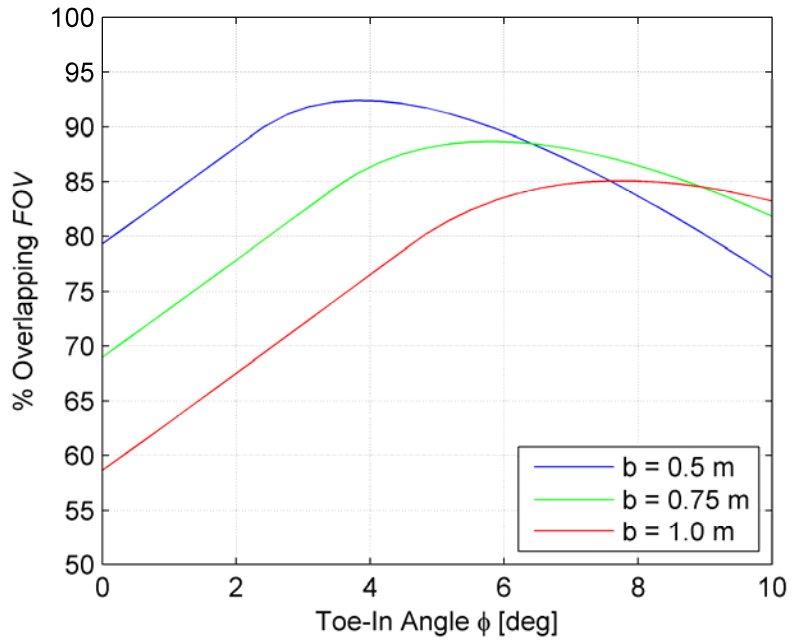

Fig. 6 – Variation in volumetric field of view overlap as a function of toe-in angle and camera spacing (*b*).

With a baseline separation (*b*) of 0.5 and 1 m the maximum overlapping field of view occurs when the cameras are towed-in to an angle of 3.8° and 7.6°, respectively. Fig. **7** shows a boxplot distribution of the calibration pixel errors for these two arrangements. There is no statistical difference between the two arrangements, suggesting that triangulation accuracy is not sensitive to the baseline separation over the range of values tested. The optimized system arrangement, therefore, is based purely on maximization of the overlapping field of view, given by $b = 0.5$, $\varphi = 3.8°$, and $w = 0^o$.

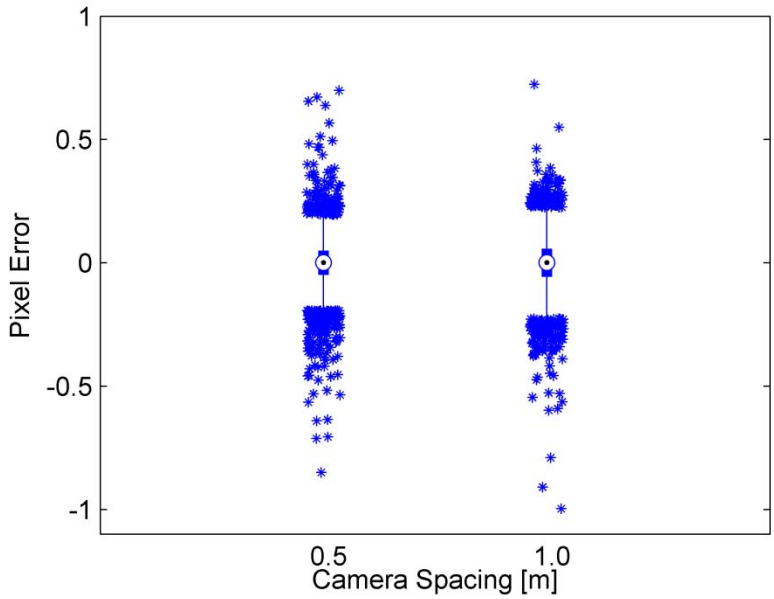

Fig. 7 - Calibration pixel errors at baseline separations (*b*) of 0.5 and 1 m. Circles denote median values, solid lines denote the 25th to 75th percentile, thin bars denote the extent of measurements beyond the interquartile range, asterisks denote outliers that are beyond 1.5 times the interquartile range.

4.1.3 Target Tracking Capability

The system's ability to measure and track a complex target in three-dimensional space is demonstrated in the 30 seconds of imagery shown in **Video 1**. For each image pair with the killer whale model visible, the projected points at the head and tail are plotted along with the corresponding coordinates relative to the left camera in the 3-D plot below the image pairs. The target length measurements conducted in this video have a mean of 212 mm (N = 47), which is equal to the actual length of the model killer whale, and a standard deviation of 15 mm.

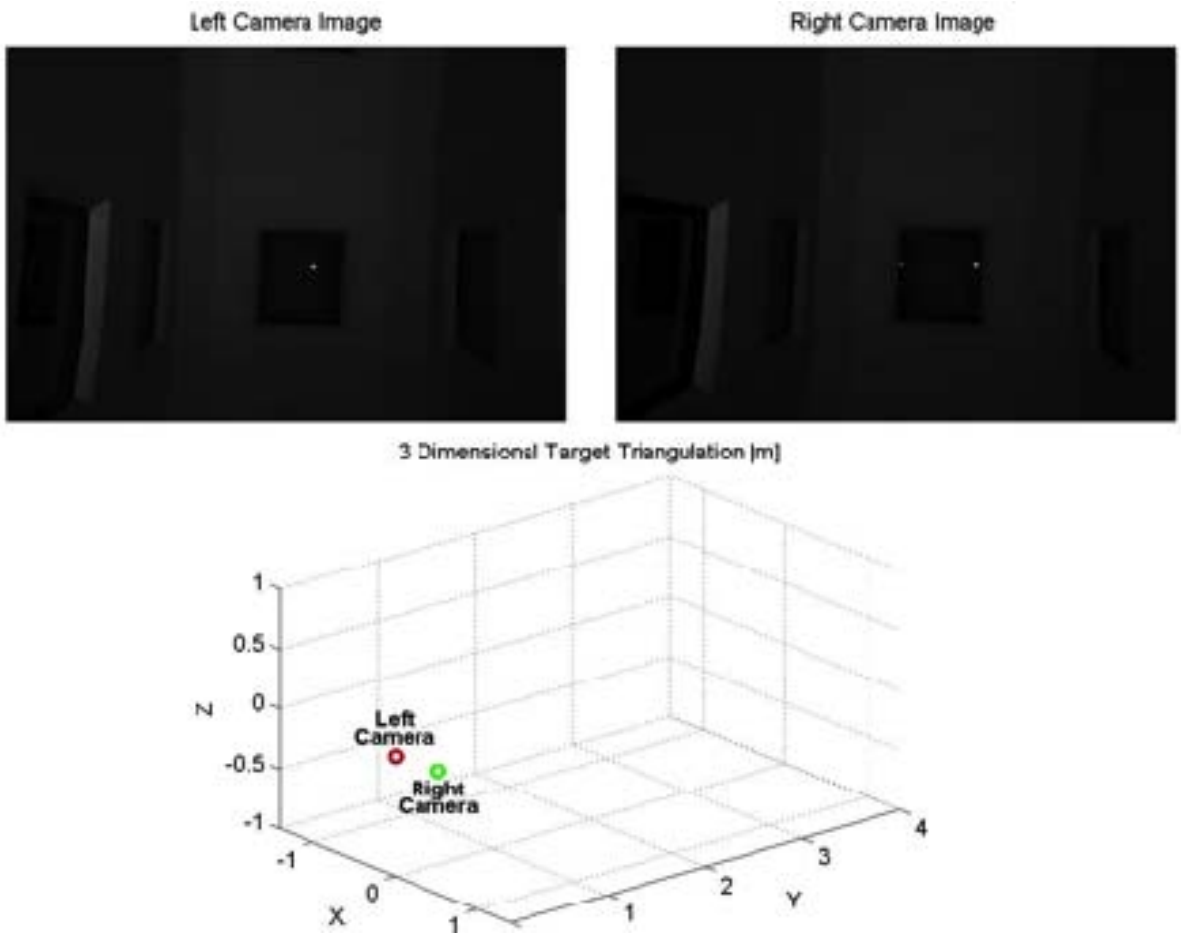

Video 1 - Target tracking demonstration using a scale-model killer whale (MPEG, 5.8 MB).

4.2 System Field Testing

4.2.1 Site-Specific Attenuation Coefficient

Four co-temporal depth/light profiles are evaluated to characterize ambient light at testing depth using the procedure described in Sec. 3.4. These were collected on August 13-16, 2012. Values for the attenuation coefficient (c) range from 0.15 to 0.24 m^{-1}, which is within the range of values expected for coastal waters[32] and confirms qualitative expectations for turbidity. Attenuation in embayments can be an order of magnitude higher,[42] which would significantly degrade the performance of the optical cameras. Review of optical camera imagery indicates that artificial

lighting is required below a depth of approximately 30 m to detect targets. This corresponds to an ambient illumination threshold of 5 Lux for these optical cameras.

4.2.2 Functional Range and Performance

Table 5 details the conditions tested, in terms of the experimental variables and site conditions. Specifically, z is the depth of the camera frame, H is the total water depth, and u is the actual relative velocity between the imaging frame and the water. Two gain settings were not evaluated for quiescent conditions (i.e., 0 m/s nominal) with a 3.5 m camera-target separation because, even with the surface vessel drifting, the relative velocity between the test frame and currents exceeded 1 m/s. Quiescent conditions for other tests correspond to a relative velocity of less than 0.5 m/s.

Table 5 – Camera evaluation cases from tow testing.

		Digital Gain		
Camera-Target Separation	**Nominal Relative Velocity**	G = 0x (no gain)	$G = 10x$	$G = 20x$
2.5 m	0 m/s	z = 46 m H = 61 m u = 0.2 m/s	z = 46 m H = 61 m u = 0.7 m/s	z = 46 m H = 60 m u = 0.2 m/s
	2 m/s	z = 30 m H = 70 m u = 1.9 m/s	z = 33 m H = 70 m u = 2.0 m/s	z = 31 m H = 69 m u = 1.8 m/s
3.5 m	0 m/s	*Not tested*	*Not tested*	z = 51 m H = 60 m u = 0.3 m/s
	2 m/s	z = 36 m H = 56 m u = 2.1 m/s	z = 37 m H = 56 m u = 1.7 m/s	z = 36 m H = 57 m u = 1.8 m/s
4.5 m	0 m/s[a]	$z \approx$ 46 m H = 60 m u = 0.3 m/s	$z \approx$ 46 m H = 60 m u = 0.2 m/s	$z \approx$ 46 m H = 61 m u = 0.2 m/s
	2 m/s[b]	$z \approx$ 30 m H = 66 m u = 2.1 m/s	$z \approx$ 30 m H = 66 m u = 1.9 m/s	$z \approx$ 30 m H = 66 m u = 1.9 m/s

[a] Pressure logger data unavailable. Camera depth estimated from umbilical length.
[b] Pressure logger data unavailable. Camera depth estimated from umbilical length and wire angle for other comparable platform tests and level of ambient light (zero reading on light meters).

Qualitatively, the optical imaging system performs well, as shown in Fig. 8. As expected, image clarity degrades with distance (Fig. 9) due to a combination of light attenuation, backscatter, and increasing pixel size. Strobe illumination is effective at freezing motion, with the streamers captured crisply in the frame (e.g., Fig. 8*f*, 3.5 m, 20*x* gain). At most camera-target separations, some degree of digital gain is required to detect the targets, though the high gain setting washes out images at small separation distance (e.g., Fig. 8*c*, 2.5 m, 20*x* gain). Flocculent is apparent in video sequences as black flecks, but the 1 m camera-strobe separation suppresses the majority of backscatter from strobe illumination. There are no distinguishing qualitative differences between images captured under tow, with a high flocculent flux through the field of view, and those captured free drifting, with a low flocculent flux.

The acoustical camera is capable of imaging the test frame and detecting streamer motion, but the two-dimensional images could, obviously, not be used to detect the static targets on the frame, as shown in **Video 2** for co-temporal video obtained by the two types of cameras.

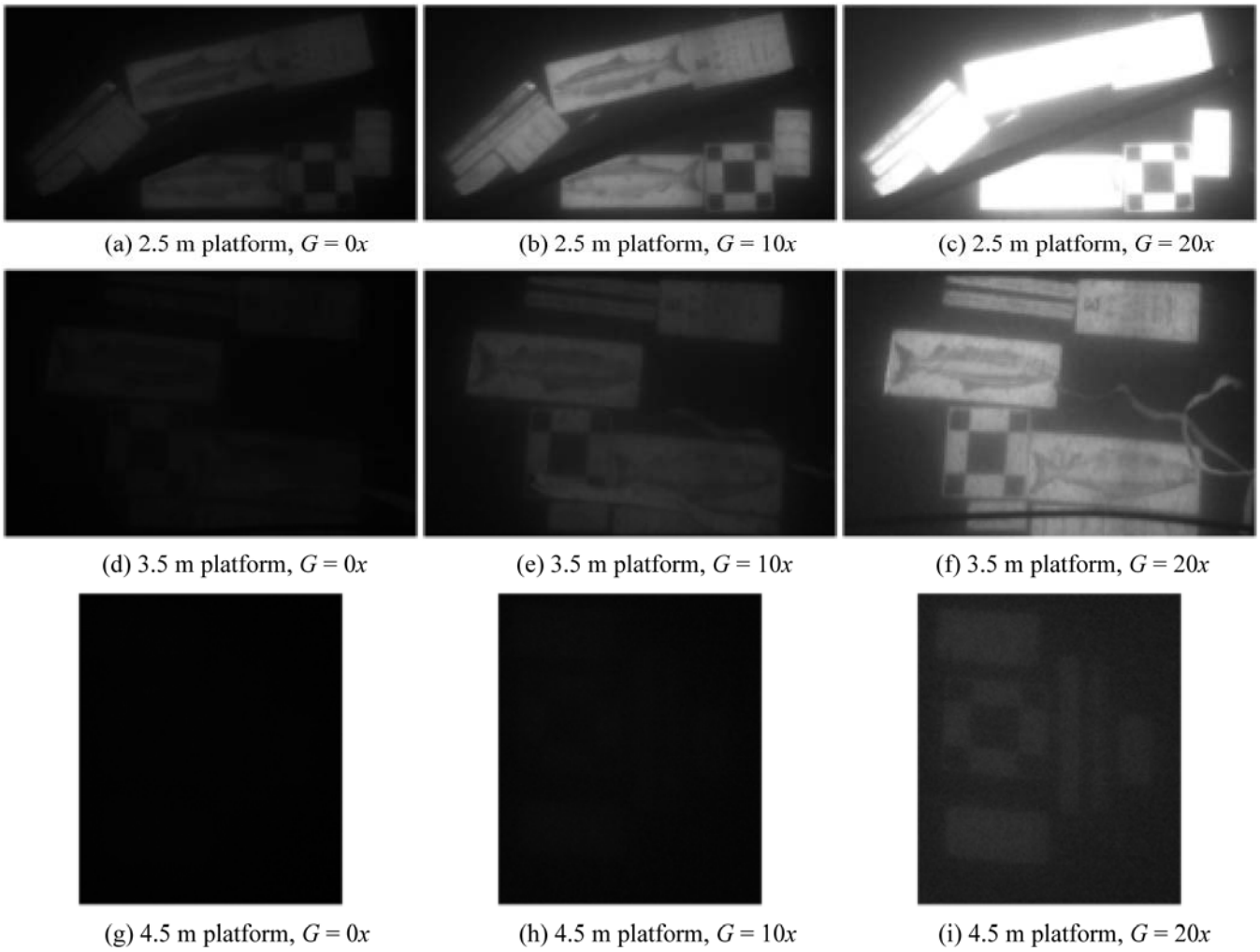

(a) 2.5 m platform, $G = 0x$ (b) 2.5 m platform, $G = 10x$ (c) 2.5 m platform, $G = 20x$

(d) 3.5 m platform, $G = 0x$ (e) 3.5 m platform, $G = 10x$ (f) 3.5 m platform, $G = 20x$

(g) 4.5 m platform, $G = 0x$ (h) 4.5 m platform, $G = 10x$ (i) 4.5 m platform, $G = 20x$

Fig. 8 – Images acquired during testing under tow ($u \approx 2$ m/s) (image *h* detectable at full resolution on a large screen).

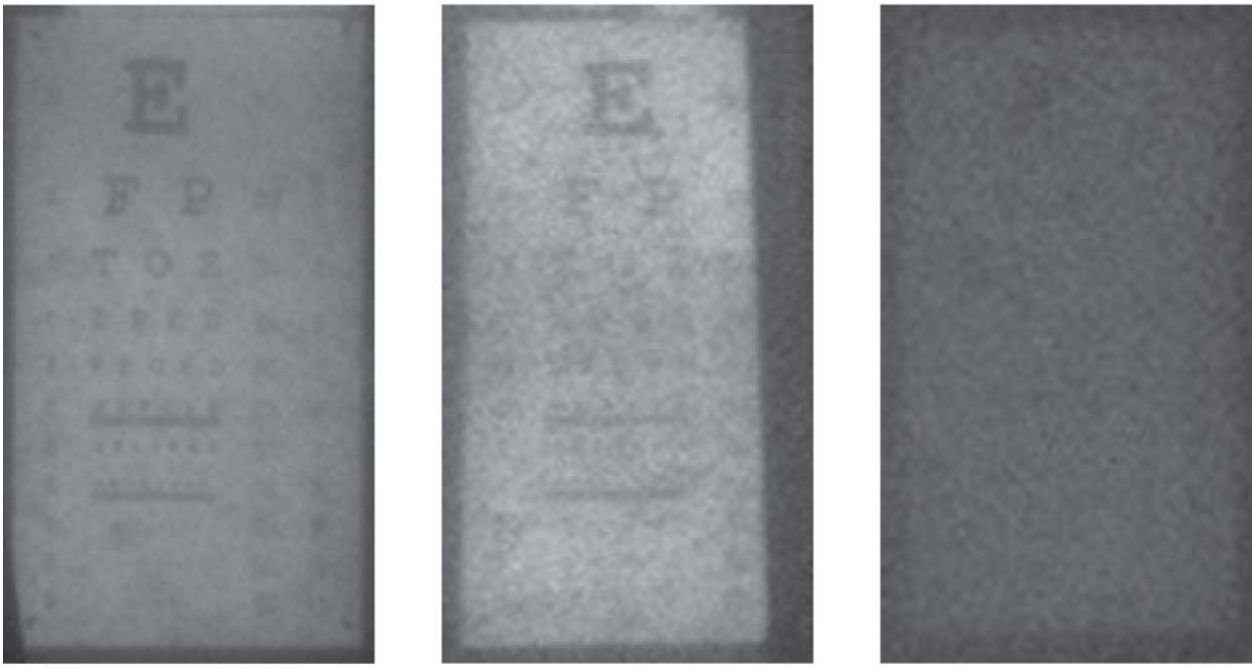

(a) 2.5 m platform, $G = 10x$ (b) 3.5 m platform, $G = 20x$ (c) 4.5 m platform, $G = 20x$

Fig. 9 – Detail of eye charts (detail from same images as Fig. 8).

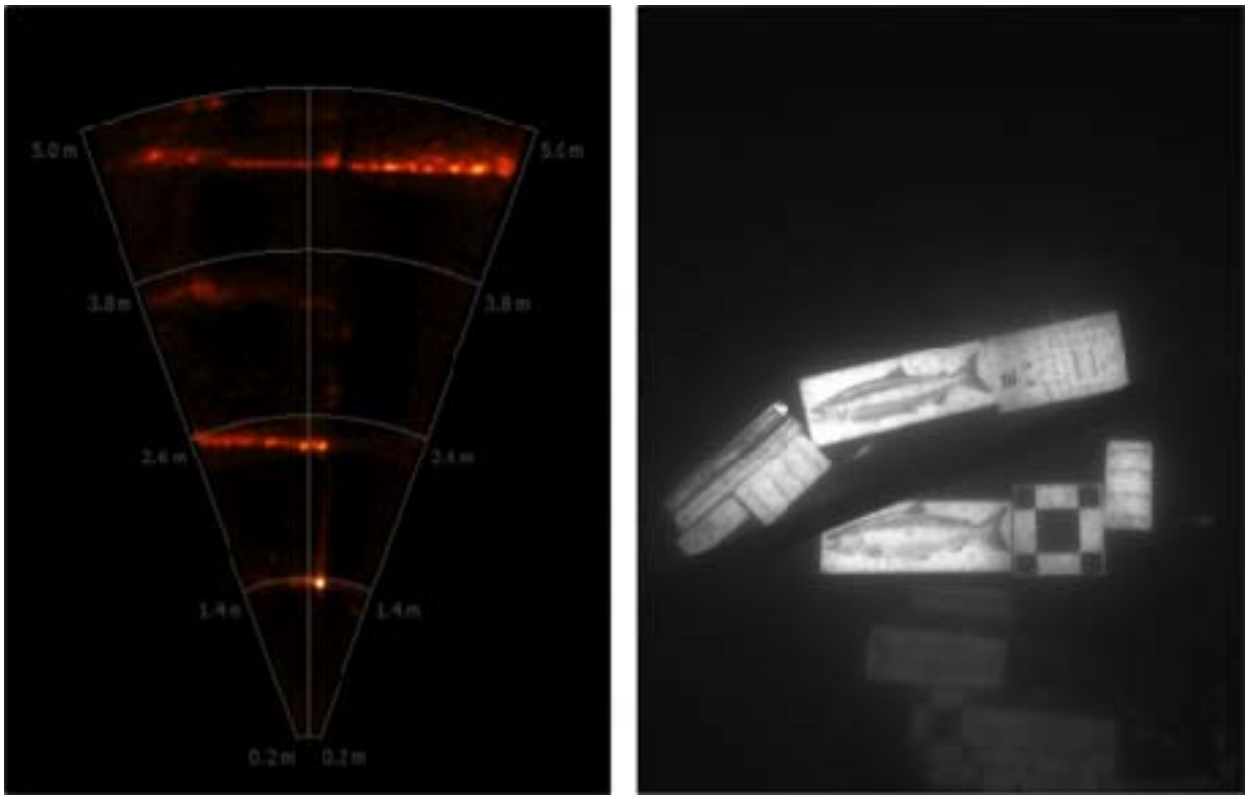

Video 2 – Simultaneous acoustical (left) and optical (right) videos. Acoustic returns at 1 m spacing correspond to the target-mounting platforms. Optical video with streamers and targets on 2.5 and 4.5 m platforms (MPEG, 6.1 MB).

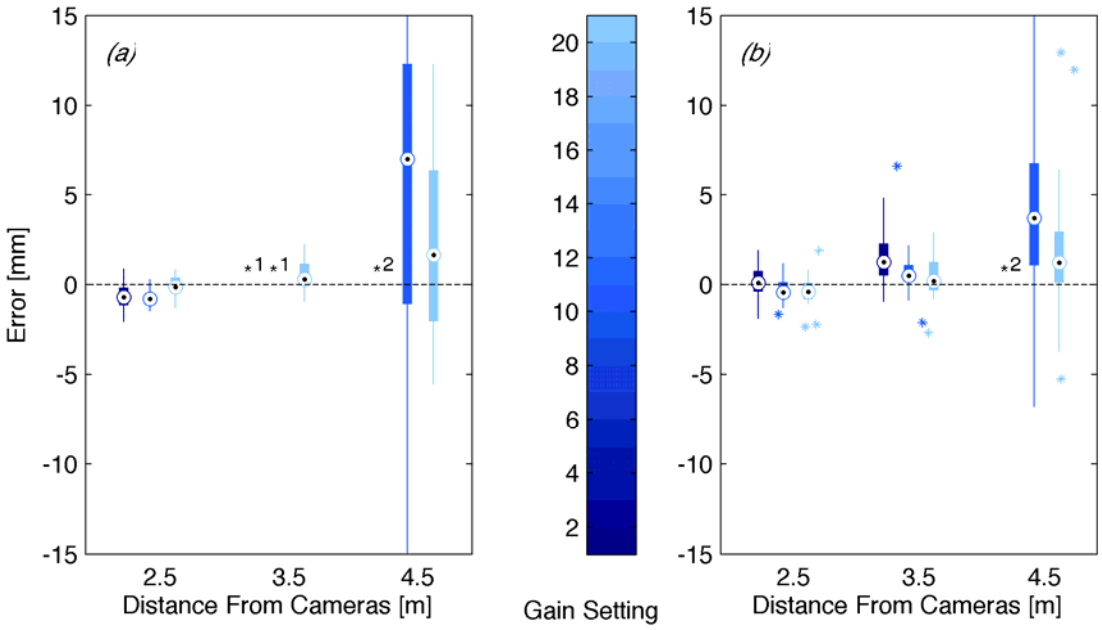

Fig. 10 – Absolute measurement error for each gain setting and camera-target separation. (a) No relative water velocity. (b) Relative water velocity of ≈ 2 m/s. Circles denote median values, lines denote the 25th to 75th percentile, thin bars denote the extent of measurements beyond the interquartile range, asterisks denote outliers that are beyond 1.5 times the interquartile range. 1: Case not tested. 2: Targets not visible at this gain setting.

Fig. **10** shows absolute measurement errors in the length of the calibration target square for each combination of gain setting and camera-target separation for the optical camera. At 2.5 m and 3.5 m camera-target separation there is a slight negative bias (length contraction) on the order of 2 mm and uncertainties are of similar magnitude. Bias may be due to "trimming" of the black target area by over-exposure of the surrounding white space or errors in the in the estimates for camera system extrinsic parameters related to the calibration procedure. Although the individual camera pixel error is an order of magnitude smaller than the observed bias, compounding biases from both cameras and the identification of corresponding positions in the image pairs may approach 2 mm. At a separation of 4.5 m, uncertainties are higher due to the degradation in image quality and length errors can exceed 1 cm (10% of target length). As

shown in Fig. 8, images at this distance have little contrast and the precision of corner detection is reduced. Difficulty associated with identifying the same target position in image pairs with low resolution and contrast contribute to greater uncertainty in the length measurement. Measurement errors under test conditions with high relative water velocity are not markedly different for the 2.5 m and 3.5 m separations. Error decreases for the 4.5 m separation, likely due to decreased frame depth (30 m submersion due to high wire angle for fixed length umbilical) which increased ambient light levels to ~5 Lux. Consequently, ambient light is sufficient to illuminate the targets and provide additional contrast.

5 Discussion

The results of laboratory and field evaluations indicate that the hybrid optical-acoustical imaging system will be able to perform its desired function of monitoring near-turbine inactions between the rotor and marine animals. Measurement errors, even at 4.5 m camera-target separation, are relatively small, less than 10% of the length of expected small targets (e.g., 10 cm herring). A digital gain setting between 10*x* and 20*x* appears optimal for target detection, discrimination, and classification over a range of camera-target separation distances. The system performs well in currents up to 2 m/s, with no obvious degradation in image quality associated with higher levels of flocculent flux.

Based on the results of field testing, the capability of the optical imaging system to detect, discriminate, and classify fish targets are summarized in Table 6. 'Detection' denotes the ability to locate a target in the camera field of view. 'Discrimination' denotes the ability to distinguish between fish and other targets, such as woody debris or kelp. 'Classification' denotes the ability to achieve a degree of taxonomic grouping. Test data indicates that visual imagery from an individual camera is unlikely to be sufficient for species-level classification at this specific

location, but species-level classification may be possible if supplemented by stereographic information (e.g., length) and known patterns species presence/absence. The acoustical camera is capable of detecting targets within the optical camera field of view and is likely to be an effective complement to characterize the behavioral response of fish to strobe illumination. While classification and discrimination of targets from the acoustical imagery alone is not possible, it may be possible for the acoustical camera (or other active sonar) to trigger the optical imaging system. This could reduce data bandwidth and the amount of optical imagery requiring manual review for target detection. The volume of data produced by optical imaging systems of this type is daunting, and, disregarding the potential for behavior modification, the use of such a system in a continuous manner poses a challenge for data management. Targeted use to evaluate specific hypotheses is recommended.

Table 6 – Optical imaging capabilities at different target separation distances (green images are likely and red images are unlikely).

Camera-Target Separation Distance	Detection	Discrimination	Classification
2.5 m	Small and large fish 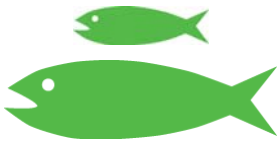	Small and large fish 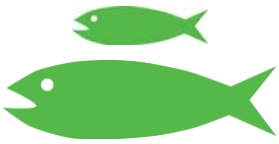	Small and large fish 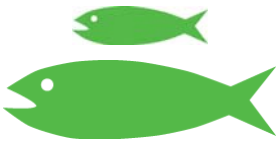
3.5 m	Small and large fish 	Small and large fish 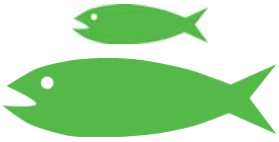	Large fish only 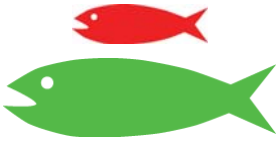
4.5 m	Large fish only 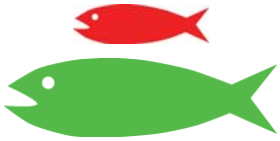	Large fish only 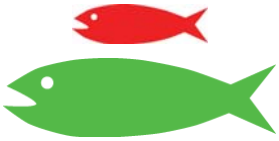	Unlikely for any fish 

Based on field testing, to evaluate interactions between marine animals and the turbine rotor, the imaging system should be deployed at turbine hub height at a slant distance of no more than 3-4 m from the turbine rotor. The capabilities of an imaging system deployed in this manner are shown, conceptually, in Fig. 11 for an OpenHydro turbine. Detection may be possible over the entire rotor swept area, but discrimination and classification are only likely to be possible over some of this region.

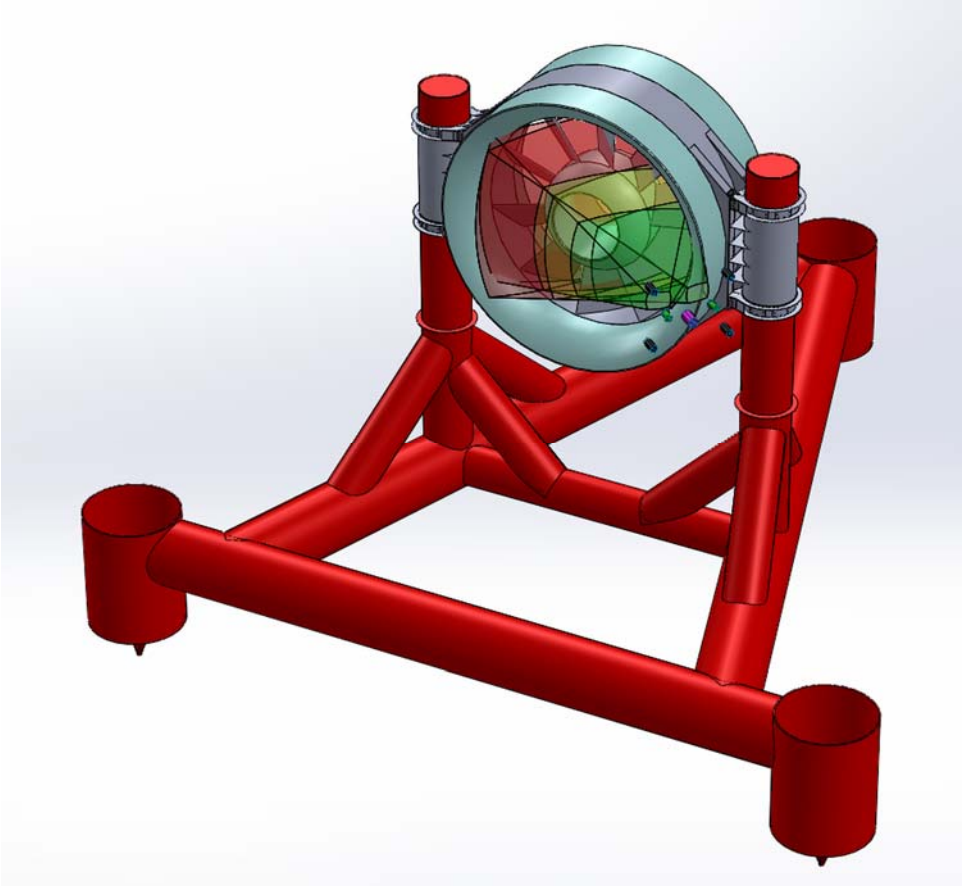

Fig. 11 - OpenHydro turbine with camera system and field of view. Green prism denotes range at which classification is likely, yellow for discrimination, and red for the extent of possible target detection.

6 Conclusion

Environmental monitoring in the near-field of tidal turbines would ideally be able to provide continuous coverage, differentiate between target collisions with turbine blades and near-misses,

allow taxonomic classification of marine animals, and not cause behavioral disturbances. The hybrid optical-acoustical camera system described in this paper has been developed to meet these monitoring needs in the conditions of the Admiralty Inlet site. Field evaluations conducted in Admiralty Inlet indicate that the system will be able characterize marine animal interactions with turbine blades while providing some level of taxonomic categorization over the majority of the rotor swept area. The accuracy of the stereographic target triangulation will likely be suitable to differentiate between strike/collision and a near-miss. The addition of an acoustical camera will allow evaluation of behavioral disturbance associated with the strobe lighting and could potentially serve as a trigger for the optical camera to enable continuous monitoring.

Acknowledgements

Funding for this project is provided by the US Department of Energy and Public Utility District No. 1 of Snohomish County. BlueView provided the acoustical camera under a no-cost lease agreement for evaluation purposes. The authors would also like to thank Jim Thomson for coordination of the field deployments, Sharon Kramer for recommendations on system testing, Capt. Andy Reay-Ellers for captaining the R/V Jack Robertson during the field tests, Alex DeKlerk for designing and fabricating the imaging frame, Joe Talbert and Tim McGinnis for building the tow umbilical, Nick Stelzenmuller for developing a number of prototype targets, Heather Eberhart for helping with general assembly and cable management, Keith van Thiel for the design of the pressure housings and optical ports, Rick Towler and Kresimir Williams for insight into component selection and stereographic calibration, and last, but certainly not least, Randy Sindelar for his adaptable, custom electronics for power and communication.

References

1. B. Polagye et al., "Environmental effects of tidal energy development," U.S. Dept. Commerce, NOAA Tech. Memo, F/SPO-116, 181 p, (2011).
2. G. Cada et al., "Potential impacts on hydrokinetic and wave energy conversion technologies on aquatic environments," *Fisheries* **32**(4), 174–180 (2007) [http://dx.doi.org/10.1577/1548-8446(2007)32[174:PIOHAW]2.0.CO;2].
3. G. Boehlert and A. Gill, "Environmental and ecological effects of ocean renewable energy development," *Oceanography* **23**(2), 68– 81 (2010) [http://dx.doi.org/10.5670/oceanog.2010.46].
4. H. Viehman and G. Zydlewski, "Fish interaction with a commercial-scale tidal energy device in a field setting," *Estuaries and Coasts*, *in revision*.
5. B. Williamson and P. Blondel, "Multibeam imaging of the environment around marine renewable energy devices," *Proc. of Meetings on Acoustics* **17** (2012).
6. M. Khan et al., "Hydrokinetic energy conversion systems and assessment of horizontal and vertical axis turbines for river and tidal applications: A technology status review," *Applied Energy*, **86**(10), 1823–1835, (2009) [http://dx.doi.org/10.1016/j.apenergy.2009.02.017].
7. S. H. Salter, "Are nearly all tidal stream turbine designs wrong?," *International Conference on Ocean Energy*, Dublin, Ireland (2012).
8. M. Kawase, P. Beba, and B. C. Fabien, "Finding and optimal placement depth for a tidal in-stream energy conversion device in an energetic, baroclinic tidal channel," NNMREC Tech. Report (2011).
9. C. C. Coutant and R. R. Whitney, "Fish behavior in relation to passage through hydropower turbines: a review," *Transactions of the American Fisheries Society*, **129**(2), 351–380 (2000) [http://dx.doi.org/10.1577/1548-8659(2000)129<0351:FBIRTP>2.0.CO;2].
10. M. J. Dadswell and R. A. Rulifson, "Macrotidal estuaries: a region of collision between migratory marine animals and tidal power development," *Biological Journal of the Linnean Society*, **51**(1-2), pp. 93– 113 (1994) [http://dx.doi.org/10.1111/j.1095-8312.1994.tb00947.x].

11. L. Barrios and A. Rodriguez, "Behavioral and environmental correlates of soaring-bird mortality at on-shore wind turbines," *Journal of applied ecology*, **41**(1), 72–81 (2004) [http://dx.doi.org/10.1111/j.1365-2664.2004.00876.x].
12. Normandeau Associates, "An estimation of survival and injury of fish passed through the hydro green energy hydrokinetic system, and a characterization of fish entrainment potential at the Mississippi Lock and Dam No. 2 hydroelectric project (FERC No. 4306)," Hastings, MN, Final Report Prepared for Hydro Green Energy, LLC (2009).
13. S. Amaral et al., "Evaluation of fish injury and mortality associated with hydrokinetic turbines," Palo Alto, CA, Final Report 1024569 for EPRI (2011).
14. S. Barr, "Short term behavioural responses in fish species to the open –centre turbine," Open Hydro Unpublished memorandum, (2010).
15. N. B. Furey, M. A. Dance, and J. R. Rooker, "Fine-scale movements and habitat use of juvenile southern flounder paralichthys lethostigma in an estuarine seascape," *Journal of Fish Biology*, **82**(5), 1469–1483 (2013) [http://dx.doi.org/10.1111/jfb.12074].
16. G. A. McMichael et al., "The juvenile salmon acoustic telemetry system: a new tool," *Fisheries*, **35**(1), 9-22 (2010) [http://dx.doi.org/10.1577/1548-8446-35.1.9].
17. C. J. Bridger and R.K. Booth, "The effects of biotelemetry transmitter presence and attachment procedures on fish physiology and behavior," *Reviews in Fisheries Science*, **11**(1), 13-34 (2003) [http://dx.doi.org/10.1080/16226510390856510].
18. Snohomish PUD, "Final Pilot License Application for the Admiralty Inlet Pilot Tidal Project," FERC Project No. 12690-000 (2012).
19. B. Polagye, M. Kawase, and P. Malte, "In-stream tidal energy potential of Puget Sound, Washington," *Proc. Inst. MechE, Part A: J. Power and Energy*, **223**(5), 571–587 (2009) [http://dx.doi.org/10.1243/09576509JPE748].

20. B. Polagye and J. Thomson, "Tidal energy resource characterization: methodology and field study in Admiralty Inlet, Puget Sound, US," *Proc. IMechE, Part A: J. Power and Energy*, **227**(3), 352-367 (2013) [http://dx.doi.org/10.1177/0957650912470081].
21. H. G. Greene, "Habitat characterization of the SnoPUD turbine site - Admiralty Head, Washington State," Final Report (2011).
22. J. Howland et al., "Development of a towed survey system for deployment by the fishing industry," *MTS/IEEE Oceans* (2006).
23. G. Rosenkranz et al., "Development of a high-speed, megapixel benthic imaging system for coastal fisheries research in Alaska," *Fish. Res.*, **92**, 340–344 (2008) [http://dx.doi.org/10.1016/j.fishres.2008.03.014].
24. K. Williams, C. N. Rooper, and R. Towler, "Use of stereo camera systems for assessment of rockfish abundance in untrawlable areas and for recording pollock behavior during midwater trawls," *Fishery Bulletin*, **108**, 352–362 (2010).
25. S. T. Barnard and M. A. Fischler, "Computational stereo," *ACM Computing Survey*, **14**(4), 553–572 (1982) [http://dx.doi.org/10.1145/356893.356896].
26. N. Alvertos, D. Brzakovic, and R. C. Gonzalez, "Camera geometries for image matching in 3-d machine vision," *IEEE Transactions on Pattern Analysis and Machine Intelligence*, **11**(9), 897–915 (1989) [http://dx.doi.org/10.1109/34.35494].
27. G. Wesheimer, "Three-dimensional displays and stereo vision," *Proc. R. Soc. B*, **278**(1716), 2241–2248 (2011).
28. W. L. Aylsworth et al., "Stereographic digital cinema: Production and exhibition techniques in 2012," *Proceedings of the IEEE*, **101**(1), 169-189 (2013) [http://dx.doi.org/10.1109/JPROC.2012.2191610].
29. G. A. Jones, "Constraint, optimization, and hierarchy: Reviewing stereoscopic correspondence of complex features," *Computer Vision and Image Understanding*, **65**(1), 57–78 (1997) [http://dx.doi.org/10.1006/cviu.1996.0482].

30. J. B. Joslin et al., "Development of an adaptable monitoring package for marine renewable energy," *MTS/IEEE Oceans* (2013).
31. S. Gallager et al., "High resolution underwater imaging and image processing for identifying essential fish habitat," *Report of the National Marine Fisheries Service Workshop on Underwater Video Analysis*, U.S. Dept. of Commerce, NOAA Tech. Memo no. NMFS-F/SPO-68 (2005).
32. J. S. Jaffe, "Underwater optical imaging: the design of optimal systems," *Oceanography*, 40–41 (1988) [http://dx.doi.org/10.5670/oceanog.1988.09].
33. M. Marchesan et al., "Behavioural effects of artificial light on fish species of commercial interest," *Fish. Res.*, **73**, 171-185 (2005) [http://dx.doi.org/10.1016/j.fishres.2004.12.009].
34. C. H. Ryer et al., "Effects of simulated underwater vehicle lighting on fish behavior," *Mar. Ecol. Prog. Ser.*, **391**, 97-106 (2009), [http://dx.doi.org/10.3354/meps08168].
35. A. W. Stoner et al., "Evaluating the role of fish behavior in surveys conducted with underwater vehicles," *Can. J. Fish. Aquat. Sci.*, **65**, 1230-1243 (2008), [http://dx.doi.org/10.1139/F08-032].
36. M. Lehaitre, L. Delauney, and C. Compere, "Biofouling and underwater measurements," *Real-time observation systems for ecosystem dynamics and harmful algal blooms*, UNESCO, Paris (2005).
37. C. Wohler, *3D Computer Vision: Efficient Methods and Applications*, 2nd ed., Springer, London (2013) [http://dx.doi.org/10.1007/978-1-4471-4150-1].
38. J. Y. Bouguet. "Camera calibration toolbox for Matlab," 9 July 2010 (accessed 12 September 2013).
39. C. Harris and M. Stephens, "A combined corner and edge detector," *Proceedings of the 4th Alvey Vision Conference*, 147-151 (1988).
40. G. Xu and Z. Zhang, *Epipolar geometry in stereo, motion, and object recognition: a unified approach*, Kluwer Academic Publs., Norwell, MA (1996) [http://dx.doi.org/10.1007/978-94-015-8668-9].
41. A. Beer, "Determination of the absorption of red light in colored liquids," *Annalen der Physik und Chemie*, **86**, 78–88 (1852).

42. J. S. Jaffe, “Multi autonomous underwater vehicle optical imaging for extended performance,” *MTS/IEEE Oceans*, San Diego, CA (2007)

Author Biographies and Photographs

James Joslin is a PhD student working with the Northwest National Marine Renewable Energy Center at the University of Washington in Seattle. His research focuses on the development of instrumentation to increase monitoring capabilities of tidal and wave energy converters. He completed his undergraduate and masters degrees at Dartmouth College and was introduced to marine engineering while working with Sea Education Association out of Woods Hole, MA.

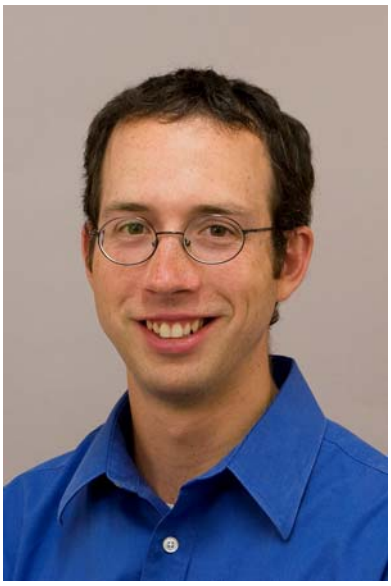

Dr. Brian Polagye is the co-Director of the Northwest National Marine Renewable Energy Center and an assistant professor in the Department of Mechanical Engineering at the University of Washington. His research focuses on marine renewable energy conversion. Dr. Polagye holds a bachelors degree from Princeton University and doctoral degree from the University of Washington.

Dr. Sandra Parker-Stetter is a Research Scientist in the School of Aquatic and Fishery Sciences at the University of Washington. Her research focuses on the application of acoustic and direct sampling techniques to evaluate the distributions of fish and large invertebrates. Dr. Parker-

Stetter holds a bachelors degree from the University of Windsor and masters and doctoral degrees from Cornell University.

Caption List

Fig. 1 – Prototype imaging system showing principal components and scale.

Fig. 2 - General 3 dimensional stereo camera arrangement.

Fig. 3 – (a) Camera arrangement variables in the x-z plane and (b) variables describing the overlapping volumetric field of view at a given distance (*d*) from the camera.

Fig. 4 – Imaging frame for camera testing.

Fig. 5 - Camera 1 (left) and Camera 2 (right) calibration images before (a and b) and after (c and d) rectification. Effects of barrel distortion are visible in the curvature of the tank windows and target frame in the unrectified image.

Fig. 6 – Variation in volumetric field of view overlap as a function of toe-in angle and camera spacing (*b*).

Fig. 7 - Calibration pixel errors at baseline separations (*b*) of 0.5 and 1 m. Circles denote median values, solid lines denote the 25^{th} to 75^{th} percentile, thin bars denote the extent of measurements beyond the interquartile range, asterisks denote outliers that are beyond 1.5 times the interquartile range.

Fig. 8 – Images acquired during testing under tow ($u \approx 2$ m/s) (image *h* detectable at full resolution on a large screen).

Fig. 9 – Detail of eye charts (detail from same images as Fig. 8).

Fig. 10 – Absolute measurement error for each gain setting and camera-target separation. (a) No relative water velocity. (b) Relative water velocity of ≈ 2 m/s. Circles denote median values, lines denote the 25^{th} to 75^{th} percentile, thin bars denote the extent of measurements beyond the interquartile range,

asterisks denote outliers that are beyond 1.5 times the interquartile range. 1: Case not tested. 2: Targets not visible at this gain setting.

Fig. 11 - OpenHydro turbine with camera system and field of view. Green prism denotes range at which classification is likely, yellow for discrimination, and red for the extent of possible target detection.

Video 1 - Target tracking demonstration using a scale-model killer whale (MPEG, 5.8 MB).

Video 2 – Simultaneous acoustical (left) and optical (right) videos. Acoustic returns at 1 m spacing correspond to the target-mounting platforms. Optical video with streamers and targets on 2.5 and 4.5 m platforms (MPEG, 6.1 MB).

Table 1 – Capabilities of potential near-turbine monitoring technologies.

Table 2 - Component, manufacturer, description, and equipment cost for the stereo-camera portion of the turbine monitoring instrumentation.

Table 3 - Component power requirements at maximum data acquisition rates.

Table 4 - Calibration reprojection error values for each camera.

Table 5 – Camera evaluation cases from tow testing.

Table 6 – Optical imaging capabilities at different target separation distances (green images are likely and red images are unlikely).